

# DEVELOPMENT OF DESIGN RESPONSE SPECTRAL SHAPES FOR CENTRAL AND EASTERN U.S. (CEUS) AND WESTERN U.S. (WUS) ROCK SITE CONDITIONS\*

W. J. Silva, R.R. Youngs, and I.M. Idriss

## 1 INTRODUCTION

In developing response spectral shapes for both the WUS and CEUS tectonic regions, three issues of particular significance arise: (1) selection of an appropriate normalization frequency and fractile level, (2) the paucity of data in the CEUS for  $M > 4.5$ , and (3) the likelihood that CEUS earthquake source processes for magnitudes larger than about  $M 6$  produce significantly less intermediate frequency energy than corresponding WUS source processes.

The first issue, selection of an appropriate normalization frequency and fractile level, is complicated somewhat by the desirability of having the fractile level uniform across frequency. This uniformity is highly desirable, as it is implicit in maintaining risk consistency or a constant level of conservatism in design analyses. Unfortunately, strong ground motions in the WUS (the tectonic regime with the most complete database in terms of magnitude and distance ranges) are characterized by a frequency-dependent, as well as magnitude-dependent, variability. Regression analyses on WUS strong ground motion data generally show empirical scatter (variation about the median) that decreases with increasing frequency (Abrahamson and Shedlock, 1997). This variability also decreases with increasing magnitude (Youngs et al., 1995) or ground motion amplitude (Campbell, 1993), particularly for  $M \geq 6$ . These statistical properties are likely real and stable, not reflecting spurious trends due to a sparse sample size. They are probably related to fundamental physics of earthquake source, path, and site processes and can reasonably be expected to occur in the CEUS as well as the WUS.

The second issue relevant to developing response spectral shapes for the CEUS, the paucity of strong motion data, precludes a purely statistical approach to developing shapes. The direct effect of a small sample size is the necessity of using physical models, resulting in a significantly higher uncertainty in the shapes for applications to CEUS sites.

The third issue, the possibility that source processes in tectonically stable regions emit less intermediate frequency energy than corresponding sources in active regions (WUS) is driven largely by the lack of CEUS data for  $M \geq 6$  and contributes substantially to the larger uncertainty in CEUS shapes. This difference in spectral content manifests itself seismologically in a second corner frequency, which results in response spectral shapes that contain a well-developed spectral sag in a frequency range (near 1 Hz) that varies with magnitude. WUS sources do not show such a well-developed spectral sag, and it is not reflected in empirical attenuation relations. Recent studies, (Atkinson and Silva, 1997) however, suggest that the sag may be present in a much more subtle

---

\* Silva, W. J., R.R. Youngs, and I.M. Idriss (2001). "Development of design response spectral shapes for Central and Eastern U.S. (CEUS) and Western U.S. (WUS) rock site conditions." *Proc. of the OECE-NEA (Organization For Economic Coordination and Development of the Nuclear Energy Agency) Workshop on Engineering Characterization of Seismic Input, Nov., 15-17, 1999 NEA/CSNI/R(2000)2*, vol. 1: 185-268.

form, being obscured (filled in) by amplification due to generally softer crustal rocks in the WUS compared to CEUS crustal conditions. Theoretically this is appealing, suggesting an intrinsic commonality between WUS and CEUS source processes, although there is no compelling argument to prove this should be the case. The possibility of commonality does not increase our confidence (lower the level of uncertainty) in CEUS shapes because the current state of knowledge does not reflect a high level of confidence in the physical process that produces a stable and predictable spectral sag for large magnitude ( $M > 6$ ) earthquakes. As a result, until more CEUS data become available for  $M > 6$  earthquakes, some uncertainty will exist as to the appropriateness and degree of sag in CEUS spectral shapes. The approach taken in developing shapes for the CEUS is not to attempt resolution of this issue, but to produce spectral shapes using models that reflect both possibilities, i.e., with and without an intermediate frequency spectral sag.

## 2 APPROACH

The overall approach taken to define response spectral shapes applicable to WUS and CEUS conditions is to rely as much as possible on recorded motions. These motions are supplemented, where necessary, by well-validated models. This approach is intended to result both in confidence in the use of the spectral shapes as well as reasonable stability over time.

To develop shapes for WUS conditions that incorporate appropriate magnitude and distance scaling, a suite of empirical attenuation relations were averaged for a set of magnitude and distance bins. The empirical relations were weighted based on a goodness of fit evaluation with statistical shapes (Kimball, 1983). The statistical shapes are computed for the magnitude and distance bins from recorded motions listed in the strong motion catalog (Table 1). The use of empirical relations rather than the statistical shapes directly (Mohraz et al., 1972; Newmark et al., 1973) provides a formalism for sampling expert opinion in smoothing, interpolation, and extrapolation within the poorly sampled bins and oscillator frequencies. Incorporating a robust weighting scheme based on how well each relation fits statistical shapes reduces potential bias in the development of average shapes.

The response spectral shapes computed from the weighted empirical relations were then fit to a functional form with magnitude and fault distance as independent variables. This process results in an attenuation relation for smooth WUS shapes that is largely driven by recordings and that incorporates the experience and background of a number of researchers in strong ground motion. The approach of producing an attenuation relation for shapes has the advantage of simplicity as well, being a continuous function of magnitude, distance, and frequency.

For applications to the CEUS, insufficient data preclude a similar empirical approach, necessitating consideration of physical models. In general, reliance on model predictions for regions of sparse data results in increased uncertainty in computed motions. For CEUS conditions, this is further complicated by observations that strongly suggest the possibility that the spectral content in the intermediate frequency range for large magnitude CEUS sources is significantly different (lower) than corresponding WUS sources. Because this issue is currently unresolved, consideration must be given to multiple CEUS source spectral models.

To minimize the dependence on models in developing CEUS shapes, we used model predictions in the form of ratios to produce transfer functions. The transfer functions, which are ratios of CEUS shapes to WUS shapes, were then applied to the empirical WUS shapes to produce shapes appropriate for CEUS conditions. We then develop attenuation relations for the CEUS shapes.

The use of ratios of model predictions rather than model results directly is intended to minimize the impact of potential model deficiencies. Another advantage of this approach is the emphasis placed on model validations for both WUS and CEUS conditions.

### 3 WUS Statistical Shapes

Statistical response spectral shapes (Kimball, 1983) were developed for a suite of magnitude and distance bins by sampling the WUS strong motion data base. Shapes (for 5% damping) were developed by normalizing each response spectrum by the spectral ordinate at the selected frequency and then averaging the scaled records within each bin. A lognormal distribution was assumed. The resulting suites of normalized spectra provides a basis for assessing both an appropriate normalization frequency as well as fractile level.

#### 3.1 Magnitude and Distance Bins for WUS Spectral Shapes

Implicit in the selection of appropriate magnitude ( $M$ ) and distance (fault distance,  $R$ ) bins is the classic tradeoff between resolution and stability. In this context, resolution refers to the ability to clearly distinguish  $M$  and  $R$  dependencies in spectral shapes (which is enhanced by more bins) while stability relates to low variability or statistical stability (which is enhanced by fewer bins, with more data in each bin). In terms of spectral shapes, high stability also results in the desirable feature of smoothness, or less variability from frequency to frequency.

The selection of bin widths and boundaries, in addition to achieving an acceptable compromise between resolution and stability based upon the distribution (in  $M$  and  $R$ ) of data, is also conditioned by knowledge of shape sensitivity to  $M$  and  $R$ . In general, the distance dependency for WUS shapes is small (less than about 30%) within about 30 to 50 km from the source. For CEUS shapes the corresponding distance is about 50 to 100 km (Silva and Green, 1989). On the other hand, near-source effects are particularly strong for fault distances within about 10 to 15 km, particularly for vertical strike-slip mechanisms (Somerville et al., 1997). Additionally, seismic hazard is generally dominated by sources within about 100 km for WUS (about 200 km for Cascadia subduction zone sources), and within about 300 km for CEUS sources. For response spectral shapes, beyond about 50 km for WUS and 70 to 100 for CEUS conditions, a factor of 2 change in distance results in about a 30% (factor of 1.3) change in spectral shape (Silva, 1991). With these considerations, distance bins of 0 to 10, 10 to 50, 50 to 100, 100 to 200 km for both WUS and CEUS shapes were considered appropriate with an additional bin of 200 to 400 km for CEUS shapes.

For magnitude bins,  $M$  of 5 up to about 8 (except for Cascadia subduction zone sources) dominate the hazard for both the WUS and CEUS. While a half magnitude change in  $M$  results in a 30% to 50% change in PGA normalized shapes (Silva and Green, 1989; Silva, 1991) depending upon  $M$  and frequency, half  $M$  bins are too sparse at the larger  $M$  ( $M > 6.5$ ). As a result, unit magnitude wide

bins were selected centered on half magnitudes: **M** 5.5, 6.5, and 7.5 with ranges of 5 to 6, 6.01 to 7, and 7.01 and larger. Table 1 shows the bins along with summary statistics. For completeness, statistics for soil sites (taken as Geomatrix classifications C and D, Appendix A) were included, in addition to a 0 to 50 km distance bin.

### **3.2 Development of WUS Statistical Spectral Shapes**

The first issue to resolve in developing the set of shapes for applications to WUS and CEUS conditions was the appropriate normalization frequency and fractile level. To approach this issue, median bin shapes were computed for a suite of normalization frequencies to determine the degree of similarity between the shapes. Figure 1 shows an example for the **M** 6.5 and  $R = 10$  to 50 km bin for normalization frequencies of 0.5, 1.0, 5.0, 10.0, 20.0, 34.0, and 100.0 Hz (100 Hz = PGA). The shapes were computed down to frequencies that were 125% (factor of 1.25) of processing corner frequencies. This resulted in an increase in variability at lower frequencies as records dropped out due to noise contamination. For all seven normalization frequencies, the shapes were quite similar, and scaling each shape to unity at 100 Hz (PGA) presents a more convenient display (Figure 2). Similar results were obtained for the other bins suggesting a convenient resolution to the issue of selecting an appropriate normalization frequency. Since peak ground acceleration has the lowest variability among response spectral ordinates in the frequency range of 100.0 to 0.2 Hz (Abrahamson and Silva, 1997; Campbell, 1997; Boore et al., 1997; Sadigh et al., 1997), it is an attractive as well as conventional normalization parameter (Seed et al., 1976). Similar results would be obtained if normalization were done using spectral acceleration at any other frequency.

The selection of an appropriate fractile level for spectral shapes must consider the manner in which the shapes are to be used. Current regulatory guidance (R.G. 1.165) recommends probabilistic seismic hazard evaluations for rock outcrop (or its equivalent), with coupling to deterministic evaluations using deaggregation of the uniform hazard spectrum (UHS), the deaggregation being done at several frequencies. Deterministic spectra are then scaled to the UHS at the deaggregation frequencies as a check on the suitability of the UHS and to provide control motions for site response evaluations. The deterministic spectra may be computed from the attenuation relations used in the UHS or may be based on the recommended spectral shapes. Additionally, the recommended spectral shapes may be used to evaluate existing design motions at the rock outcrop level. As a result, the development of median shapes is most consistent with intended uses, particularly in the context of UHS, where the desired hazard is appropriately set at the UHS exceedence level.

The bin statistical shapes (median  $\pm$  1 sigma) normalized by peak ground acceleration are shown in Figures 3 to 5 for rock and Figures 6 to 8 for soil.

### **3.3 Ground Motion Model for Spectral Shapes**

The most desirable feature in a ground motion model for spectral ordinates is the ability to reliably and accurately capture magnitude, distance, and site dependencies with a minimum of parameters. A necessary aspect of any ground motion model implemented in engineering design practice is a thorough validation with recorded motions. Since all models are mathematical approximations to complicated physical processes, rigorous validation exercises are necessary to assess model accuracy,

reveal strengths and shortcomings, and constrain parameter values and their uncertainties (Roblee et al., 1996). Ideally, a ground motion model will be validated over the ranges of magnitudes, distances, site conditions, and tectonic environments for which it is implemented. In this sense, the model is more an interpolative tool that can be used with a confidence level reflected in quantified validation exercises (Abrahamson et al., 1990; EPRI, 1993; Silva et al., 1997). While this is becoming possible for WUS tectonic conditions, it is clearly not the case for the CEUS. Because of the paucity of recording in CEUS conditions, thorough validation exercises to assess model accuracy and parameter distributions are not possible. This situation necessarily results in significantly higher uncertainty, which can be assessed only in a qualitative manner.

### 3.3.1 Point-Source Model

Since response spectral shapes are intended to reflect average horizontal motions at sites distributed at the same fault distance from the source, the effects of source finiteness are expected to be minimal (Silva and Darragh, 1995). The effects of rupture directivity and source mechanism on spectral shapes (Section 3.6) increase the variability associated with spectral shapes at close distances ( $R \leq 15$  km) and at low frequency ( $\leq 1$  Hz) but have little effect on the *average* shape. As a result, a point-source model with its attractive simplicity is considered appropriate. The stochastic point-source model, in the context of strong ground motion simulation, was originally developed by Hanks and McGuire (1981) and refined by Boore (1983; 1986). It has been validated in a comprehensive manner by modeling 18 earthquakes at about 500 sites (Silva et al., 1997). Table 2 lists the parameters used to develop the spectral shapes and transfer functions.

For applications to the CEUS, a single significant set of observations may fundamentally increase uncertainty in model predictions of spectral shapes. This phenomenon was illustrated with ground motions generated by the 1988 **M** 5.8 Saguenay, Ontario earthquake. Even prior to this earthquake, high frequency ( $> 5$  Hz) motions at hard rock CEUS sites were known to be significantly greater than motions recorded on typical WUS soft rock conditions. A number of small earthquake ( $\mathbf{M} \leq 5$ ) CEUS data showed this increase in high-frequency content, and less damping in the shallow crust (1 to 2 km) of the CEUS was considered the likely cause for the difference (Silva and Darragh, 1995). This difference was observed for the Saguenay earthquake as well as the **M** 6.4 1985 Nahanni aftershock earthquakes. However, the Saguenay earthquake also showed anomalously low intermediate-frequency (0.5 to 2 Hz) energy (Boore and Atkinson, 1992; Atkinson, 1993; Silva and Darragh, 1995). This observation along with others (Choy and Boatwright, 1988; Boatwright and Choy, 1992; Atkinson, 1993; Boatwright, 1994) has led to the speculation that CEUS source processes may possess differences from WUS source processes that result in stable and significant differences in intermediate frequency content for earthquakes with magnitude (**M**) greater than about 5 (Atkinson and Boore, 1995; 1998). Seismologically this spectral sag may be interpreted as the presence of second corner frequency or change in slope of the earthquake source spectrum (Boatwright, 1994; Atkinson and Boore, 1998). Interestingly, recent observations have suggested this may be the case for WUS earthquake source as well (Silva et al., 1997; Atkinson and Silva, 1997), but manifested in a much more subtle effect on response spectra due to differences in crustal conditions between WUS and CEUS. To illustrate the differences in WUS and CEUS rock site crustal conditions, Figure 9 shows generic velocity profiles for both regions. The differences in the

shallow (top 5 km) velocities is quite large resulting in large differences in amplification (Figure 10) as well as crustal damping (Table 2) (Silva and Darragh, 1995).

An example comparison of response spectra computed for **M** 6.5 at a distance of 25 km using both WUS and CEUS single and double corner frequency point-source models is shown in Figure 11 for shapes and Figure 12 for absolute spectral levels using parameters listed in Table 2. The two single corner frequency shapes for the WUS and CEUS (solid lines) show large differences over the entire frequency range. The WUS shape exceeds the CEUS for frequencies less than about 10 Hz where the shapes cross. The WUS shape peaks near 5 Hz while the CEUS shape has a maximum amplification in the 30 to 50 Hz frequency range.

Comparing the single and double corner frequency spectra for WUS and CEUS, Figure 11 shows the spectral sag significantly more pronounced for the CEUS. At low frequencies (below about 1 Hz) the double corner CEUS spectrum is about a factor of 3 lower than the single corner CEUS spectrum. Over the same frequency range, the difference between single and double corner shapes for the WUS is only about 10 to 20%.

Comparing the absolute levels, Figure 12 shows that at low frequencies, the single corner frequency model (solid lines) predicts similar motions for WUS and CEUS conditions. Peak accelerations for CEUS conditions are predicted to be larger than for WUS conditions, reversing the trends between spectral shapes (normalized by peak acceleration) and absolute spectral levels (Silva, 1991).

Though shifted in frequency, the differences between WUS and CEUS rock site shapes are not unlike the differences in the WUS statistical spectra between soft rock and deep soil shown in Figure 13. This is consistent with the explanation that CEUS spectral shapes are caused by the hard crustal conditions found there.

### 3.3.2 Comparison Of Model Shapes to WUS Statistical Shapes

To provide a qualitative evaluation of model performance, Figure 14 compares model shapes to WUS statistical shapes in the distance range of 10 to 50 km and for magnitudes near 5.5, 6.5, and 7.5. Model shapes for both single and double corner source spectra are shown illustrating the generally small difference between the alternative source models for WUS conditions. In general, the model shapes reflect the statistical shapes very well for the **M** 5.5 and **M** 6.5 bins and over-predict for the **M** 7.5 statistical shape.

The well developed spectral sag in the **M** 7.5  $R = 10$  to 50 km statistical shape bin is also not matched by the empirical attenuation equations (Figure 16c). Since this magnitude bin is sparsely populated (Table 1), the statistical shapes may be biased by sampling only a few earthquakes and rock sites. It is intriguing nonetheless that the statistical shapes for **M** greater than 7 at rock sites show evidence of a well-developed second corner frequency source spectrum. The developers of the empirical attenuation relations used here have chosen to ignore this observation, because of the few data on which it is based.

### 3.3.3 WUS to CEUS Transfer Functions

Using the point-source model, median spectral shapes were computed for single-corner WUS conditions and both double and single corner CEUS conditions using the parameters listed in Table 2. Ratios of the shapes, CEUS/WUS, for a dense grid in magnitude and distance were taken to provide transfer functions to apply to the weighted empirical shapes (Section 4.4). An example suite of the transfer functions is shown in Figure 15.

## **3.4 Development of Design Response Spectra**

### 3.4.1 Western US Spectral Shapes

The approach used to develop spectral shapes for rock site conditions appropriate for the WUS consisted of the following steps:

1. Use a number of empirical strong ground motion attenuation relationships to compute spectral amplification values, the ratio SA/PGA for the magnitude range ( $5 \leq \mathbf{M} \leq 8$ ) and fault distance range ( $0.1 \leq R^* \leq 200$  km) of interest.
2. Develop weights to apply to the relationships based on comparisons with a common set of recorded strong motion data.
3. Compute a weighted average of the empirical attenuation relationship spectral shapes for a dense grid of magnitude and distance pairs.
4. Develop a functional form to define spectral amplification over the magnitude and distance range of interest.

Five recently published empirical attenuation relationships were chosen to develop the spectral shapes for the WUS: Abrahamson and Silva (1997), Boore and others (1997), Campbell (1997), Idriss (1991), and Sadigh and others (1997). These relationships are henceforth referred to as A&S 97, Bao 97, C 97, I 91, and Sao 97, respectively. The spectral shapes predicted by these relationships are compared on Figure 16 to the statistical spectral shapes developed in Section 3.2. Note that the Bao 97 relationship is limited to  $5.5 \leq \mathbf{M} \leq 7.5$  and  $R \leq 80$  km and the C 97 relationship is limited to  $R \leq 60$  km. The selected attenuation relationships have 14 spectral frequencies in common: 0.2, 0.25, 0.333, 0.5, 0.667, 1.0, 2.0, 3.33, 5.0, 6.67, 10.0, 13.33, 20, and 34 Hz. (Note that C 97 does not contain 0.2 Hz and Bao does not contain 0.2, 0.25, and 0.333 Hz. Also, the Bao 97 spectral accelerations for frequencies between 10 and 40 Hz were calculated here by linear interpolation in log-log space as recommended by D. Boore [personal communication, 1998]. Spectral amplifications were computed for each attenuation relationship by dividing the predicted spectral acceleration at each frequency by the predicted peak ground acceleration.

---

\*For each empirical relation the appropriate distance definition is used.

### 3.4.2 Development of Weighted Empirical Spectral Shapes

The weights to be applied to the spectral shapes defined by the five empirical attenuation relationships were based on the relative ability of the relationships to predict the spectral shapes computed from the strong motion data base described in Section 3.2. To allow for the possibility that the relative prediction ability varies as a function of magnitude and distance, weights were computed for each of the 12 magnitude and distance bins defined in Section 3.2.

We defined the residual  $(\varepsilon(f)_{ij})_k$  to be the difference between the log of the spectral amplification for frequency  $f$  of the  $j^{\text{th}}$  recorded motion from the  $i^{\text{th}}$  earthquake,  $(SA(f)/PGA)_{ij}^r$  (the geometric mean of the two horizontal components) and the log of the spectral amplification predicted by the  $k^{\text{th}}$  attenuation relationship for magnitude  $\mathbf{M}_i$  and source-to-site distance  $R_{ij}$ .

$$(\varepsilon(f)_{ij})_k = \ln[(SA(f)_{ij})_{ij}^r] - \ln[(SA(f)_{ij})_{ij}^k] \quad (1)$$

These residuals are assumed to be normally distributed with a random effects variance structure (e.g. Brillinger and Preisler 1984, 1985; Youngs and others, 1995):

$$(\varepsilon(f)_{ij})_k = \varepsilon_1(f)_{ij} + \varepsilon_2(f)_{ij} \quad (2)$$

where  $\varepsilon_1(f)_{ij}$  and  $\varepsilon_2(f)_{ij}$  are independent, normal variates with variances  $\tau_1^2(f)$  and  $\tau_2^2(f)$ , respectively.

Two approaches were used to assign weights to the five attenuation relationships for each spectral frequency within each magnitude and distance bin. The first approach was based on the relative bias of the relationships. For each frequency in each  $\mathbf{M}$  and  $R$  bin, the mean residual for the  $k^{\text{th}}$  attenuation relationship,  $\mu(f)_k$ , is found by maximizing the generalized normal distribution likelihood function:

$$L(\mu(f)_k, \tau_1(f)_k, \tau_2(f)_k) = \frac{\exp\left[-\frac{[(\varepsilon(f)_{ij})_k - \mu(f)_k]^T V(f)_k^{-1} [(\varepsilon(f)_{ij})_k - \mu(f)_k]}{2}\right]}{2\pi |V(f)_k|^{1/2}} \quad (3)$$

where  $V(f)_k$  is the block-diagonal variance matrix of  $(\varepsilon(f)_{ij})_k - \mu(f)_k$ . Figure 17 shows the mean residuals and their 90% confidence intervals for the five attenuation relationships and 12 magnitude-distance bins.

The  $t$  statistic,  $t_k = |\mu(f)_k|/\sigma[\mu(f)_k]$ , together with the cumulative  $T$  distribution can be used to compute the probability a sample of size  $n$  from a population with zero mean would have a mean residual as large as  $|\mu(f)_k|$ ,  $P(T \leq t_k | n-1)$ . If one considers that the relationships with the higher probability of

producing the computed  $t$  statistic should be given higher weight, then the relative weight for the  $k^{\text{th}}$  attenuation relationship,  $W(f)_k^T$  can be defined as:

$$W(f)_k^T = \frac{P(T \leq t(f)_k | n-1)}{\sum P(T \leq t(f)_k | n-1)} \quad (4)$$

These are referred to as "T" weights.

The second weighting approach uses relative likelihoods under the assumption that the mean residual is zero. The likelihood function is given by:

$$L(\mu(f)_k=0, \tau_1(f)_k, \tau_2(f)_k) = \frac{\exp\left[-\frac{[(\mathcal{E}(f)_{ij})_k^T V(f)_k^{-1} (\mathcal{E}(f)_{ij})_k]}{2}\right]}{2\pi |V(f)_k|^{1/2}} \quad (5)$$

where  $V(f)_k$  is the block-diagonal variance matrix of  $(\mathcal{E}(f)_{ij})_k$ . Equation (5) gives the probability of observing the sample set of residuals, given that the mean residual is zero. If one considers that the relationships with the higher likelihood should be given higher weight, then the relative weight for the  $k^{\text{th}}$  attenuation relationship,  $W(f)_k^L$  can be defined as:

$$W(f)_k^L = \frac{L(f)_k}{\sum_k L(f)_k} \quad (6)$$

These are referred to as "L" weights.

The top plots in the two columns of Figure 18 show examples of the "T" and "L" weights for one of the 12 magnitude-distance bins. The weights display a highly irregular pattern, reflecting the variability in the mean residuals shown on Figure 17. The approach to developing the response spectral shapes outlined in Section 3.1 is based on the use of the empirical attenuation relationships to provide smoothly varying estimates of response spectral shapes over a magnitude and distance range that extends beyond the bulk of the recorded data. The use of the highly variable weights shown at the top of Figure 18, while providing a close match to the recorded data set, would rapidly switch from strongly favoring one attenuation relationship to favoring another over short frequency intervals, and thus tend to defeat the purpose of using the smooth empirical attenuation relationship spectra. In addition, limitations in the band-width of the processed data for the smaller recordings results in no weight estimates for some frequencies. These two issues were addressed by smoothing the weights across frequency with a Gaussian smoothing operator. The smoothed weights are defined by:

$$W(f_i)_k^* = \frac{\sum_{j=1}^J W(f_j)_k \cdot \exp(-\ln(f_j/f_i)^2/h^2)}{\sum_{j=1}^J \exp(-\ln(f_j/f_i)^2/h^2)} \quad (7)$$

where  $f_j, j = 1$  to  $J$  are the 14 common spectral frequencies defined above and  $h$  determines the width of the smoothing operator. Larger values of  $h$  produce greater smoothing. The remaining plots on Figure 18 show smoothed weights for values of  $h$  of 0.25, 0.5, and 1.0.

Figure 19 shows examples of the weighted average empirical spectral shapes computed for the average magnitude and distance of two of the magnitude-distance bins using smoothed "L" and "T" weights. As indicated on the plot, variations in  $h$  have a very minor effect on the computed spectral shapes. Also, the "L" and "T" weights produce very similar spectral shapes. Therefore, the smoothed "L" and "T" weights were averaged to produce the final set of weights. A smoothing parameter of  $h = 1.0$  was chosen for the final weights to produce a smoothly varying final set of weights. These are shown on Figure 20. Figure 21 shows examples of the weighted empirical response spectral shapes for magnitude of **M** 5 to 8 and distances of 1 to 200 km.

### 3.4.3 Magnitude and Distance Dependencies of Weighted Empirical Spectral Shapes

The response spectral shapes shown on Figure 21 vary with magnitude and distance. In order to provide relationships for specifying a response spectral shape for any magnitude and distance within the specified range of the attenuation relationships, a function form was fit to the weighted empirical spectral shapes. Figure 22 shows the statistical spectra for magnitude **M** 6 to 7 and  $R$  10 to 50 km data. This spectral shape can be closely matched by the ad hoc relationship:

$$\ln[SA(f)/PGA] = \frac{C_1}{\cosh(C_2 f^{C_3})} + C_4 \left[ \frac{\exp(C_5 f)}{f^{C_6}} \right] \quad (8)$$

The form of Equation (8) is not based on a physical model, but is rather designed to fit the general characteristics of the spectral shapes. The first term fits the high frequency portion of the spectrum, decreasing exponentially to zero with increasing frequency. The second term models the low frequency portion of the spectrum. The factor  $\exp(C_5 f)$  controls the transition of control from the low frequency to high frequency terms.

Coefficients  $C_1$  through  $C_6$  were defined as functions of magnitude and/or distance by creating a data set of 651 response spectral shapes (31 magnitudes times 21 distances) at 0.1 magnitude units from **M**5 to **M**8 and at fault distances ( $R$ ) of 0.1, 1, 2, 3, 5, 10, 12, 15, 20, 25, 30, 40, 50, 60, 70, 85, 100, 125, 150, 175, and 200 km. Each response spectral shape contained spectral amplifications at the 14 frequencies common to the five empirical attenuation relationships. In addition, fitting time histories to the response spectral shapes requires specification of the spectral amplifications in the frequency range of 0.1 to 100 Hz. The solid diamonds shown on Figure 22 indicate the spectral amplifications predicted by an extrapolation of Equation (8), which was fit to the frequency range of 0.2 to 34 Hz. As indicated, the functional form provides a good fit in the extrapolated range both for  $f > 34$  Hz and

$f < 0.2$  Hz. The poorest fit is at 0.1 Hz, where the statistical spectra are becoming somewhat biased due to the exclusion of records with limited band-widths. The 651 weighted empirical spectral shapes were extended from the frequency range of 0.2 to 34 Hz to the frequency range of 0.1 to 100 Hz by fitting Equation (8) to each spectral shape and then using the parameters of that fit to predict spectral amplifications in the frequency range of 0.1 to 0.2 Hz and 34 to 100 Hz.

The entire extended data set was then used to obtain expressions for coefficients  $C_1$  through  $C_6$  by nonlinear least squares. The best fit was found by the parameter set listed in Table 3. Figure 23 shows examples of the response spectral shapes predicted using these relationships.

#### 3.4.4 Model for Central and Eastern US Spectral Shapes

The approach used to develop spectral shapes for rock site conditions appropriate for the CEUS consisted of the following steps:

1. Use numerical modeling to develop scaling relationships between CEUS and WUS response spectral shapes.
2. Use the scaling relationships from step 1 to convert the weighted empirical WUS spectral shapes to CEUS spectral shapes.
3. Develop a functional form to define spectral amplification over the magnitude and distance range of interest.

##### 3.4.4.1 Scaling of WUS Weighted Empirical Spectral Shapes to CEUS Conditions

The scaling relationships for transferring WUS spectral shapes to CEUS spectral shapes are described in Section 3.3 and are shown on Figure 15. These scaling relationships were used to scale the extended (0.1 to 100 Hz) weighted empirical WUS response spectral shapes to produce CEUS spectral shapes. As discussed in Section 3.3, two sets of scaling relationships were defined, one based on single corner frequency CEUS earthquake source spectra and one based on double corner frequency CEUS earthquake source spectra. Both scaling relationships assume a single corner frequency WUS earthquake source spectra. Figure 24 shows examples of the CEUS response spectral shapes scaled from the weighted empirical WUS spectral shapes using the scaling relationships shown on Figure 15.

One problem that was encountered was an inconsistency or flat portion in CEUS spectral shapes around 10 Hz. Close comparison of the model and attenuation-based WUS spectral shapes indicated that the model shapes showed slightly higher spectral amplifications than the attenuation-based spectra around 10 Hz. This over-prediction or bias of WUS model spectral shapes caused an under-prediction of the CEUS/ WUS transfer function. As a result, the transfer function was slightly increased around 10 Hz. Figure 25 shows examples of the scaled (before adjustment) and adjusted spectral amplifications, for both the single- and double-corner CEUS spectral models.

##### 3.4.4.2 Modeling the Effect of Magnitude and Distance on CEUS Spectral Shapes

Using the same approach as for WUS response spectral shapes, a functional form was fit to the scaled and adjusted empirical spectral shapes. A modified form of Equation (8) was used to model the CEUS shapes. The relationship is:

$$\ln[SA(f)/PGA] = \frac{C_1}{\cosh(C_2 f^{C_3})} + C_4 \left[ \frac{\exp(C_5 f)}{f^{C_6}} + \frac{C_7 \exp(C_8 f)}{f^{C_9}} \right]^{1/2} \quad (9)$$

A second term was added to the low-frequency portion of the model to provide more flexibility in the shape. Coefficients  $C_1$  through  $C_9$  were defined as functions of magnitude and/or distance using the data set of 651 CEUS response spectral shapes (31 magnitude values times 21 distances) by nonlinear least squares with the spectral amplifications in the frequency range of the adjustment down weighted to reduce their influence on the fitted parameters.

For the single and double corner frequency CEUS earthquake spectra, the resulting coefficients are listed in Table 3. Figures 26 and 27 shows examples of the response spectral shapes predicted using these relationships.

### 3.5 Comparison of Recommended Shapes to Current Regulatory Guidance

In this section we compare Newmark and Hall (1978) and Regulatory Guide 1.60 (1973) design spectra to both WUS and CEUS recommended design spectra for the most populated distance bin (0 to 50 km) and mean magnitudes of  $M$  5.6,  $M$  6.4, and  $M$  7.3 (Table 1). Figure 28 shows comparisons to WUS recommended shapes and Figure 29 shows analogous comparisons to CEUS shapes. For Newmark and Hall design shapes, WUS bin median values for peak accelerations, velocities, and displacements are used for both WUS and CEUS conditions. Both median and 1-sigma amplification factors are used for the Newmark and Hall design spectra.

For the WUS motions, Figure 28 shows a reasonably good comparison between the Newmark and Hall spectra and the recommended shapes. The empirical PGV/PGA ratio is about 60 cm/sec/g for  $M$  6.3 and 7.3. Increasing this ratio to the value recommended by Newmark and Hall (1978) of about 90 cm/sec/g would increase the low frequency levels but result in peak velocities not supported by the data. The dependence of the Newmark and Hall design shapes on peak parameters captures some of the effects of the empirical magnitude dependency and would presumably capture elements of the distance dependency as well. Conversely, the fixed R.G. 1.60 shape is quite conservative even for  $M$  7.3, since it was based on  $M \approx 6.7$ , used a mixture of rock and soil data, and was derived with 1-sigma amplification factors (Figure 28).

For the CEUS, Figure 29 shows a similar suite of plots but with recommended shapes for both the single- and double-corner CEUS source models. The Newmark-Hall design shapes use the WUS bin parameters because comparable empirical CEUS data are not available. The expected peak accelerations for CEUS rock motions are larger than corresponding WUS rock motions, so the CEUS shapes (SA/PGA) appear to be lower than WUS shapes at low frequencies. In absolute levels

however, single corner WUS and CEUS spectra have comparable spectral levels for frequencies below about 3 Hz (see Figure 12). Normalizing at a frequency around 1 to 5 Hz would be more indicative of absolute levels and would result in similar comparisons with WUS shapes (Figure 28) at frequencies  $\leq 5$  Hz while showing a larger difference between the R.G. 1.60 and recommended shapes at high frequencies (as illustrated in Figure 12).

### **3.6 Effects of Source Mechanism and Near-Fault Conditions on Response Spectral Shapes**

Since both the WUS and CEUS shapes are intended to reflect an average horizontal component for a random source mechanism located at a fixed rupture distance (but at a random azimuth with respect to a rupture surface), it is important to assess the effects implied by these limitations. Both source mechanism (reverse, oblique, strike-slip, normal) as well as hanging-wall vs. foot-wall site location for dipping faults have frequency-dependent effects (Abrahamson and Shedlock, 1997). Additionally, for potential sites located in the NW Pacific region of WUS, the tectonic environment may include the contribution of large ( $M \geq 9$ ) subduction zone earthquakes. Such sources may dominate the low frequency portion of the UHS requiring appropriate shapes for scaling.

For large magnitude ( $M \geq 6.5$ ) earthquakes, rupture directivity affects both low frequency spectral levels ( $\leq 1$  Hz) and time domain characteristics. Rupture towards a site enhances average spectral levels and reduces durations, while rupture away from a site reduces motions and increases durations, all of these changes are relative to average conditions (Somerville et al., 1997; Boatwright and Seekins, 1997). Differences in fault normal and fault parallel motions are also affected by rupture directivity and can be large at low frequencies (Somerville et al., 1997). Design decisions on whether to incorporate component differences in spectral levels and time domain characteristics should be made on a site-specific basis with consideration of uncertainties and the implications for analyses. Fault normal and fault parallel motions may not define principal directions for design purposes and these implications must be considered in two-dimensional analyses.

These source mechanism and near-fault issues become relevant when a high degree of certainty exists in the nature of the controlling sources as well as the source-site geometry. In calculating the hazard levels for a site, it is assumed that the appropriate degree of seismotectonic knowledge as well as epistemic uncertainty is incorporated in the attenuation relations used in the probabilistic hazard analysis. The UHS levels will then reflect appropriate contributions of source mechanism and site location. The recommended spectral shapes developed here, which are appropriate for average conditions, are scaled to the UHS at selected frequencies and do not reflect either conservatism or unconservatism in the frequency dependence of spectral levels based on source mechanism and site location.

#### **3.6.1 Effects of Source Mechanism**

Assessment of the effects of source mechanism, which is taken to include hanging wall vs. foot wall effects, relies on WUS empirical motions and is strictly appropriate for those conditions. Of the five empirical attenuation relations considered in the development of the WUS shapes (Section 3.4.1), two include frequency-dependent source mechanism effects (Abrahamson and Silva, 1997; Boore et al., 1997) and only one includes frequency-dependent hanging wall vs. foot wall effects

(Abrahamson & Silva, 1997). To illustrate possible source mechanism effects on the revised WUS shapes, Figure 30 shows spectral shapes computed for the two relations for  $M$  5.5 and  $M$  6.5 earthquakes at a distance of 25 km. When normalizing by peak acceleration, the maximum effect of source mechanism is at low frequency (0.2 Hz) and shows a maximum expected range of about 50%.

The shape for the strike-slip mechanism, the base case for the recommended shapes, is highest for frequencies below about 1 Hz, while normal faulting shapes are expected to be slightly higher than strike-slip shapes for frequencies in the range of about 1 to 5 Hz. Since the normal faulting shape exceeds the strike-slip shape by less than 10%, use of the recommended shapes for normal faulting conditions is not considered to significantly underestimate design motions.

However, for large magnitude ( $M \geq 6.4$ ) earthquakes occurring on reverse faults, Figure 30 shows that the expected shape is lower than the strike-slip shape by about 10% in the 1 to 2 Hz frequency range. Scaling the reverse mechanism shape to a UHS in the 1 to 2 Hz range could then result in larger predicted motions for frequencies above the scaling frequency than scaling the recommended spectral shape. For sites controlled by reverse mechanism sources, care should be taken in evaluating the development of the low frequency design motions for frequencies in the range of the low frequency UHS scaling frequency (1.0 to 2.5 Hz, R.G. 1.165).

To examine the expected effects of site location for dipping faults, Figure 31 compares shapes computed for strike-slip mechanism to shapes computed for a dipping fault for both hanging-wall and foot-wall site locations. These site dependencies are strongest in the fault distance range of 8 to 18 km and are based on Somerville and Abrahamson (1995) and included in the Abrahamson and Silva, (1997) relationship. The Boore et al., (1997) relation includes an  $M$ ,  $R$ , and frequency-independent hanging wall vs. foot wall effect implicitly in its distance definition. As a result their shapes are largely site location (hanging wall vs. foot wall) independent.

The hanging-wall vs. foot-wall frequency dependencies illustrated in Figure 31 are actually strongest for large magnitude ( $M \geq 6.5$ ) and at high frequency (PGA) and represent a maximum factor of about 1.4 for the horizontal component and about 1.9 for the vertical component (ratio of hanging-wall to “not-hanging-wall” PGA values). Since the hanging-wall shape is lower than the strike-slip shape (the basis mechanism for the recommended spectral shapes) by about 10% in the 1 to 2 Hz frequency range, scaling the hanging-wall shape instead of the strike-slip shape to the UHS in the 1 to 2 Hz frequency range will result in higher spectral levels for frequencies above the scaling frequency. Modifications to the recommended spectral shapes should be made on a site-specific basis, using all relevant records applicable to the site and the fault generating the hazard.

### 3.6.2 Subduction Zone Spectral Shapes

The possible occurrence of Cascadia subduction zone earthquakes with magnitudes up to  $M$  9 can be significant contributors to the low frequency UHS for sites located in the Pacific Northwest (including Northern California), particularly near the Pacific coast. As a result, comparisons of empirical (Youngs et al., 1997)  $M$  9.0 shapes at a suite of distances were made to the recommended shape for  $M$  8.0 (the largest magnitude for which the empirical WUS relations are considered valid).

The recommended shape is computed for a distance of 25 km since the dependence on distance is small within about 50 km. The comparisons are shown in Figure 32. Interestingly, for the same

peak accelerations, the crustal earthquakes for **M** 8.0 are expected to have larger low frequency ( $\leq 2$  Hz) motions than **M** 9.0 subduction zone earthquakes. The maximum difference in the 1 to 2 Hz range is about 10% and would be larger for smaller magnitude Cascadia sources. As with the source mechanism comparisons, if large magnitude (**M** > 8) subduction zone earthquakes contribute substantially to the low frequency hazard, appropriate spectral shapes should be developed on a site-specific basis.

### 3.7 Vertical Motions

Current regulatory guidance for vertical (V) ground motions specifies spectral levels that are equal to the horizontal (H) at frequencies > 3.5 Hz and that are 2/3 the horizontal for frequencies < 0.25 Hz, with the ratio varying between 1 and 2/3 between 3.5 Hz and 0.25 Hz (R.G. 1.60). As with the horizontal spectral shape, the implied V/H ratio is independent of magnitude, distance, and site condition and is shown in Figure 33. For the Newmark-Hall design motions, the V/H ratio is taken as independent of frequency as well as magnitude, distance, and site condition, having a constant value of 2/3 (Figure 33). With the dramatic increase in strong motion data since the development of these design specifications in the 1970's, the conclusion that the vertical and average horizontal ground motions vary in stable and predictable ways with magnitude, distance, and site condition has become increasingly compelling. In general, vertical motions exceed horizontal (average of both component) motions at high frequency and at close fault distances (within about 10 to 15 km). The amount and frequency range of the exceedence depends on magnitude, distance, and site conditions. For different site conditions, time domain characteristics of vertical motions can be quite different at close distances and may be a consideration in selecting input motions for spectral matching or scaling procedures. A recent workshop proceedings (Silva, 1997) illustrates the expected differences in vertical and horizontal motions based on magnitude, distance, and site conditions and forms a background for the procedures recommended to develop vertical component spectra that are consistent with the WUS and CEUS revised rock horizontal component shapes.

Because structures, systems, and components have limited capacities for dynamic vertical demands, it is important to accommodate stable and predictable differences in vertical loads based on significant contributors (**M** and **R**) to the seismic hazard at a site. Since there are fewer attenuation relations for vertical motions in the WUS and currently none available for the CEUS, the general approach to developing vertical component design spectra is to use a frequency-dependent V/H ratio. It is difficult to capture the appropriate degree of uncertainty in the V/H ratio as well as the corresponding hazard level of the vertical component design spectrum after scaling the horizontal UHS spectrum by the V/H ratio. Thus, the usual assumption is that the derived vertical motions reflect a hazard level consistent with the horizontal UHS. To maintain consistency with the horizontal median shapes developed earlier in this Section, median V/H ratios are developed.

#### 3.7.1 V/H Ratios for WUS Rock Site Conditions

Of the five empirical WUS attenuation relations used in developing the horizontal spectral shapes (Section 3.4.1), three include vertical motions: Abrahamson and Silva, 1997; Campbell, 1997; and Sadigh et al., 1997 (verticals from Sadigh et al., 1993). To develop V/H ratios for WUS rock site conditions, median V/median H ratios for strike-slip mechanisms were produced for each relation

and averaged assuming equal weights. The resulting V/H dependencies on magnitude and distance are illustrated in Figures 34 and 35. Figure 34 shows expected ratios for **M** 5.5, **M** 6.5, and **M** 7.5 earthquakes for a suite of distances ranging from 1 to 50 km. The ratios are magnitude-dependent, decreasing with decreasing magnitude and with the sensitivity to magnitude decreasing with increasing distance.

These effects are likely driven by the differences in magnitude scaling (change in spectral levels with magnitude) between the horizontal and vertical components. The dependence of the V/H ratios on magnitude decreases with distance (Figure 34) as the difference in magnitude scaling between the vertical and horizontal components decreases.

The effects of source mechanism on the V/H ratios (included only in the Abrahamson and Silva, 1997 relation) is small, with strike slip ratios generally exceeding the ratios for oblique, reverse, and normal faulting mechanisms. For hanging wall sites and for fault distances in the 4 to 24 km range, V/H ratios are higher at high frequencies by a maximum of about 30% for **M** greater than about 6 (Abrahamson and Somerville, 1996; Abrahamson and Silva, 1997). These effects should be considered in developing vertical component spectra for both WUS and CEUS sites, when the geometry of a site with respect to a dominant fault is known.

Figure 35 illustrates the distance dependencies for each magnitude, showing a stronger distance effect with increasing magnitude. The peaks in the V/H ratios near 15 Hz are stable with magnitude and distance, and are controlled by the frequency of maximum spectral amplification for the vertical motions. The slight troughs in the ratios in the 1-3 Hz frequency range vary with magnitude (see Figure 34) and are controlled by the peaks (maximum spectral amplifications) in the horizontal component spectra. These features, as well as the differences in magnitude scaling between horizontal and vertical spectra, are illustrated in Figures 36 and 37. These figures show expected median spectra (5% damped) for horizontal and vertical components from the Abrahamson and Silva (1997) empirical relations for a suite of magnitudes. For the horizontal component spectra, Figure 36 shows the strong shift in peak values with increasing magnitude while the vertical spectra (Figure 37) show peaks at a constant frequency in the 10-20 Hz range.

The location of peaks in V/H ratios results from peaks in the vertical spectra and are likely controlled by the shallow crustal amplification (Figure 9) and damping (Table 2). As a result, these peaks are expected to occur at a higher frequency for CEUS hard rock conditions, which have lower damping values (Silva, 1997). Additionally, for WUS empirical relations, smaller V/H ratios occur at low frequency ( $\leq 2$  Hz) with soil sites (Silva, 1999) where the effects of nonlinearity in the horizontal component is small. This suggests that for linear response conditions, the V/H ratio increases with profile stiffness. As a result, V/H ratios for hard rock conditions in the CEUS would be expected to be somewhat higher overall than WUS soft rock conditions.

These trends suggest that magnitude and distance dependencies may be largely captured by the expected peak acceleration of the horizontal motions, with larger V/H ratios associated with higher expected horizontal peak accelerations. The trends in Figures 34 and 35 clearly show V/H ratios exceeding unity at high frequencies for distances out to about 20 km for **M** 7.5 earthquakes. The average expected horizontal peak acceleration for **M** 7.5 at 20 km is about 0.3g suggesting that the

current R.G. 1.60 ratio may be appropriate for conditions where the design peak accelerations are less than about 0.3g. The conventional assumption of vertical spectra taken as a constant 2/3 the horizontal is unconservative in the 10 to 30 Hz frequency range even out to 50 km.

To provide for a reasonable accommodation of magnitude and distance dependency in the revised vertical motions for WUS rock site conditions, Figure 38 shows recommended V/H ratios for ranges of expected horizontal peak accelerations. These ratios are simply the averages of the empirical relations. The values are listed in Table 4. The ranges in horizontal peak accelerations are intended to capture important **M** and **R** dependencies, maintain reasonable conservatism, and result in a procedure that is simple to implement. Direct multiplication of the revised horizontal shapes by these smooth V/H ratios is intended to result in smooth vertical spectra appropriate for design and analyses.

### 3.7.2 V/H Ratios For CEUS Rock Site Conditions

For applications to CEUS hard rock site conditions, the only empirical V/H ratios available are for small magnitude ( $M \leq 5$ ) earthquakes recorded at distances beyond about 20 km at hard rock sites (Atkinson, 1993). This empirical ratio, computed using Fourier amplitude spectra, is defined only from 1 Hz to 10 Hz and decreases from a value of 0.9 at 1 Hz to 0.7 at 10 Hz. The ratio is independent of distance and is based on recordings at sites in the distance range of about 20 to 1,000 km. This trend of decreasing V/H ratio in the 1 to 10 Hz frequency range, although weak, is opposite to the trend shown in the WUS V/H ratios. This difference may reflect differences in Fourier amplitude and response spectra but the average value of about 0.8 suggests higher V/H ratios at large distance for CEUS rock sites than WUS rock sites. For linear response conditions, this trend is consistent with increasing V/H ratios as profile stiffness increases. This results from less shear-wave (SV) energy being converted from the vertical component to the horizontal component due to wave refraction, for stiffer profiles.

A few V/H ratios are available from recordings at CEUS rock sites (and other intraplate sites) for earthquakes with magnitudes greater than **M** 5. Figure 39 shows results from the **M** 5.9 Saguenay and **M** 6.8 Nahanni and Gazli earthquakes. For the Saguenay earthquake, the V/H ratio varies between about 0.7 and 1 suggesting a higher ratio in the CEUS than the WUS at large distances (average distance is 111 km). While the ratio was computed from a large number of sites, it is still a single earthquake that is both deep, with a hypocentral depth of about 30 km, and considered anomalous in its high frequency spectral levels (Boore and Atkinson, 1992). For the larger magnitude data (Gazli and Nahanni earthquakes) only three sites are available for V/H ratios. Sites Karakyr and S1, for the Gazli and Nahanni earthquakes respectively, are located very close to the rupture surfaces at an average distance of about 4.5 km. Site Karakyr is not considered a hard rock site, having about 1.4 km of sedimentary rock (with some clays) overlying a hard schist basement rock (Hartzell, 1980). This geology, with an estimated kappa value of 0.015 sec, may be considered a CEUS soft rock site (Silva and Darragh, 1995). The V/H ratio for the most distant Nahanni site at 16 km (S3, Figure 39), shows ratios consistent with those of the Saguenay earthquake, ranging from about 0.6 to about 1 for frequencies above 1 Hz. Interestingly, for frequencies  $\leq 0.6$  Hz, the V/H ratio is near 2. These V/H ratios from Nahanni are for only a single earthquake, as with Saguenay,

and at only a single site but they do suggest the possibility of higher ratios for CEUS sites as well as a high degree of uncertainty in the ratios.

For the near source V/H ratios (distance of 4.5 km), Figure 39 shows ratios near unity up to about 5 Hz and values near 2 for frequencies above 10 Hz. These trends are consistent at the two sites for the two earthquakes. Both sites (Karakyr and S1) have vertical peak accelerations exceeding 1g (1.3g for Gazli and 2.1g for Nahanni), about double the average horizontal peak accelerations. These results, reflecting few data for poorly understood earthquakes and largely unknown site conditions, indicate that very large V/H ratios may be likely at very close rupture distances to CEUS earthquakes. Larger than average high frequency ( $\geq 3$  Hz) ratios likely result from both S1 and Karakyr being located on the hanging wall of the fault. As with the more distant Nahanni site, S3, these results suggest higher V/H ratios for CEUS rock sites than WUS sites and show that ratios at near-fault sites can be quite large at high frequencies.

To develop recommended V/H values for applications to CEUS rock sites, the simple point source model (Section 3.3) was extended to consider P-SV waves and was used to estimate vertical component spectra (EPRI, 1993; Silva, 1997). The model predicts the general trends in the WUS V/H ratios and has been validated at rock sites that recorded the 1989 **M** 6.9 Loma Prieta earthquake (EPRI, 1993). As a result, V/H ratios computed for the generic CEUS rock site conditions (Figure 9) may be used with reasonable confidence to develop guidelines. The V/H ratios predicted by the model for CEUS conditions are illustrated in Figure 40. The low frequency peaks (1 to 30 Hz) result from resonances associated with compressional- and shear-wave velocity profiles and would be smoothed out if the velocities were randomized. The peak in the ratios near 60 Hz is associated with the vertical spectra and corresponds to the peak in the WUS ratios (Figures 37 and 38) but shifted from about 15 to 20 Hz to about 60 Hz because of the lower kappa values for the hard rock CEUS vertical motions ( $\kappa = 0.003$  sec; Silva, 1997). The magnitude dependencies in the CEUS ratios are smaller than for the WUS probably because the WUS model currently does not include magnitude saturation, apart from a stress drop that decreases with increasing magnitude (Atkinson and Silva, 1997). Since this stress drop scaling affects both vertical and horizontal components equally, the simple model does not show the same trends as the empirical V/H ratios (Figure 34). However, the model does show higher ratios at low frequencies ( $< 3$  Hz) than the WUS ratios, consistent with available observations. Based on the trends shown in the model predictions as well as the CEUS recordings, a reasonable approach to defining recommended ratios is to shift the WUS ratios to higher frequencies, so that the peaks correspond to about 60 Hz. Also the low frequency WUS levels should be scaled up by about 50% (factor of 1.5), a proportion reflected in comparing the CEUS and WUS model estimates of the V/H ratios (Silva, 1997). The recommended ratios are shown in Figure 41 and are listed in Table 5. Maintaining the same peak acceleration ranges in the horizontal component for the CEUS V/H ratios adds conservatism necessitated by the large uncertainties. For cases where the site is located on the hanging wall of a dipping fault within a rupture distance of about 20 km, the V/H ratio could be significantly larger ( $\approx 30\%$ ) for large magnitude earthquakes, warranting appropriate site-specific studies.

To illustrate the vertical spectra resulting from the process of scaling the horizontal spectra, Figure 42 shows WUS vertical motions while Figures 43 and 44 show corresponding CEUS vertical motions. Both WUS and CEUS verticals are based on the **M** 6.4 bin shapes shown in Figures 28 and

29 and reflect vertical motions relative to 1g horizontal motions. For the WUS verticals, the vertical peak acceleration exceeds the horizontal for horizontal peak accelerations exceeding 0.5g. For peak horizontal accelerations in the 0.2 to 0.5g range, the vertical spectra exceed the horizontal spectra in the frequency range of about 10 to 30 Hz, but the vertical peak accelerations are lower than the horizontal. At low frequency, below about 3 Hz, the verticals spectra are about one half the horizontal. For the CEUS verticals shown in Figures 43 and 44, both the single and double corner vertical spectra show trends relative to the horizontals that are similar to the WUS but shifted to higher frequencies, as expected.

In general, both WUS and CEUS V/H ratios provide smooth and reasonable vertical motions when applied to the recommended spectral shapes for horizontal components.

### **3.8 ACKNOWLEDGMENTS.**

Support for this ongoing work was provided by Nuclear Regulatory Commission under the direction of Roger Kenneally. Careful reviews by Dave Boore, Niles Chokski, Allin Cornell, Robert Rothman, Robert Kennedy, Carl Stepp, Roger Kenneally, Buck Ibrahim, and Robert Darragh contributed substantially to the quality of the work and are gratefully acknowledged.

### 3.9 REFERENCES

- Abrahamson, N.A. and W.J. Silva (1997). "Empirical response spectral attenuation relations for shallow crustal earthquakes." *Seism. Res. Lett.*, 68(1), 94-127.
- Abrahamson, N.A. and K.M. Shedlock (1997). "Overview." *Seism. Research Lett.*, 68(1), 9-23.
- Abrahamson, N.A. and P.G. Somerville (1996). "Effects of hanging wall and foot wall on ground motions and recorded during the Northridge earthquake." *Bull. Seism. Soc. Am.* 86(1B), S93-S99.
- Abrahamson, N.A., P.G. Somerville, C.A. Cornell (1990). "Uncertainty in numerical strong motion predictions" *Proc. Fourth U.S. Nat. Conf. Earth. Engin.*, Palm Springs, CA., 1, 407-416.
- Atkinson, G.M. and D.M. Boore (1998). "Evaluation of models for earthquake source spectra in Eastern North America." *Bull. Seism. Soc. Am.* 88(4), 917-934.
- Atkinson, G.M. and D.M. Boore (1995). "Ground motion relations for eastern North America." *Bull. Seism. Soc. Am.*, 85(1), 17-30.
- Atkinson, G.M. and W.J. Silva (1997). "An empirical study of earthquake source spectra for California earthquakes." *Bull. Seism. Soc. Am.* 87(1), 97-113.
- Atkinson, G.M. (1993). "Source spectra for earthquakes in eastern North America." *Bull. Seism. Soc. Am.*, 83(6), 1778-1798.
- Boatwright, J. (1994). "Regional propagation characteristics and source parameters of earthquakes in Northeastern North America." *Bull. Seism. Soc. Am.*, 84(1), 1-15.
- Boatwright, J. and G. Choy (1992). "Acceleration source spectra anticipated for large earthquakes in Northeastern North America." *Bull. Seism. Soc. Am.*, 82(2), 660-682.
- Boatwright, J. and L. Seekins (1997). "Response spectra from the 1989 Loma Prieta, California, earthquake regressed for site amplification, attenuation, and directivity." USGS Open-File Report 97-858.
- Boore, D.M., W.B. Joyner and T.E. Fumal (1997). "Equations for estimating horizontal response spectra and peak acceleration from Western North American earthquakes: A summary of recent work." *Seism. Res. Lett.* 68(1), 128-153.
- Boore, D.M., and G.M. Atkinson (1992). "Source spectra for the 1988 Saguenay, Quebec, earthquakes." *Bull. Seism. Soc. Am.*, 82(2), 683-719.
- Boore, D.M. (1986). "The effect of finite bandwidth on seismic scaling relationships." in *Earthquake*

- Source Mechanics, Maurice Ewing Ser.*, S.Das, ed., Amer. Geophys. Union, Wash. D.C. vol.6.
- Boore, D.M. (1983). "Stochastic simulation of high-frequency ground motions based on seismological models of the radiated spectra." *Bull. Seism. Soc. Am.*, 73(6), 1865-1894.
- Brillinger, D.R. and H.K. Preisler (1985). Further analysis of the Joyner-Boore attenuation data, *Bull. Seism. Soc. Am.*, 75, 611-614.
- Brillinger, D.R. and H.K. Preisler (1984). An exploratory analysis of the Joyner-Boore attenuation data, *Bull. Seism. Soc. Am.*, 74, 1441-1450.
- Campbell, K.W. (1997). "Empirical near-source attenuation relationships for horizontal and vertical components of peak ground acceleration, peak ground velocity, and pseudo-absolute acceleration response spectra." *Seism. Res. Lett.*, 68(1), 154-176.
- Campbell, K. W. (1993) "Empirical prediction of near-source ground motion from large earthquakes." in V.K. Gaur, ed., *Proceedings, Intern'l Workshop on Earthquake Hazard and Large Dams in the Himalya*. INTACH, New Delhi, p. 93-103.
- Choy, G.L. and J. Boatwright (1988). "Teleseismic and near-field analysis of the Nahanni earthquakes in the Northwest Territories, Canada." *Bull. Seism. Soc. Am.*, 78(5), 1627-1652.
- EPRI (1993). "Guidelines for determining design basis ground motions." Palo Alto, Calif.: Electric Power Research Institute, vol. 1-5, EPRI TR-102293.
- Hanks, T.C. and McGuire, R.K. (1981). "The character of high-frequency strong ground motion." *Bull. Seism. Soc. Am.*, 71(6), 2071-2095.
- Hartzell, S. (1980). "Faulting Process of the May 17, 1976, Gazli, USSR Earthquake." *Bull. Seism. Soc. Am.*, 70(5), 1715-1736.
- Idriss, I.M. (1991). "Earthquake ground motions at soft soil sites." *Proceedings: 2nd Int'l Confer. on Recent Advances in Geotechnical Earthquake Engineering and Soil Dynamics*, Saint Louis, Missouri, Invited Paper LP01, 2265-2272.
- Kimball, J.K. (1983). "The use of site dependent spectra." *Proc. Workshop on Site-Specific Effects of Soil and Rock on Ground Motion and the Importance for Earthquake-Resistant Design*, Santa Fe, New Mexico, USGS Open-File Rept. 83-845, 410-422.
- Mohraz, B., W.J. Hall and N.M. Newmark (1972). "A study of vertical and horizontal earthquake spectra." Nathan M. Newmark Consulting Engineering Services, Urbana, Illinois: *AEC Report No. WASH-1255*.

- Newmark, N.M. and W.J. Hall (1978). "Development of criteria for seismic review of selected nuclear power plants." US Nuc. Reg. Comm., NUREG/CR-0098, May.
- Newmark, N.M., W.J. Hall, and B. Mohraz (1973). *A Study of Vertical and Horizontal Earthquake Spectra*. Directorate of Licensing, U.S. Atomic Energy Commission, Rept. WASH-1255.
- Newmark, N.M., J.A. Blume and K.K. Kapur (1973). "Seismic design criteria for nuclear power plants." *Journal of the Power Division*, ASCE 99, 287-303.
- Regulatory Guide 1.60 (1973). "*Design response spectra for seismic design of nuclear power plants.*" U.S. Atomic Energy Commission, Directorate of Regulatory Standards.
- Roblee, C.J., W.J. Silva, G.R. Toro and N. Abrahamson (1996). "Variability in Site-Specific Seismic Ground-Motion Predictions." Uncertainty in the Geologic Environment: From Theory to Practice, *Proceedings "Uncertainty '96" ASCE Specialty Conference*, Edited by C.D. Shackelford, P.P. Nelson, and M.J.S. Roth, Madison, WI, Aug. 1-3, pp. 1113-1133.
- Sadigh, K., C.-Y. Chang, J.A. Egan, F. Makdisi, and R.R. Youngs (1997). "Attenuation relationships for shallow crustal earthquakes based on California strong motion data." *Seism. Res. Lett.*, 68(1), 180-189.
- Sadigh, K., C.-Y. Chang, N.A. Abrahamson, S.J. Chiou and M.S. Power (1993). "Specification of long-period ground motions: Updated attenuation relationships for rock site conditions and adjustment factors for near-fault effects." in *Proc. ATC-17-1, Seminar on Seismic Isolation, Passive Energy Dissipation, and Active Control, March 11-12, San Francisco, California, 59-70*.
- Seed, H.B., C. Ugas and J. Lysmer. (1976). "Site-dependent spectra for earthquake resistant design." *Bull. Seism. Soc. Am.*, 66(1), 221-243.
- Silva, W.J. (1997). "Characteristics of vertical strong ground motions for applications to engineering design." *Proc. Of the FHWA/NCEER Workshop on the Nat'l Rep. Of Seismic Ground Motion for New and Existing Highway Facilities*, Technical Report NCEER-97-0010.
- Silva, W.J., N.A. Abrahamson, G.R. Toro, C.J. Costantino (1997). "Description and validation of the stochastic ground motion model." Rept. submitted to Brookhaven National Laboratory, Associated Universities, Inc. Upton, New York.
- Silva, W.J. and R. Darragh (1995). "Engineering characterization of earthquake strong ground motion recorded at rock sites." Palo Alto, Calif:Electric Power Research Institute, TR-102261.

- Silva, W.J. (1991). "Global characteristics and site geometry." Chapter 6 in *Proceedings: NSF/EPRI Workshop on Dynamic Soil Properties and Site Characterization*. Palo Alto, Calif.: Electric Power Research Institute, NP-7337.
- Silva, W.J., and R.K. Green (1989). "Magnitude and distance scaling of response spectral shapes for rock sites with applications to North American tectonic environment." *Earthquake Spectra*, 5(3), 591-624.
- Somerville, P.G., N.F. Smith, R.W. Graves, and N.A. Abrahamson, (1997). "Modification of empirical strong ground motion attenuation relations to include the amplitude and duration effects of rupture directivity." *Seism. Res. Lett.*, 68(1), 199-222.
- Somerville, P.G. and N.A. Abrahamson (1995). "Ground motion prediction for thrust earth-quakes." *Proc. of the SMIP95 Seminar on Seismological and Engineering Implications of Recent Strong Motion Data*, San Francisco, California.
- Youngs, R.R., S.J. Chiou, W.J. Silva, and J.R. Humphrey (1997), "Strong ground motion attenuation relationships for subduction zone earthquakes." *Seism. Res. Lett.*, 68(1), 58-73.
- Youngs, R.R., N.A. Abrahamson, F. Makdisi, and K. Sadigh (1995). "Magnitude dependent dispersion in peak ground acceleration." *Bull. Seism. Soc. Am.*, 85(1), 1161-1176.

Table 1  
WUS STATISTICAL SHAPE BINS

<u>Magnitude Bins (M)</u>								
				<u>Bin Center</u>				
<u>Range</u>								
5 - 6				5.5				
6 - 7				6.5				
7+				7.5				
Distance Bin (km)	$\bar{M}$	$\bar{R}$ (km)	Number of Spectra	PGA* (g), $\sigma_{ln}$	PGV* (cm/sec), $\sigma_{ln}$	PGD* (cm), $\sigma_{ln}$	$\frac{PGV^*}{PGA} \left( \frac{cm/sec}{g} \right)$ , $\sigma_{ln}$	$\frac{PGA \bullet PGD^*}{PGV^2}$ , $\sigma_{ln}$
0 - 10, rock	5.54	7.91	30	0.18, 0.91	8.14, 1.14	0.80, 1.60	44.50, 0.58	2.17, 0.28
	6.53	5.75	32	0.44, 0.76	32.65, 0.93	6.22, 1.26	73.51, 0.40	2.54, 0.42
	7.27	4.20	6	0.93, 0.26	81.73, 0.25	47.42, 0.66	87.94, 0.39	6.47, 0.60
0 - 10, soil	5.76	7.80	24	0.26, 0.65	18.57, 0.56	3.11, 0.46	70.72, 0.33	2.32, 0.35
	6.46	6.00	77	0.38, 0.43	46.88, 0.59	14.79, 0.89	122.00, 0.44	2.54, 0.41
	7.05	8.90	4	0.40, 0.62	44.46, 0.56	21.27, 0.25	110.42, 0.07	4.25, 0.24
10 - 50, rock	5.57	21.80	180	0.11, 0.87	5.08, 0.85	0.54, 1.04	46.96, 0.37	2.24, 0.38
	6.43	30.28	238	0.13, 0.73	8.81, 0.76	1.96, 1.01	70.41, 0.49	3.09, 0.54
	7.27	31.00	6	0.17, 0.85	8.80, 0.88	2.50, 1.56	50.59, 0.37	5.51, 0.90

Table 1 (cont.)  
WUS STATISTICAL SHAPE BINS

<u>Magnitude Bins (M)</u>								
				<u>Bin Center</u>				
<u>Range</u>								
				5.5				
				6.5				
				7.5				
Distance Bin (km)	$\bar{M}$	$\bar{R}$ (km)	Number of Spectra	<u>Bin Center</u>				
				PGA*(g), $\sigma_{ln}$	PGV*(cm/sec), $\sigma_{ln}$	PGD*(cm), $\sigma_{ln}$	$\frac{PGV^*}{PGA} \left( \frac{cm/sec}{g} \right)$ $\sigma_{ln}$	$\frac{PGA \bullet PGD^*}{PGV^2}$ , $\sigma_{ln}$
10 - 50, soil	5.69	21.82	378	0.11, 0.73	6.63, 0.77	0.87, 0.94	59.88, 0.34	2.16, 0.33
	6.35	28.27	542	0.14, 0.63	10.77, 0.74	2.25, 1.04	78.77, 0.41	2.57, 0.41
	7.29	33.46	56	0.16, 0.35	22.38, 0.38	10.46, 0.39	141.17, 0.36	3.25, 0.56
50 - 100, rock	5.91	64.27	34	0.05, 0.40	2.22, 0.53	0.21, 0.83	41.16, 0.43	2.24, 0.57
	6.51	70.35	102	0.06, 0.51	3.87, 0.82	0.79, 1.23	69.89, 0.56	2.88, 0.56
	7.32	81.46	10	0.06, 0.52	5.16, 0.87	2.64, 1.17	80.63, 0.45	6.23, 0.50
50 - 100, soil	5.80	67.22	42	0.06, 0.80	3.12, 0.78	0.38, 0.92	53.20, 0.23	2.28, 0.49
	6.49	67.34	158	0.07, 0.67	6.23, 0.78	1.26, 0.99	88.00, 0.42	2.26, 0.44
	7.31	76.57	14	0.10, 0.12	11.24, 0.34	5.42, 0.60	111.37, 0.35	4.24, 0.50
100 - 200, rock	5.4	107.80	2	0.02, ----	1.16, ----	0.10, ----	49.72, ----	1.74, ----
	6.64	114.57	14	0.02, 0.86	2.03, 0.38	1.09, 0.68	132.54, 0.59	3.98, 0.27

Table 1 (cont.)  
WUS STATISTICAL SHAPE BINS

Magnitude Bins (M)								
Range				Bin Center				
5 - 6 6 - 7 7+				5.5 6.5 7.5				
Distance Bin (km)	$\bar{M}$	$\bar{R}$ (km)	Number of Spectra	PGA** (g), $\sigma_{ln}$	PGV* (cm/sec), $\sigma_{ln}$	PGD* (cm), $\sigma_{ln}$	$\frac{PGV^*}{PGA} (\frac{cm/sec}{g})$ , $\sigma_{ln}$	$\frac{PGA \bullet PGD^*}{PGV^2}$ , $\sigma_{ln}$
	7.30	152.01	14	0.03, 0.47	5.55, 0.66	2.43, 1.06	184.16, 0.35	2.34, 0.31
100 - 200, soil	6.0	105.00	2	0.03, ----	1.50, ----	0.11, ----	42.92, ----	1.74, ----
	6.64	132.97	28	0.03, 0.78	3.05, 0.58	0.89, 0.97	98.24, 0.53	2.90, 0.42
	7.31	147.07	88	0.04, 0.25	8.09, 0.39	3.50, 0.76	188.64, 0.36	2.25, 0.29
0 - 50, rock	5.57	19.91	208	0.12, 0.89	5.39, 0.91	0.57, 1.14	46.73, 0.40	2.22, 0.37
	6.44	27.39	270	0.15, 0.84	10.27, 0.89	2.24, 1.10	70.77, 0.48	3.02, 0.53
	7.27	17.60	12	0.40, 1.07	26.82, 1.35	10.89, 1.94	66.70, 0.46	5.97, 0.69
0 - 50, soil	5.69	21.10	398	0.12, 0.75	7.02, 0.79	0.93, 0.97	60.48, 0.34	2.16, 0.33
	6.37	25.50	619	0.16, 0.70	12.93, 0.87	2.85, 1.20	83.17, 0.44	2.57, 0.41
	7.27	31.82	60	0.17, 0.42	23.43, 0.42	10.97, 0.42	138.87, 0.36	3.30, 0.55

\*\*Median values

Table 2 POINT-SOURCE PARAMETERS*		
	WUS	CEUS
$\Delta\sigma$ (bars)	65	120
kappa (sec)	0.040	0.006
$Q_0$	220	351
$\eta$	0.60	0.84
$\beta$ (km/sec)	3.50	3.52
$\rho$ (g/cc)	2.70	2.60
Amplification	soft rock (Figure 10)	hard rock (Figure 10)
Double Corner	Atkinson and Silva (1997)	Atkinson (1993)

\* based on Silva et al. (1997)

Table 3 RESPONSE SPECTRAL SHAPE COEFFICIENTS FOR 5% DAMPING			
	WUS	CEUS (1C)*	CEUS (2C)*
C <sub>1</sub>	1.8197	0.88657	0.97697
C <sub>2</sub>	0.30163	exp(-10.411)	exp(-9.4827)
C <sub>3</sub>	0.47498+0.034356 <b>M</b> +0.0057204ln( <i>R</i> +1)	2.5099	2.3006
C <sub>4</sub>	-12.650+ <b>M</b> ·[2.4796-0.14732 <b>M</b> +0.034605ln(0.040762 <i>R</i> +1)]	-7.4408+ <b>M</b> [1.5220-0.088588 <b>M</b> +0.0073069ln(0.12639 <i>R</i> +1)]	-12.665+ <b>M</b> [2.4869-0.14562 <b>M</b> +0.024477ln(0.041807 <i>R</i> +1)]
C <sub>5</sub>	-0.25746	-0.34965	-0.21002
C <sub>6</sub>	0.29784+0.010723 <b>M</b> -0.0000133 <i>R</i>	-0.31162+0.0019646 <i>R</i>	0.74361+0.0000671 <i>R</i>
C <sub>7</sub>	n.a.	3.7841	exp[-13.476+ <b>M</b> (4.4007-0.31651 <b>M</b> +0.000235 <i>R</i> )]
C <sub>8</sub>	n.a.	-0.89019	0.95259+ <b>M</b> (-0.58275+0.000166 <i>R</i> )
C <sub>9</sub>	n.a.	0.39806+0.058832 <b>M</b>	-3.3534+0.44094 <b>M</b>

Note: Equation (8) is used for the WUS; equation (9) is used for the CEUS.

**M** = moment magnitude

*R* = fault distance

\*1C = single corner frequency model

2 C = double corner frequency model

Table 4  
RECOMMENDED V/H RATIOS FOR WUS ROCK SITE CONDITIONS

Frequency (Hz)	$\leq 0.2g^*$	$0.2 - 0.5g^*$	$> 0.5g^*$
.100+00	.503E+00	.558E+00	.696E+00
.333E+00	.503E+00	.558E+00	.696E+00
.500E+00	.461E+00	.508E+00	.651E+00
.667E+00	.458E+00	.495E+00	.645E+00
.100E+01	.440E+00	.461E+00	.608E+00
.118E+01	.434E+00	.454E+00	.597E+00
.133E+01	.431E+00	.451E+00	.592E+00
.167E+01	.420E+00	.447E+00	.585E+00
.200E+01	.416E+00	.447E+00	.583E+00
.217E+01	.417E+00	.452E+00	.592E+00
.250E+01	.426E+00	.467E+00	.616E+00
.278E+01	.436E+00	.482E+00	.638E+00
.333E+01	.456E+00	.511E+00	.681E+00
.417E+01	.495E+00	.571E+00	.758E+00
.500E+01	.536E+00	.628E+00	.836E+00
.588E+01	.581E+00	.691E+00	.918E+00
.666E+01	.625E+00	.751E+00	.997E+00
.833E+01	.715E+00	.888E+00	.119E+01
.100E+02	.796E+00	.101E+01	.137E+01
.111E+02	.840E+00	.107E+01	.144E+01
.125E+02	.885E+00	.112E+01	.150E+01
.167E+02	.904E+00	.114E+01	.152E+01
.200E+02	.888E+00	.112E+01	.148E+01
.250E+02	.810E+00	.102E+01	.133E+01
.333E+02	.744E+00	.912E+00	.117E+01
.500E+02	.704E+00	.848E+00	.107E+01
.100E+03	.704E+00	.848E+00	.107E+01

---

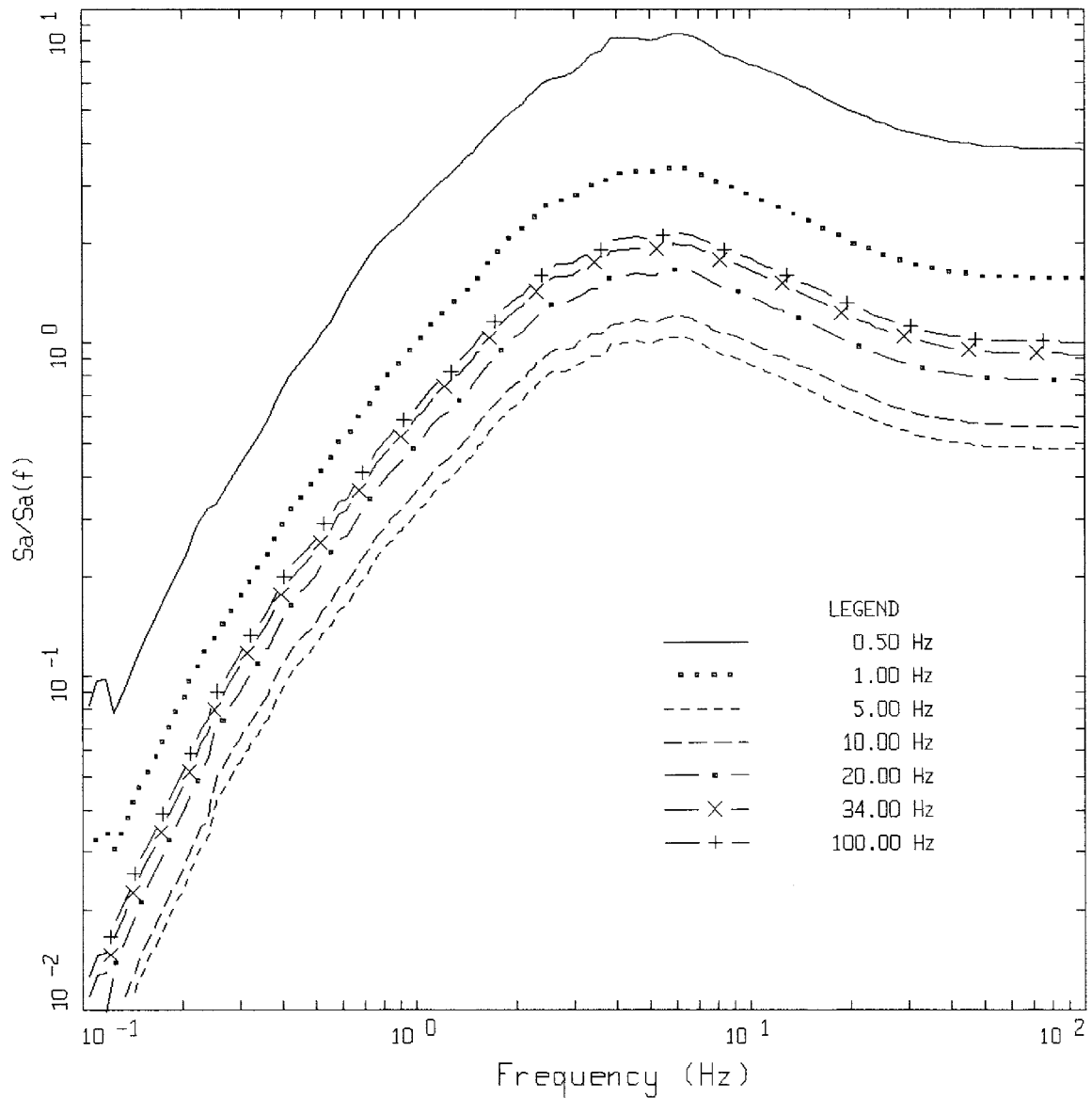
\*Range in rock outcrop horizontal component peak acceleration

Table 5  
RECOMMENDED V/H RATIOS FOR CEUS ROCK SITE CONDITIONS

Frequency (Hz)	$\leq 0.2g^*$	0.2 - 0.5g*	$> 0.5g^*$
0.10	0.67	0.75	0.90
10.00	0.67	0.75	0.90
18.75	0.70	0.81	1.01
22.06	0.73	0.85	1.08
25.00	0.75	0.88	1.12
31.25	0.77	0.95	1.25
37.50	0.81	1.00	1.37
41.67	0.84	1.07	1.44
46.88	0.85	1.12	1.50
62.50	0.90	1.14	1.52
75.00	0.89	1.12	1.48
93.75	0.81	1.02	1.33
100.0	0.78	1.00	1.30

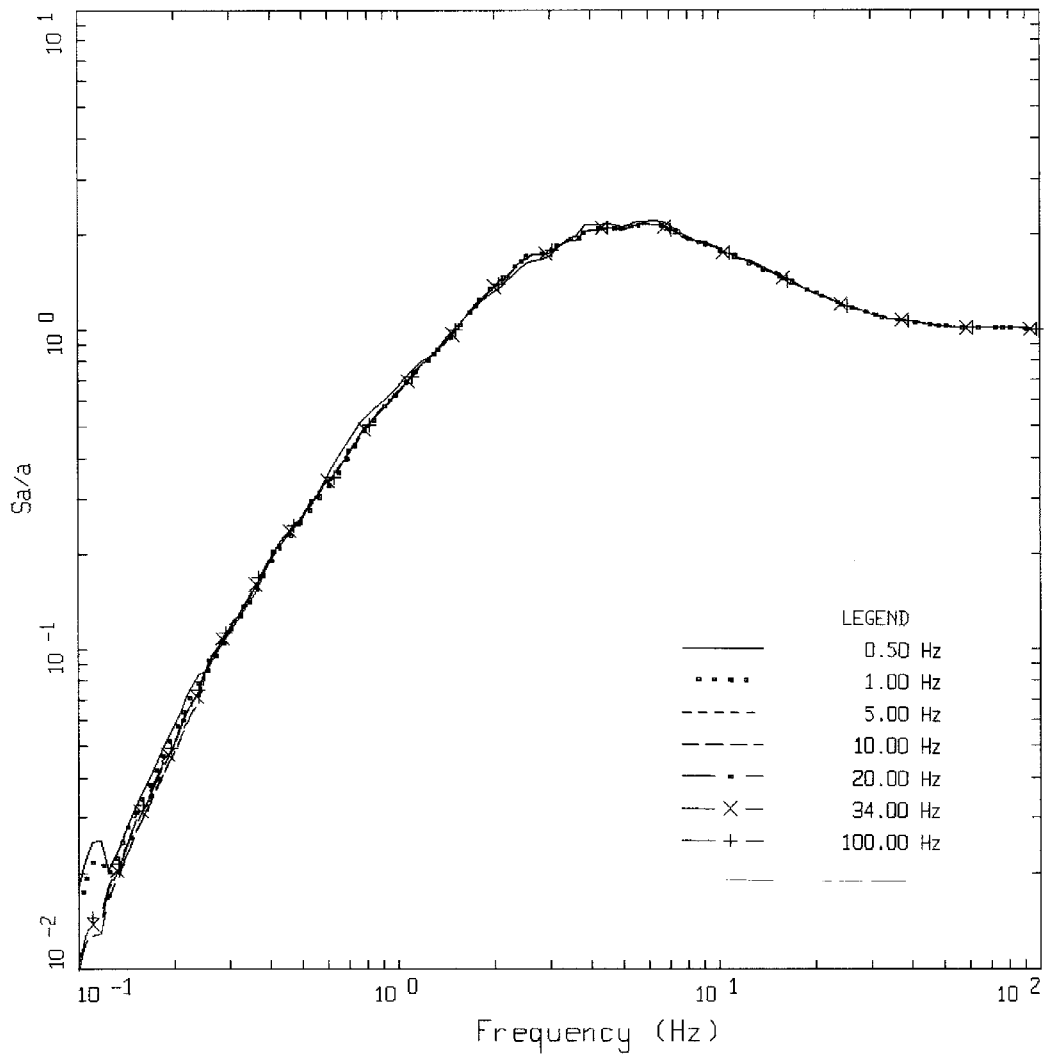
---

\*Range in rock outcrop horizontal component peak acceleration



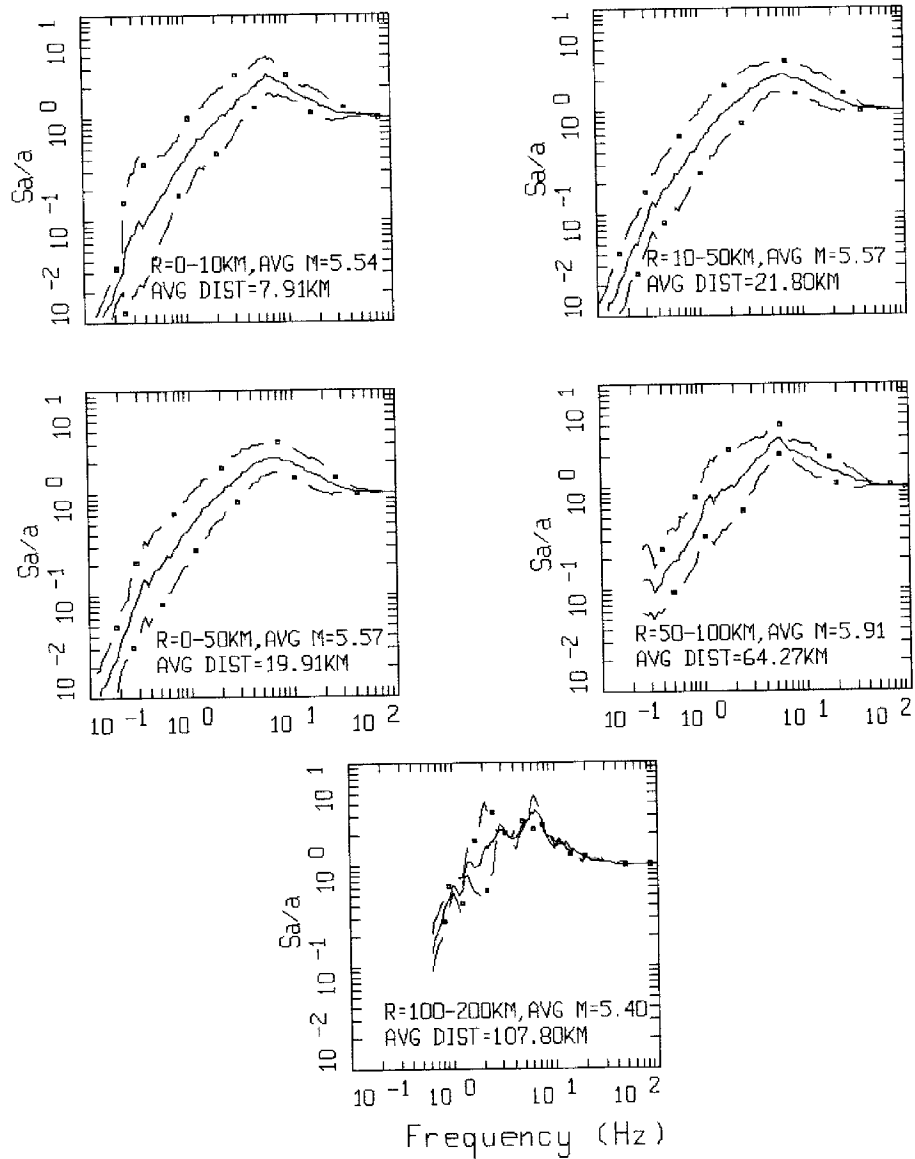
AVERAGE HORIZONTAL SPECTRA, 50TH PERCENTILE  
M=6.5 (6.0-7.0), R=10-50 KM, ROCK  
AVERAGE M = 6.43, AVERAGE DISTANCE = 30.28 KM

Figure 1. Response spectral shapes (5% damping) for the **M** 6.5, **R** = 10 to 50 km bins normalized by spectral ordinates at a suite of frequencies (0.5 to 100.0 Hz).



AVERAGE HORIZONTAL SPECTRA, 50TH PERCENTILE  
 M=6.5 (6.0-7.0), R=10-50 KM, ROCK  
 AVERAGE M = 6.43, AVERAGE DISTANCE = 30.28 KM

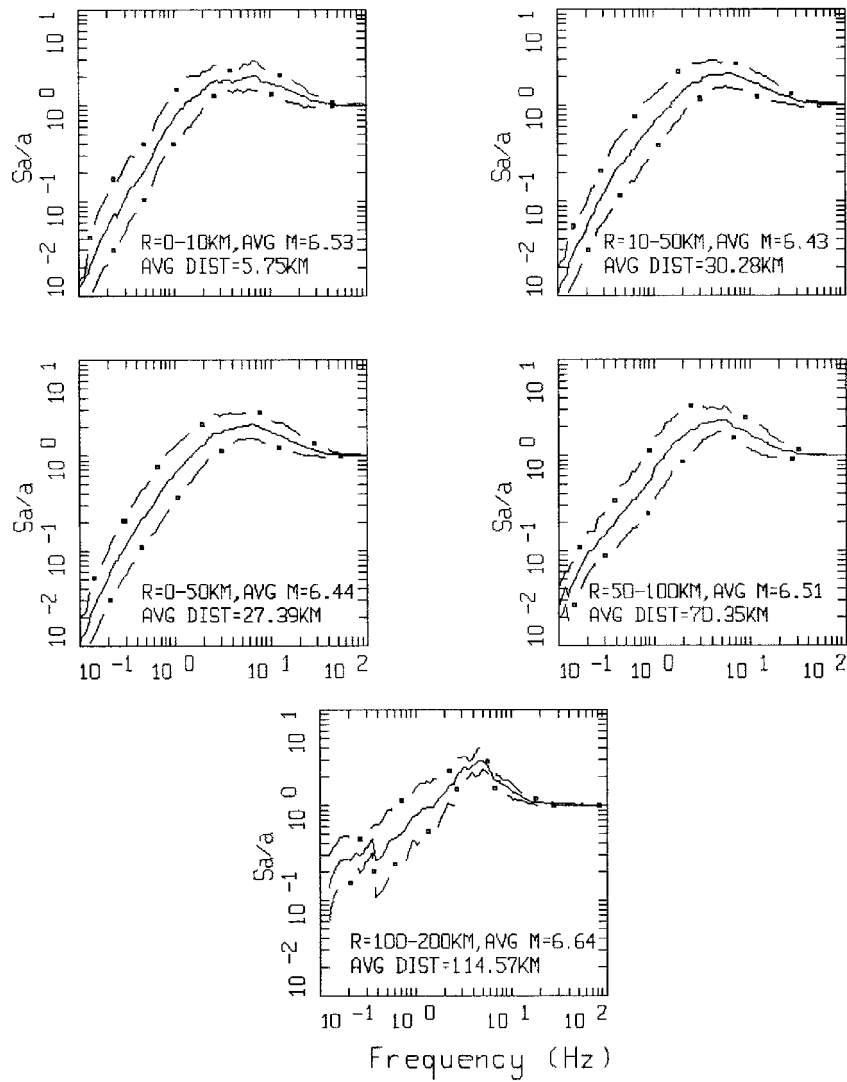
Figure 2. Response spectral shapes (5% damping) for the **M** 6.5, *R* = 10 to 50 km bins from Figure 1 renormalized by their respective 100 Hz values.



AVERAGE HORIZONTAL SPECTRA, ROCK  
 M=5.5 (5.0-6.0)

LEGEND  
 ————— 50TH PERCENTILE  
 - . - . 84TH PERCENTILE  
 - . - . 16TH PERCENTILE

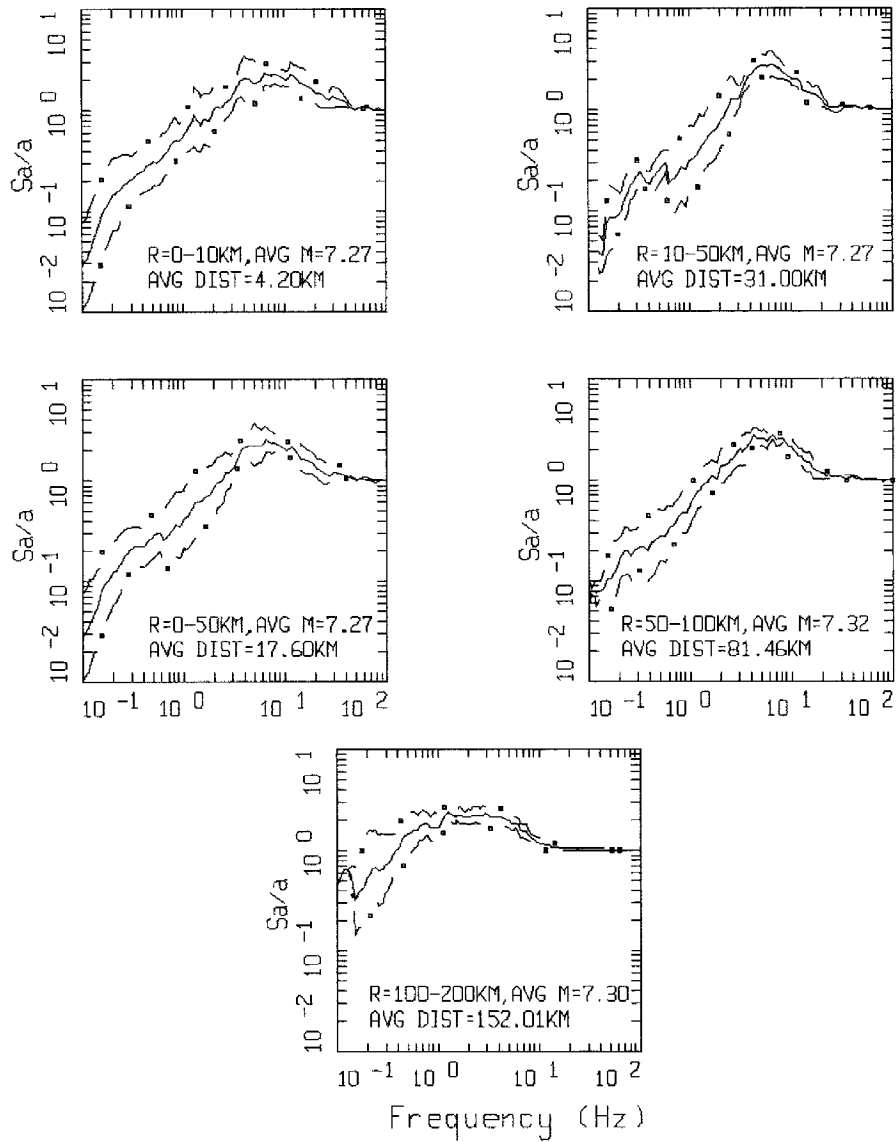
Figure 3. Response spectral shapes (5% damping) computed for the  $M = 5.5$  magnitude bin for WUS soft rock site conditions.



AVERAGE HORIZONTAL SPECTRA, ROCK  
 M=6.5 (6.0-7.0)

LEGEND  
 ——— 50TH PERCENTILE  
 - · - 84TH PERCENTILE  
 - · - 16TH PERCENTILE

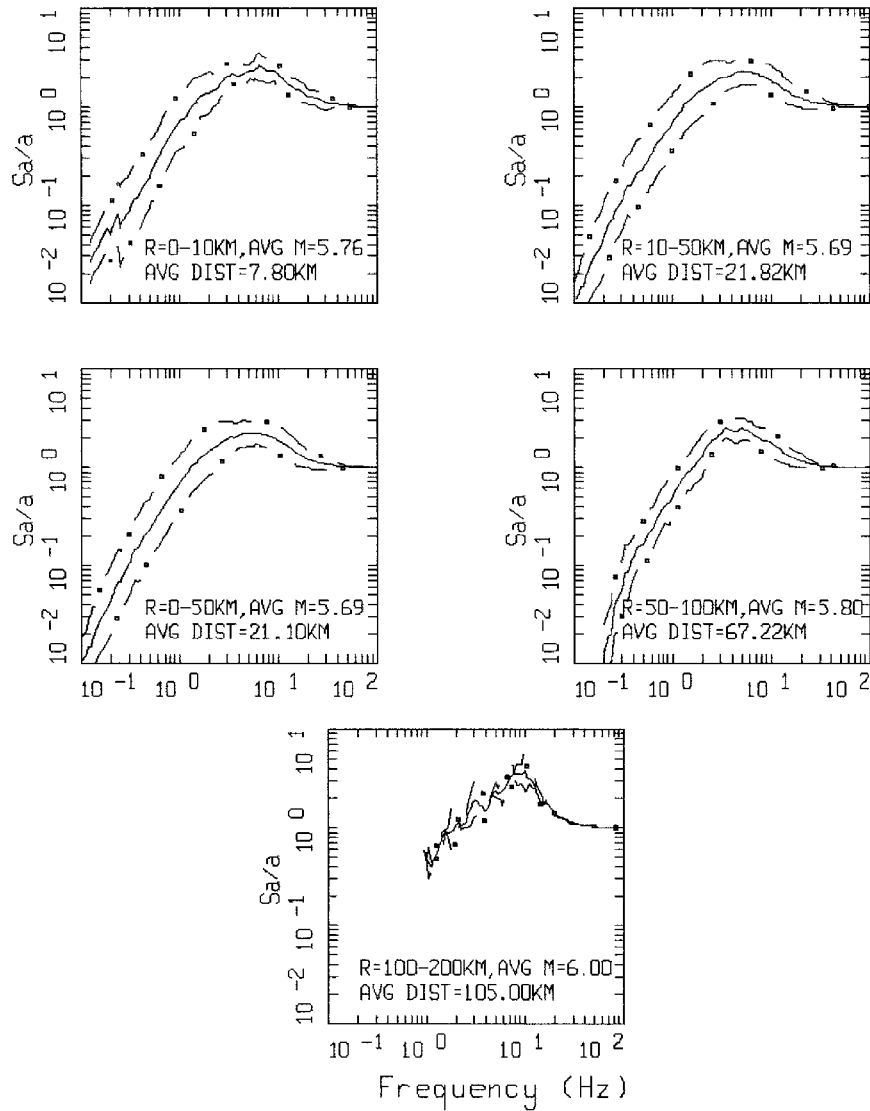
Figure 4. Response spectral shapes (5% damping) computed for the  $M = 6.5$  magnitude bin for WUS soft rock site conditions.



AVERAGE HORIZONTAL SPECTRA, ROCK  
 M=7.5 (7.0-7.0+)

LEGEND  
 ————— 50TH PERCENTILE  
 - · - 84TH PERCENTILE  
 - · - 16TH PERCENTILE

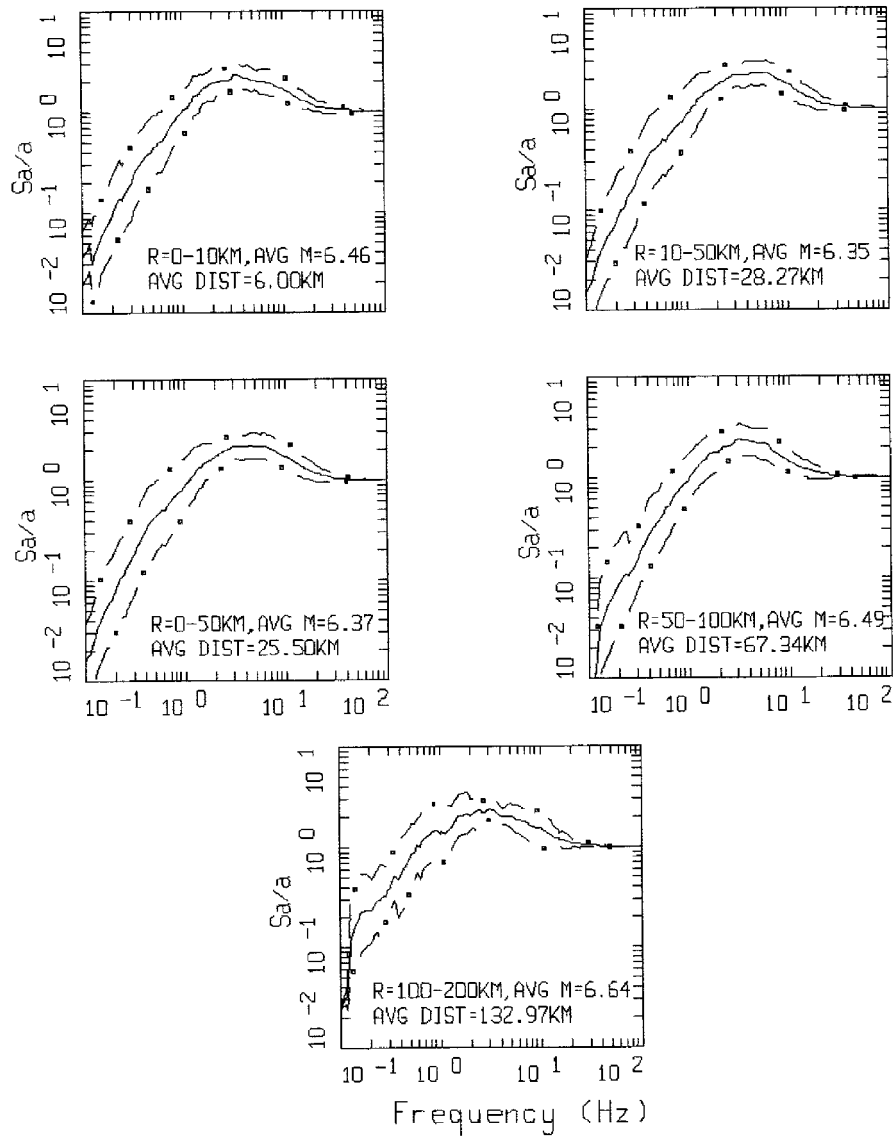
Figure 5. Response spectral shapes (5% damping) computed for the  $M = 7.5$  magnitude bin for WUS soft rock site conditions.



AVERAGE HORIZONTAL SPECTRA, SOIL  
 $M=5.5$  (5.0-6.0)

LEGEND  
 — 50TH PERCENTILE  
 - - 84TH PERCENTILE  
 - . - 16TH PERCENTILE

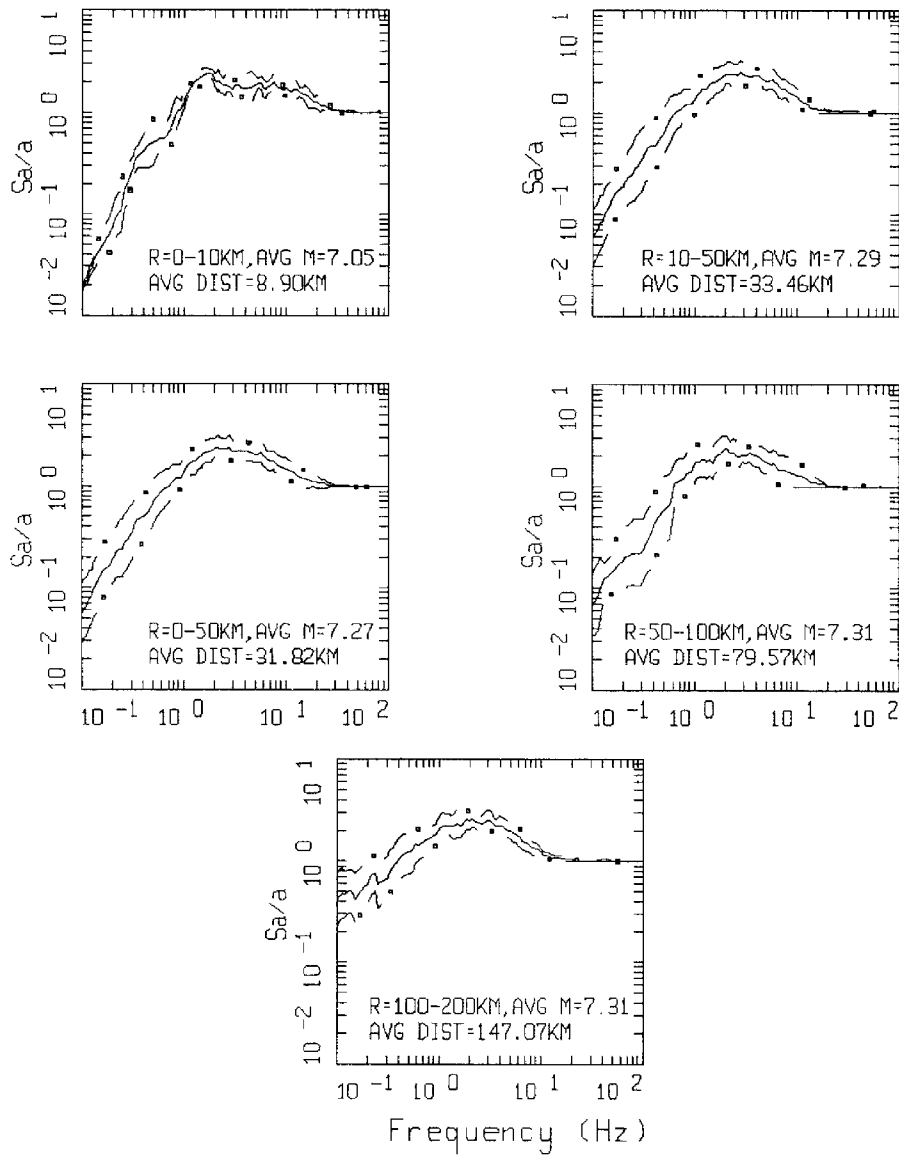
Figure 6. Response spectral shapes (5% damping) computed for the  $M = 5.5$  magnitude bin for WUS deep soil site conditions.



AVERAGE HORIZONTAL SPECTRA, SOIL  
 M=6.5 (6.0-7.0)

LEGEND  
 — 50TH PERCENTILE  
 - · - 84TH PERCENTILE  
 - · - 16TH PERCENTILE

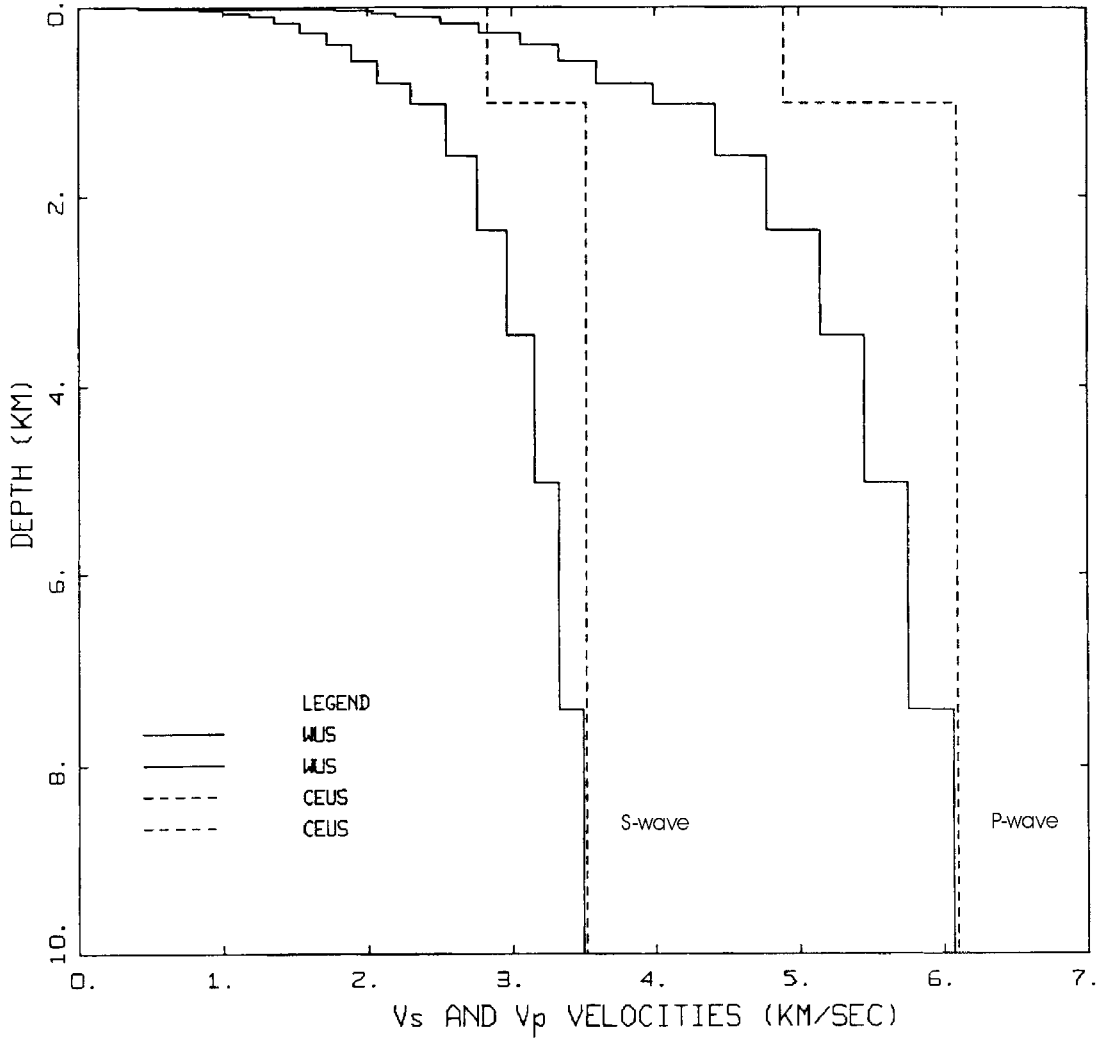
Figure 7. Response spectral shapes (5% damping) computed for the  $M = 6.5$  magnitude bin for WUS deep soil site conditions.



AVERAGE HORIZONTAL SPECTRA, SOIL  
 M=7.5 (7.0-7.0+)

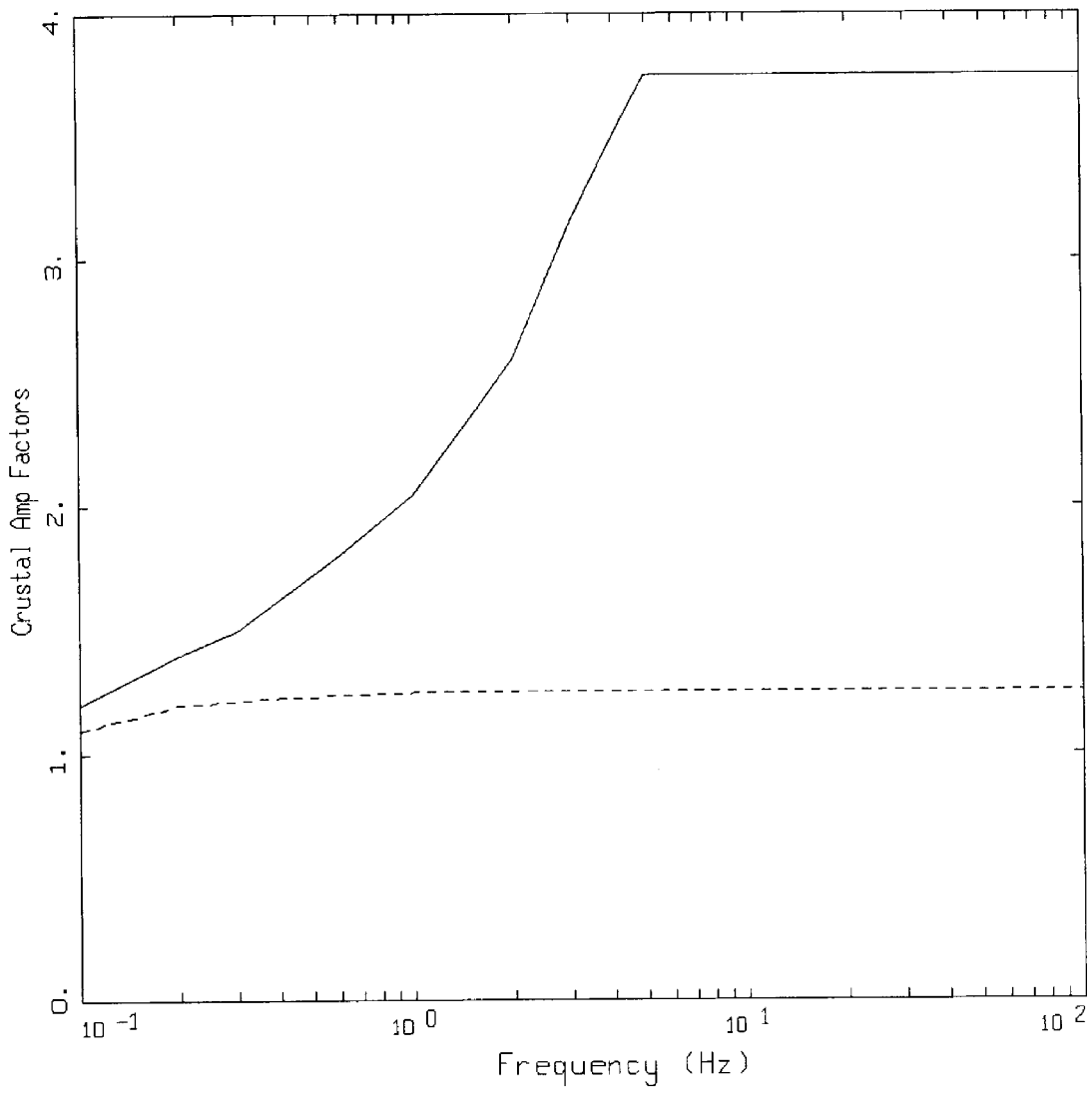
LEGEND  
 — 50TH PERCENTILE  
 — • — 84TH PERCENTILE  
 — • — 16TH PERCENTILE

Figure 8. Response spectral shapes (5% damping) computed for the  $M = 7.5$  magnitude bin for WUS deep soil site conditions.



GENERIC WUS AND CEUS  
CRUSTAL MODELS

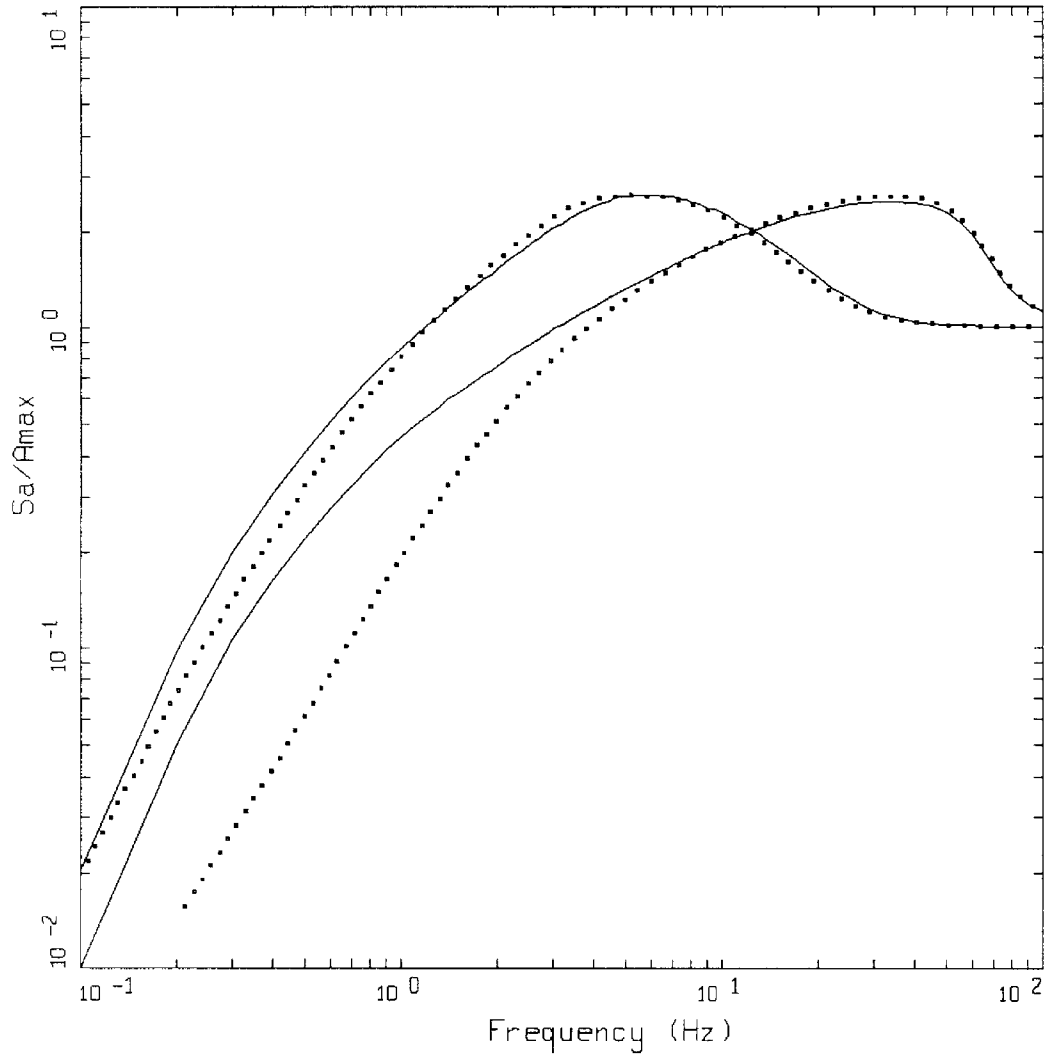
Figure 9. Comparison of generic compression- and shear-wave velocity profiles for WUS (Silva et al., 1997) and CEUS (EPRI, 1993) crustal conditions.



CRUSTAL AMPLIFICATION FACTORS

- LEGEND
- WUS, SOFT ROCK
  - - - CEUS, HARD ROCK

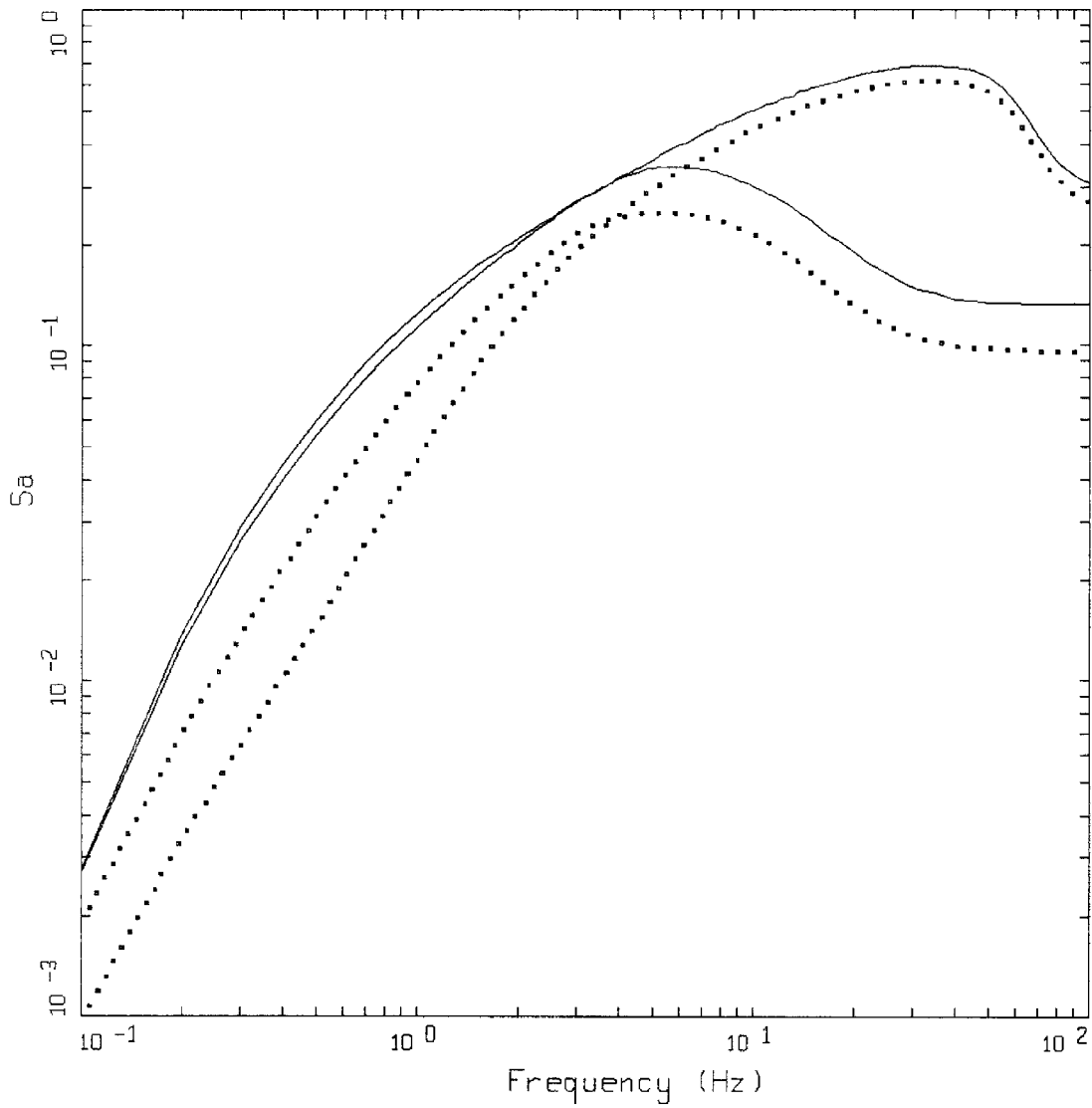
Figure 10. Crustal amplification factors (smoothed) for Fourier amplitude spectra computed for the crustal models shown in Figure 9 (10 km to the surface) using vertically propagating shear-waves.



POINT-SOURCE MODEL  
 $M = 6.5, R = 25 \text{ KM}$

- LEGEND
- WUS ROCK, SINGLE CORNER
  - ..... WUS ROCK, DOUBLE CORNER
  - CEUS ROCK, SINGLE CORNER
  - ..... CEUS ROCK, DOUBLE CORNER

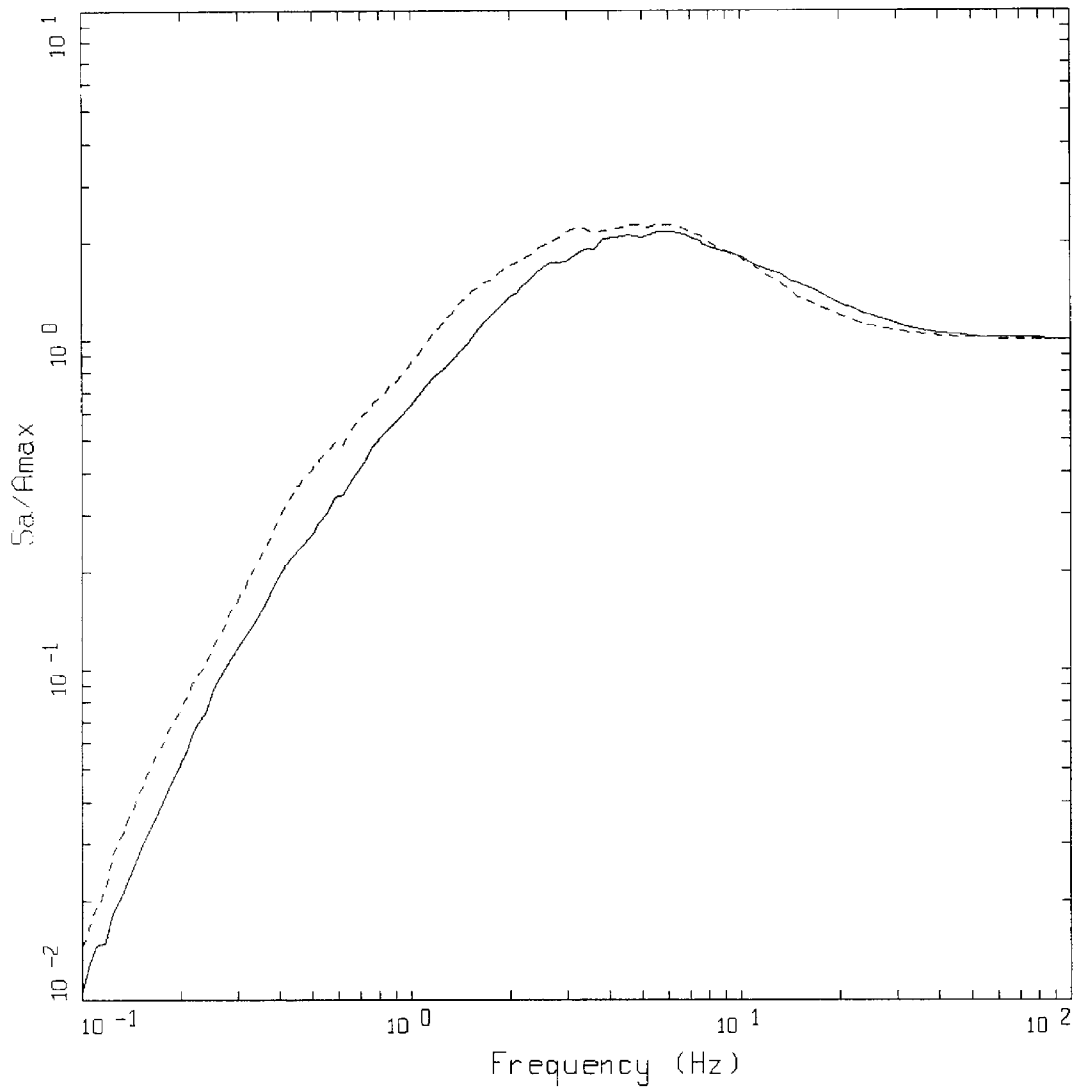
Figure 11. Response spectral shapes (5% damping) computed for  $M = 6.5$  at  $R = 25 \text{ km}$  using both single and double corner frequency source spectra for WUS and CEUS conditions.



POINT-SOURCE MODEL  
 $M = 6.5$ ,  $R = 25$  KM

- LEGEND
- WUS ROCK, SINGLE CORNER
  - ..... WUS ROCK, DOUBLE CORNER
  - CEUS ROCK, SINGLE CORNER
  - ..... CEUS ROCK, DOUBLE CORNER

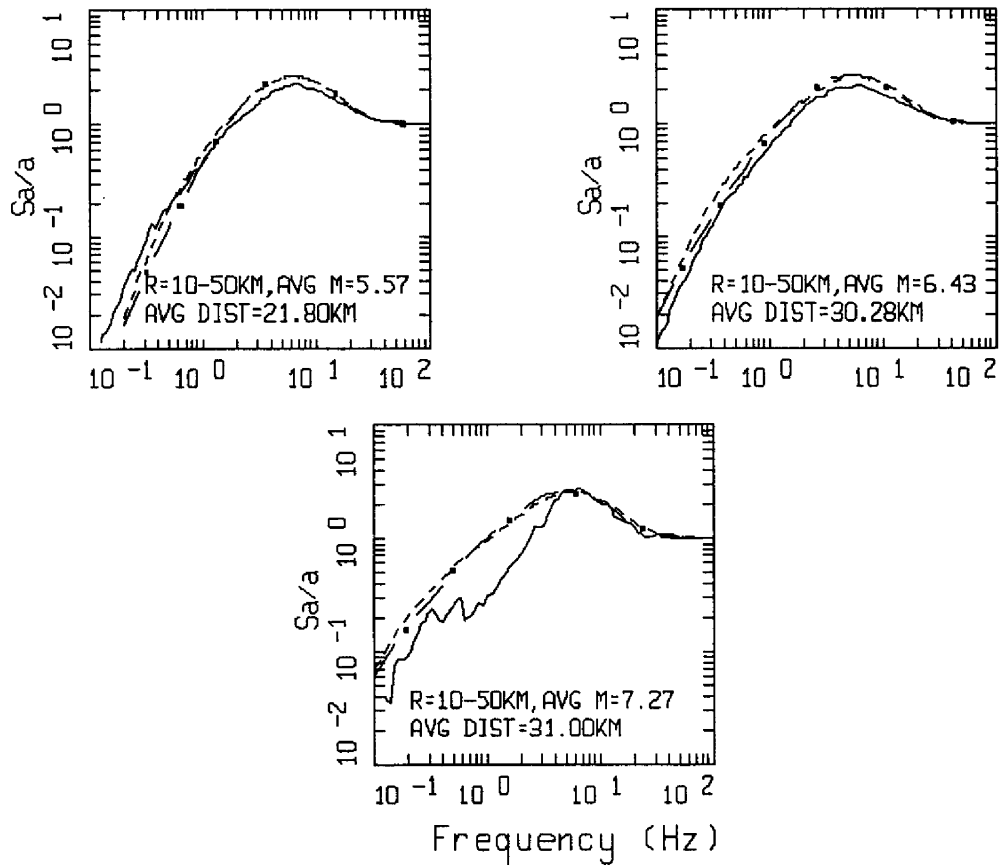
Figure 12. Absolute response spectra (5% damping) computed for  $M = 6.5$  at  $R = 25$  km using both single and double corner frequency source spectra for WUS and CEUS conditions.



AVERAGE HORIZONTAL SPECTRA  
 M=6.5 (6.0-7.0), R=10-50 KM,  
 ROCK AND SOIL

LEGEND  
 ———— ROCK, AVG M = 6.43, AVG DIST = 30.28 KM  
 - - - - - SOIL, AVG M = 6.35, AVG DIST = 28.27 KM

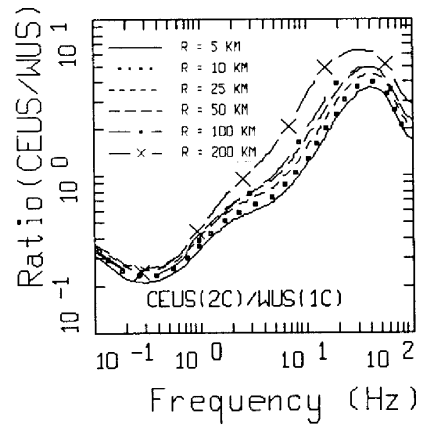
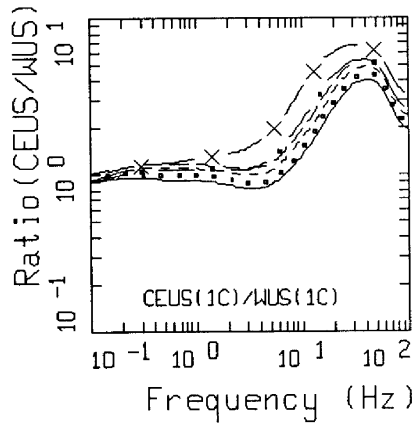
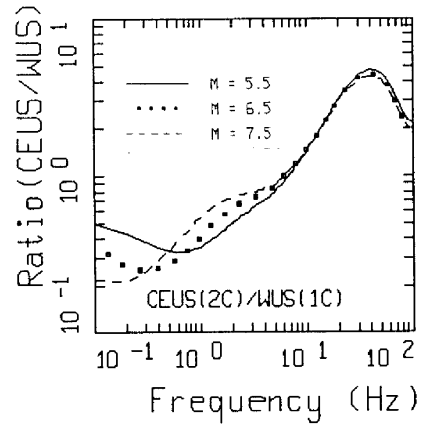
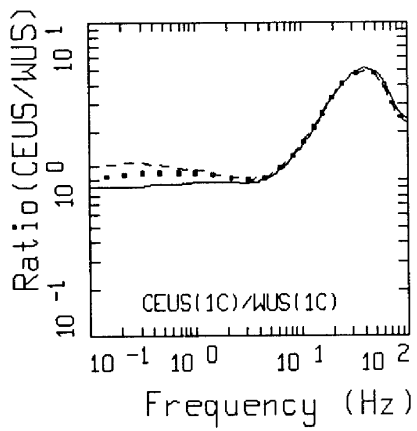
Figure 13. Comparison of WUS statistical response spectral shapes (5% damping) for the M 6.5, R = 10 to 50 km bins for rock and deep soil site conditions.



AVERAGE HORIZONTAL SPECTRA, WUS ROCK  
M=5.5, 6.5, 7.5, R=10-50 KM BINS

LEGEND  
—— STATISTICAL  
----- MODEL, SINGLE CORNER FREQUENCY  
- · - MODEL, DOUBLE CORNER FREQUENCY

Figure 14. Comparison of WUS statistical response spectral shapes to computed shapes using both the single and double corner frequency source model. The distance bin is 10 to 50 km and the magnitude bins are **M** 5.5, 6.5, and 7.5.



TRANSFER FUNCTIONS  
CEUS/WUS

Figure 15. WUS to CEUS transfer functions. Top, magnitude dependencies at a distance of 25 km; bottom, distance dependencies for  $M = 6.5$ .

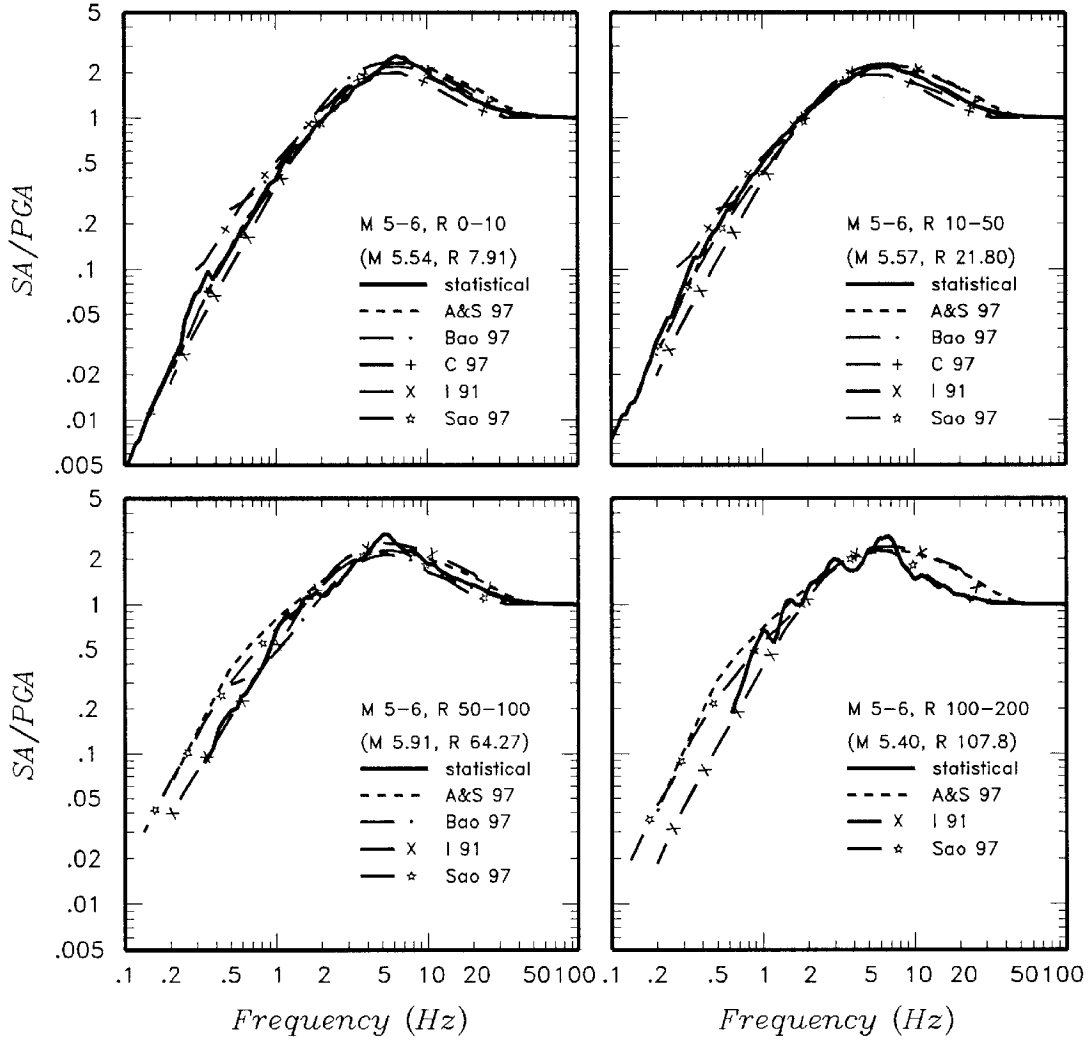


Figure Set 16a. Comparison of the statistical spectral shapes from Figures 3 to 5 with spectral shapes predicted by the attenuation relationships of Abrahamson and Silva (1997) [A&S 97], Boore and others (1997) [Bao 97], Campbell (1997) [C 97], Idriss (1991) [I 91], and Sadigh and others (1997) [Sao 97].

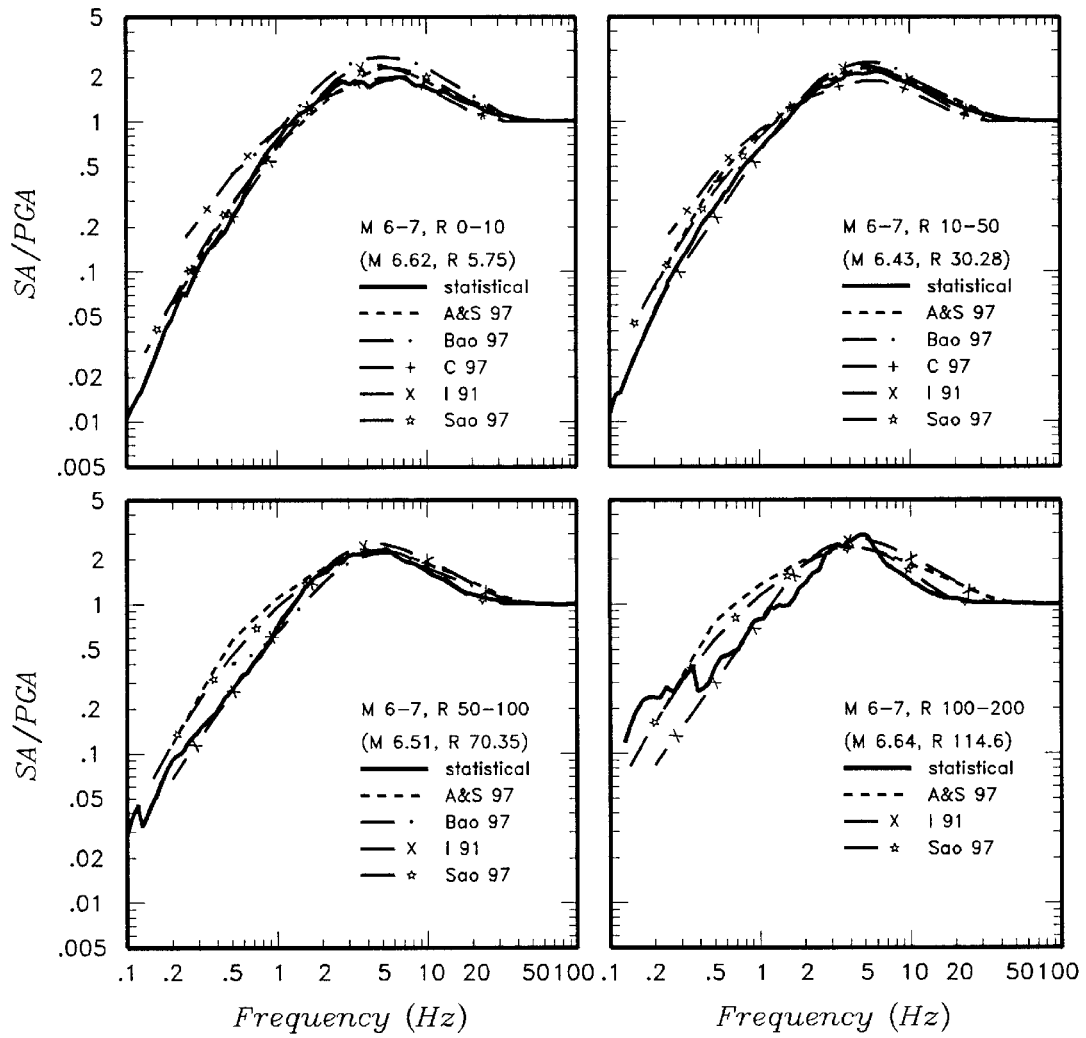


Figure 16b. (Continued)

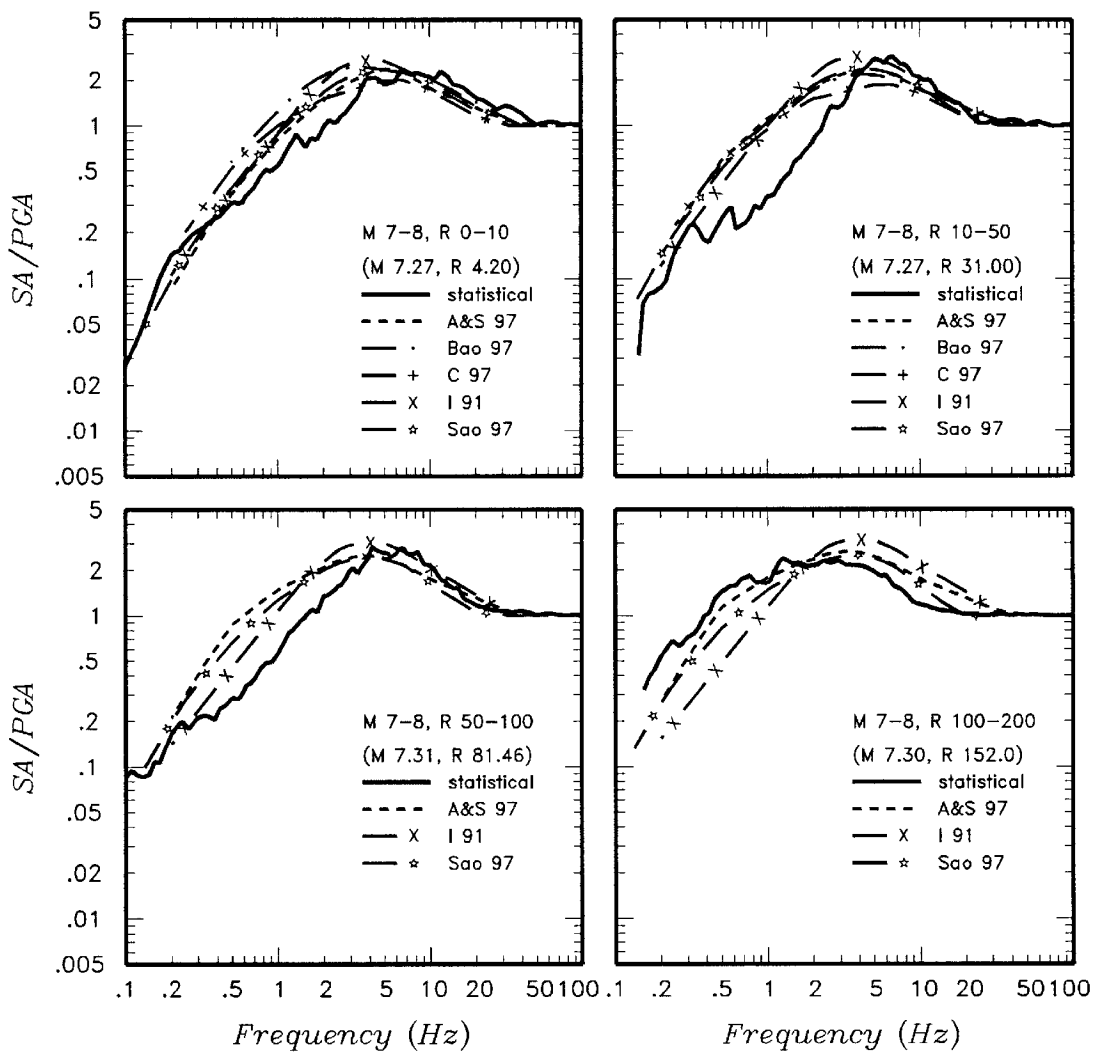


Figure 16c. (Continued)

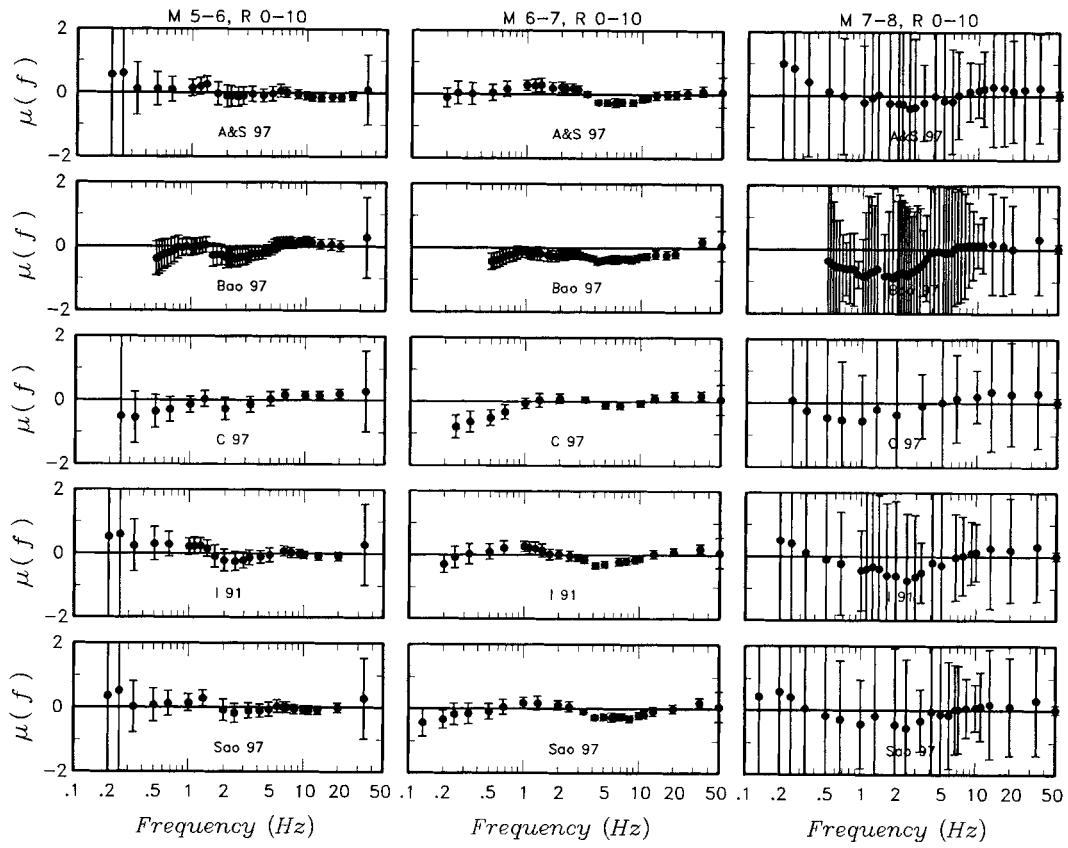


Figure Set 17a. Mean residuals and their 90% confidence intervals for the five attenuation relationships.

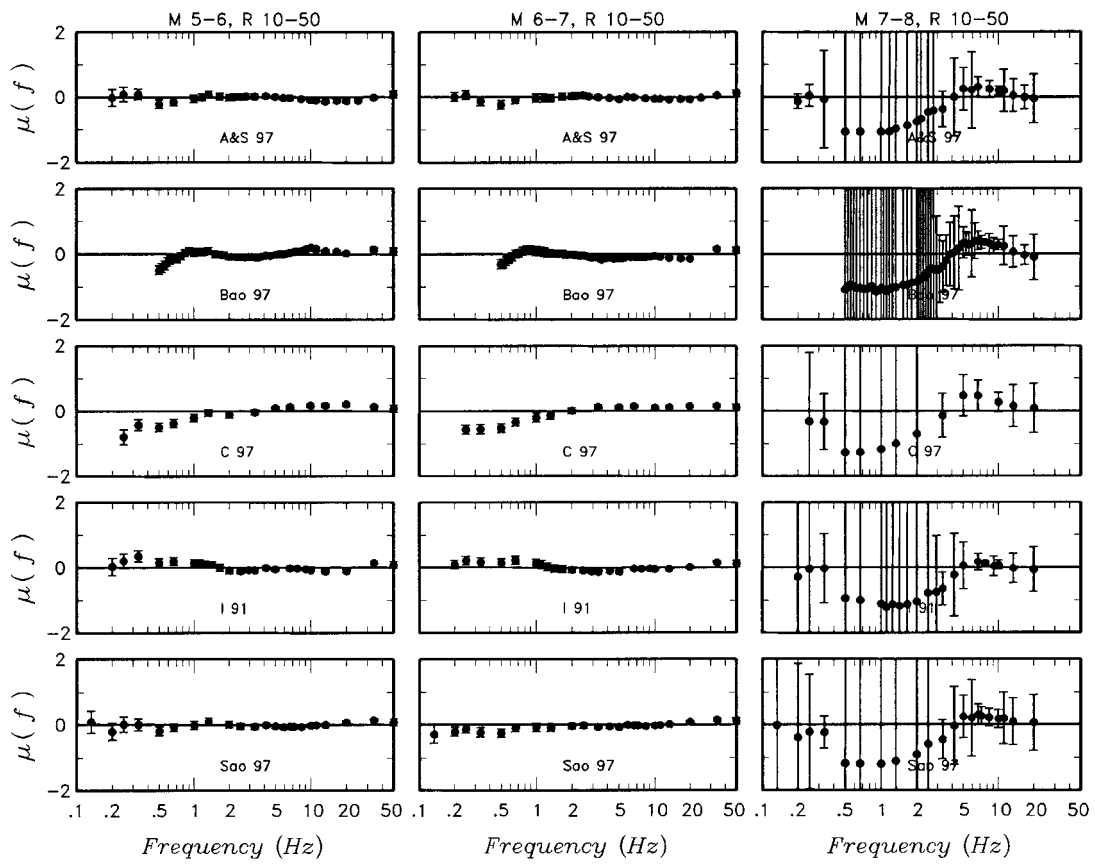


Figure 17b. (Continued)

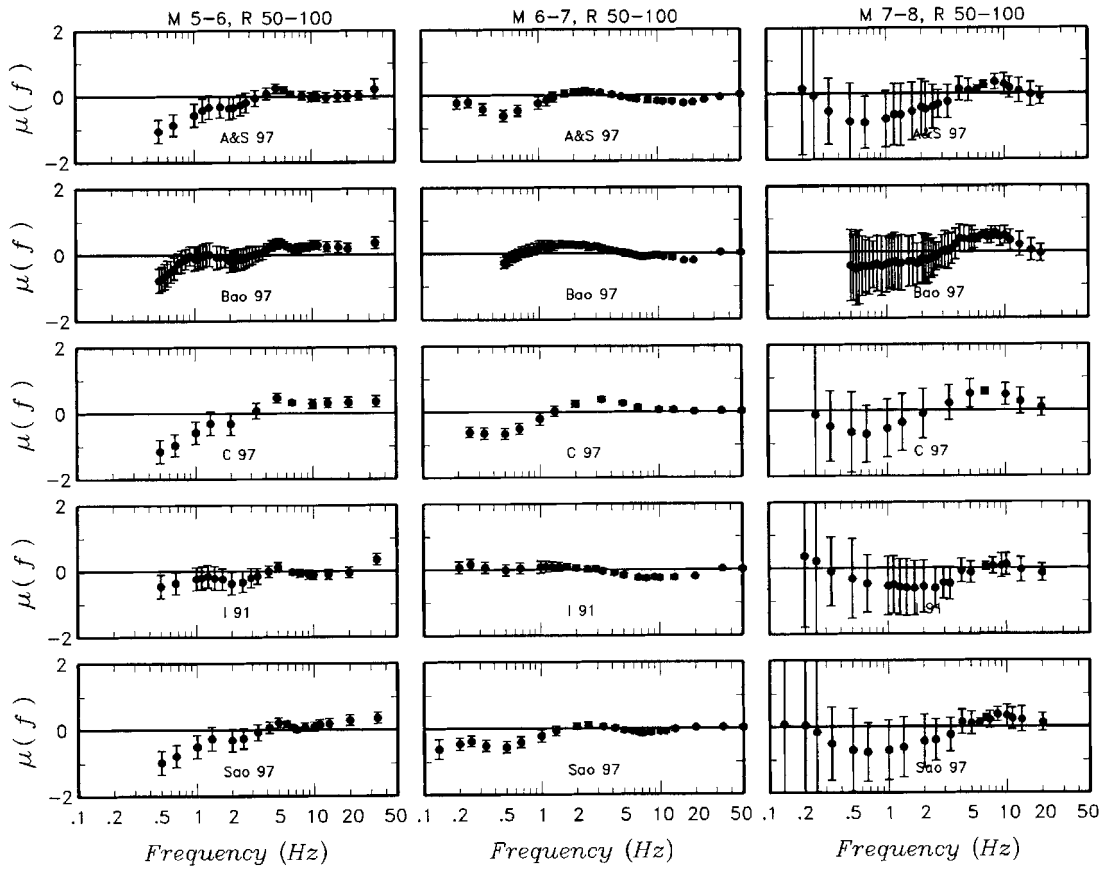


Figure 17c. (Continued)

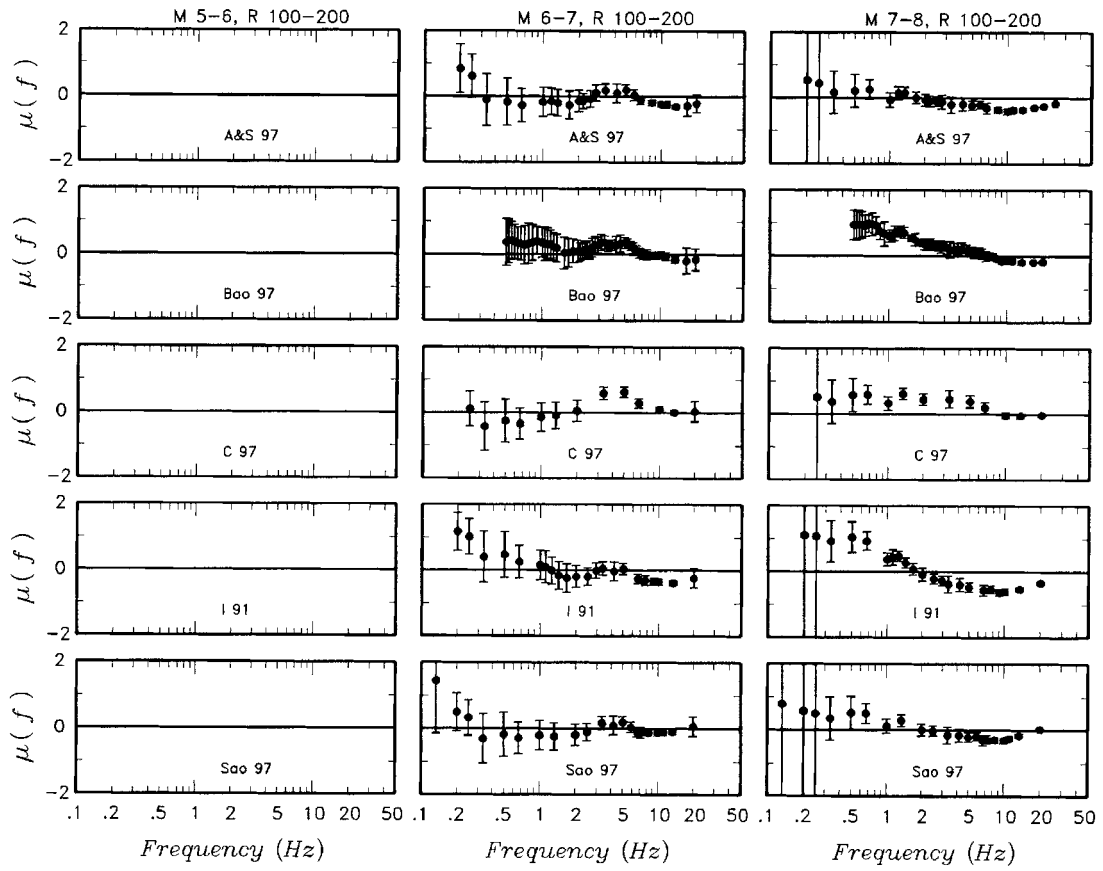


Figure 17d. (Continued)

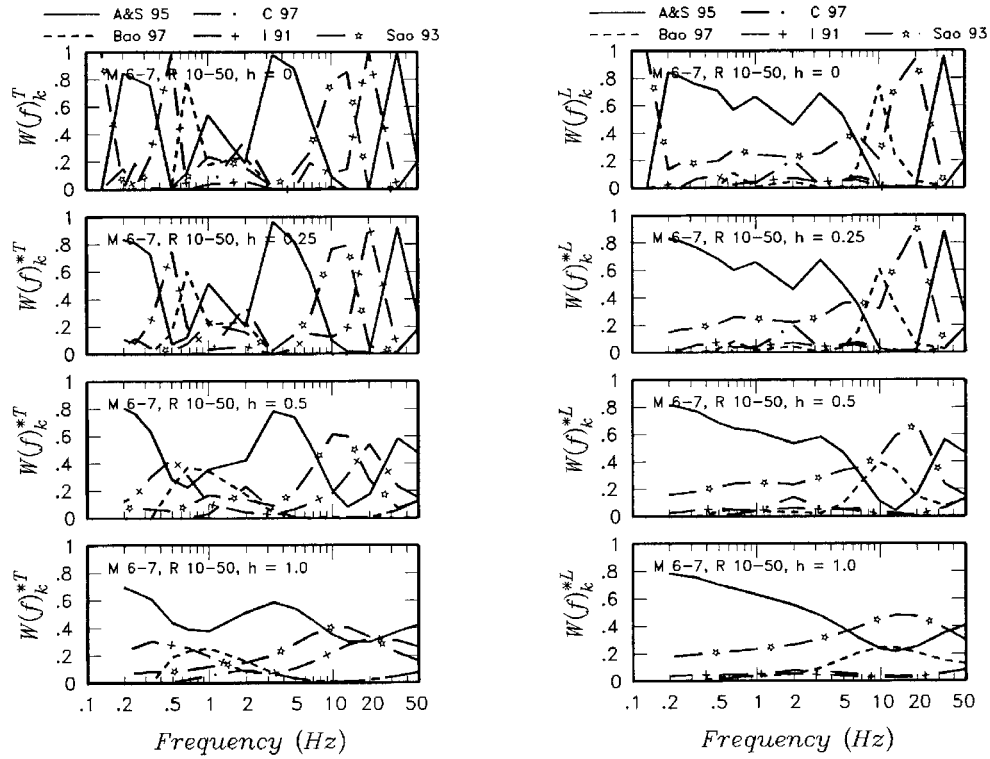


Figure 18. Relative bias ("T") weights (left column) and relative likelihood ("L") weights (right column) for M 6-7 and R 10-50 km magnitude distance bin. Top plot in each column shows weights computed using Equations (4) and (6). The remaining plots show the smoothed weights obtained using Equation (7) with values of  $h$  from 0.25 to 1.0.

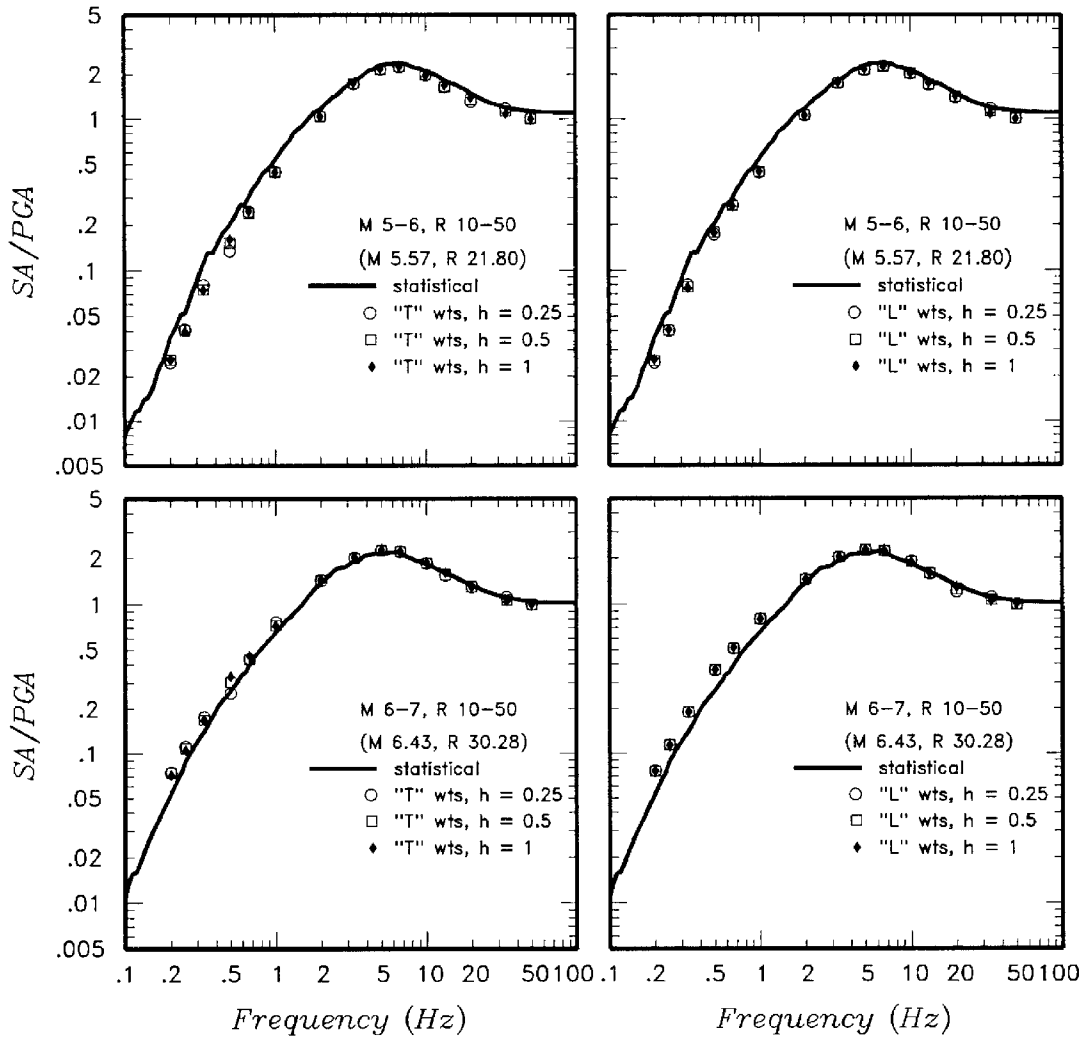


Figure 19. Example comparisons of the statistical spectral shapes from Figure 5 with spectral shapes predicted by the weighted combination of the five attenuation relationships. Weighted empirical spectral shapes are shown for smoothed "T" and "L" weights and values of  $h$  from 0.25 to 1.0.

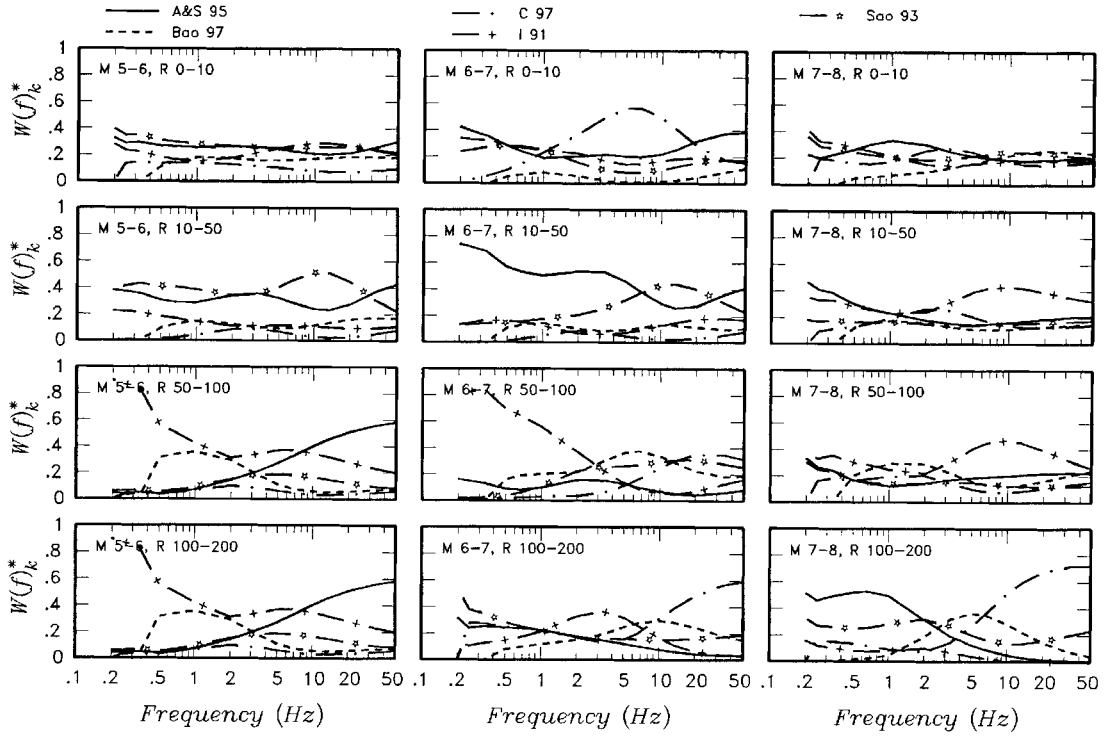


Figure 20. Relative weights used to obtain weighted empirical attenuation spectral shapes. The weights are the average of the smoothed "T" and "L" weights with  $h = 1.0$ .

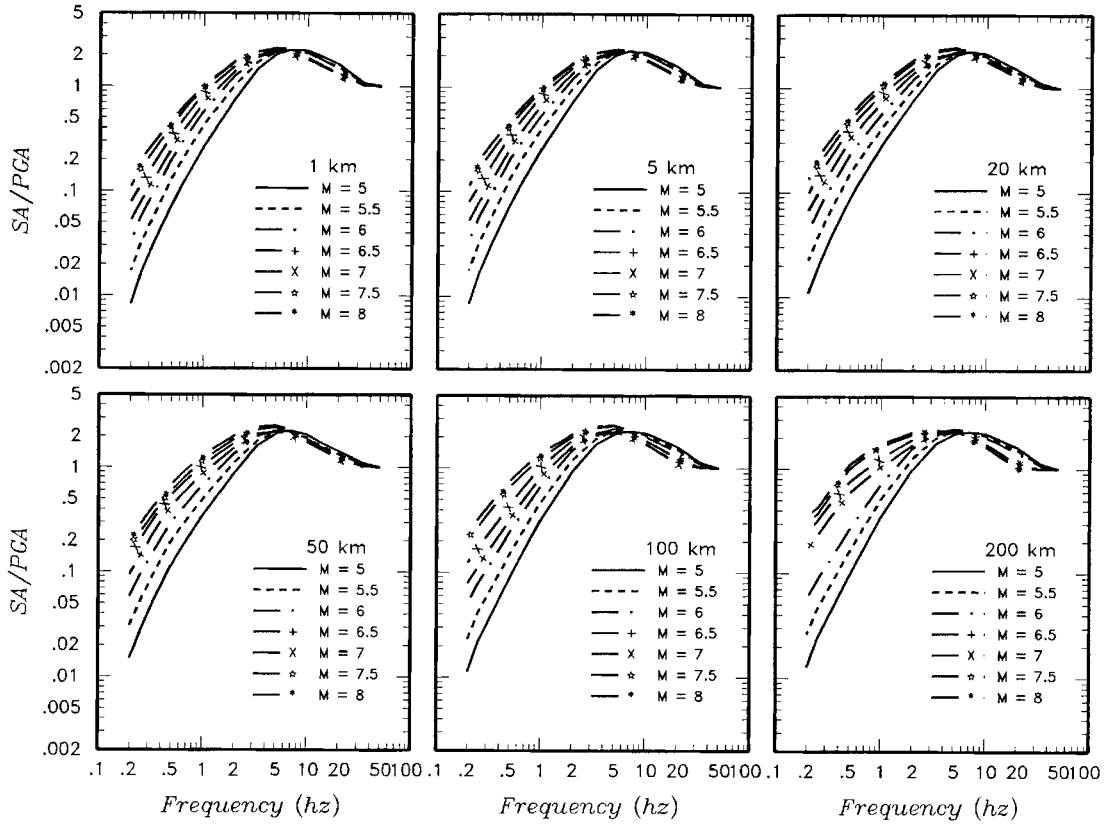


Figure 21. Weighted empirical attenuation response spectral shapes obtained using the relative weights shown on Figure 20.

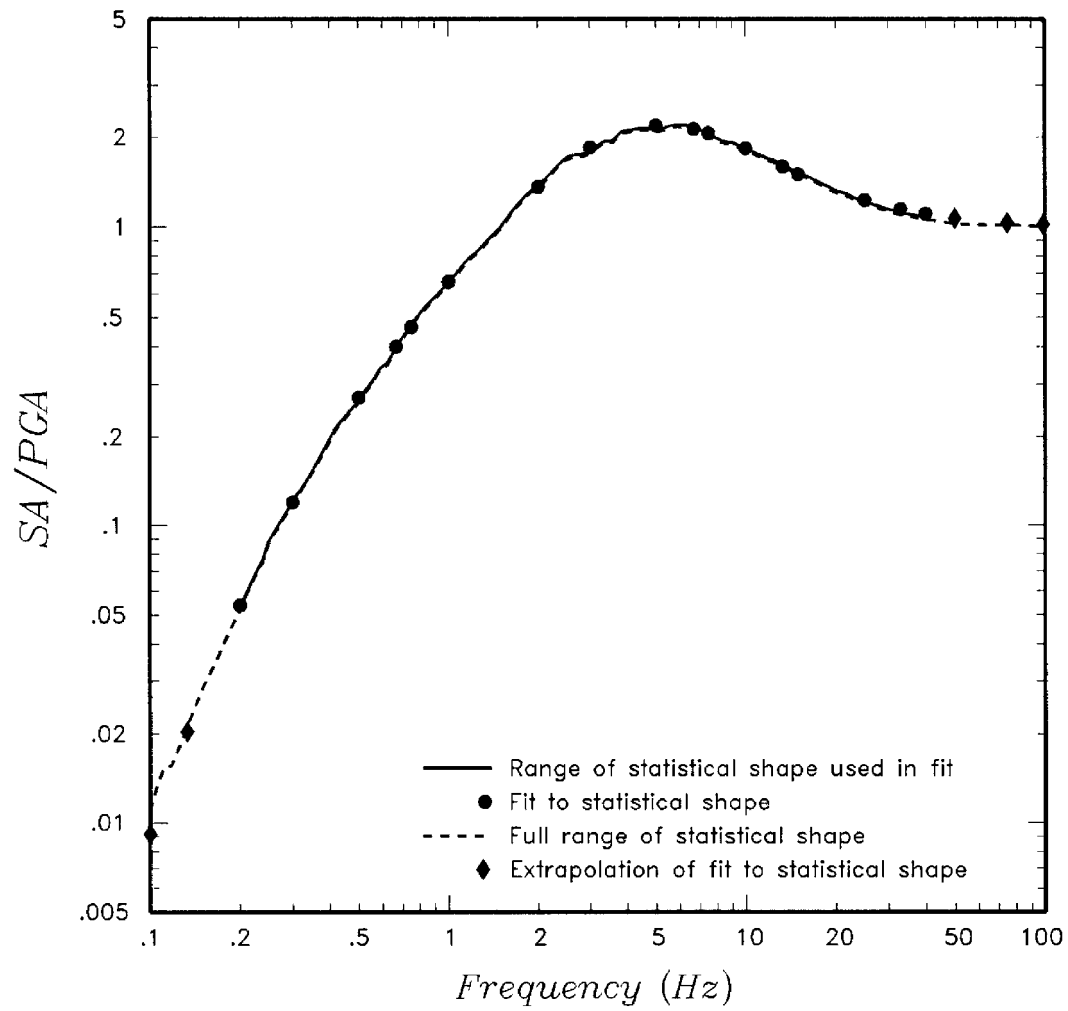


Figure 22. Example of a fit of Equation (8) to an individual spectral shape.

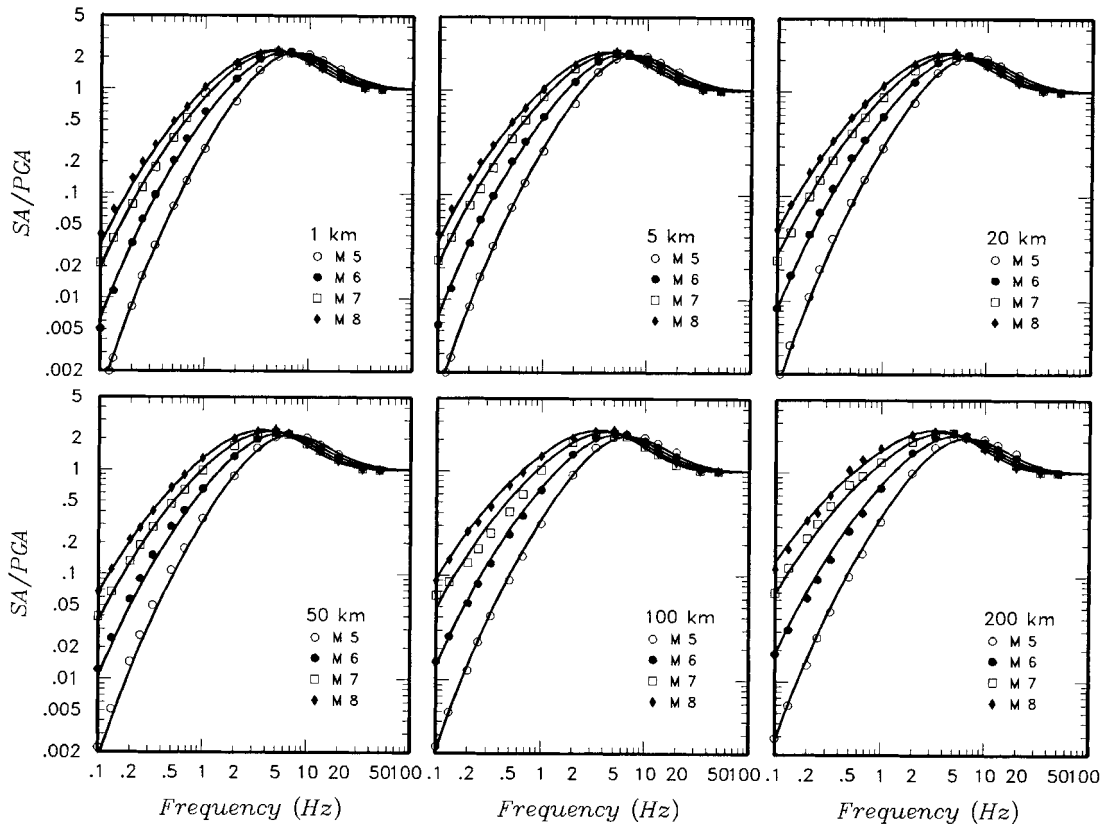


Figure 23. Example WUS response spectral shapes predicted by Equation (8) with parameters listed in Table 3 compared to the weighted empirical spectral shape data used in the fit.

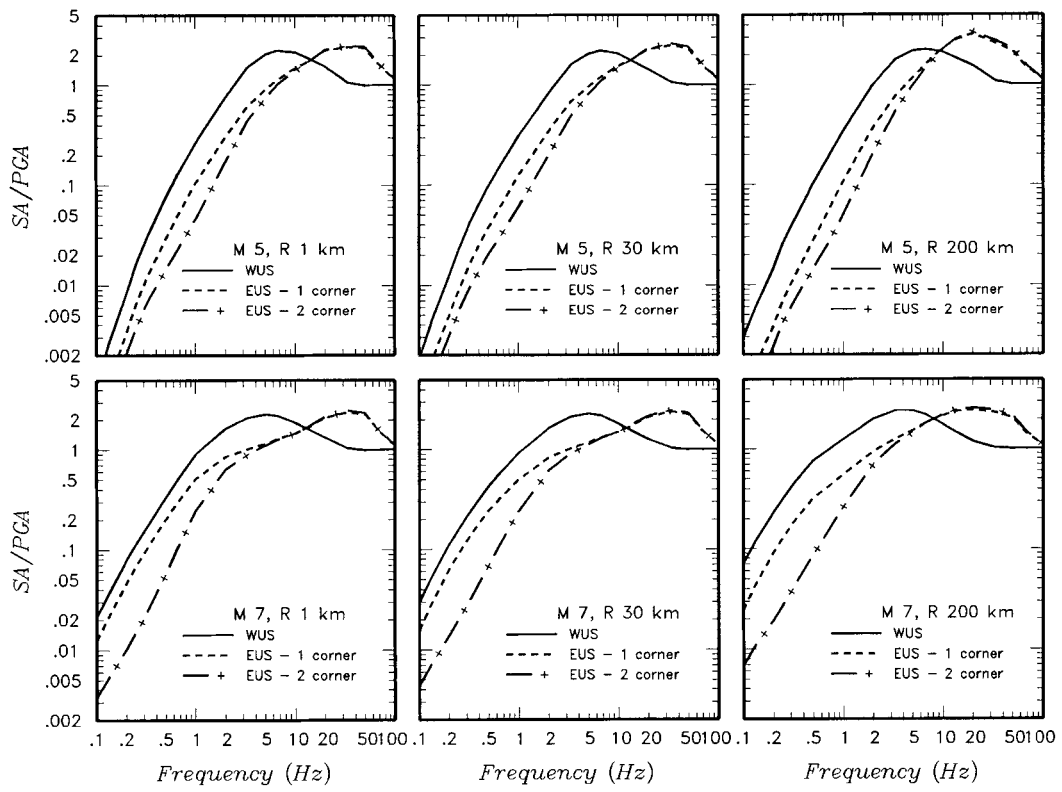


Figure 24. Example EUS response spectral shapes obtained by scaling weighted empirical WUS response spectral shapes.

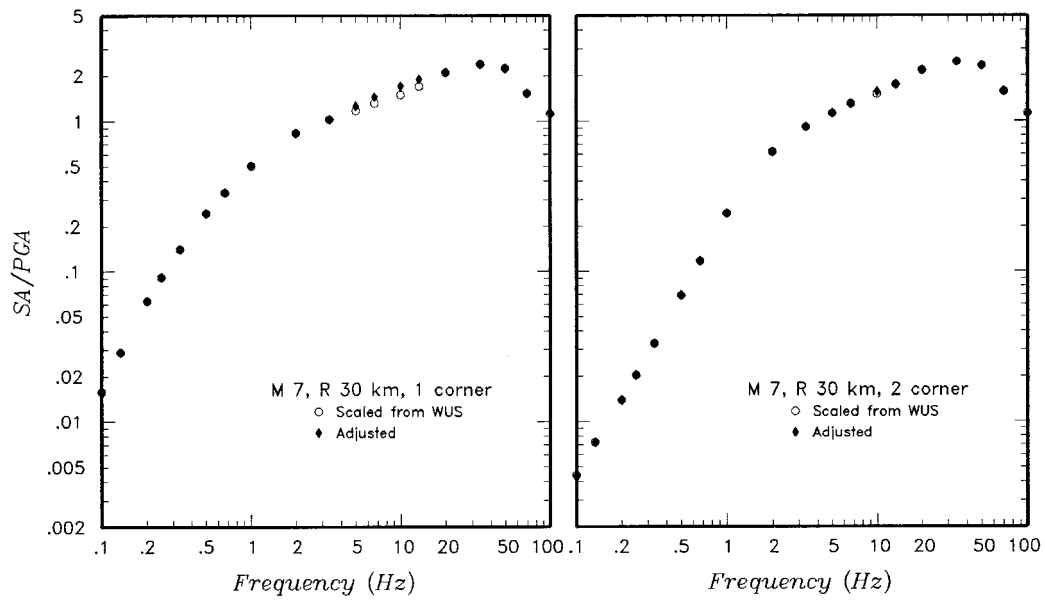


Figure 25. Examples of adjustments to scaled EUS response spectral shapes to remove sag near 10 Hz.

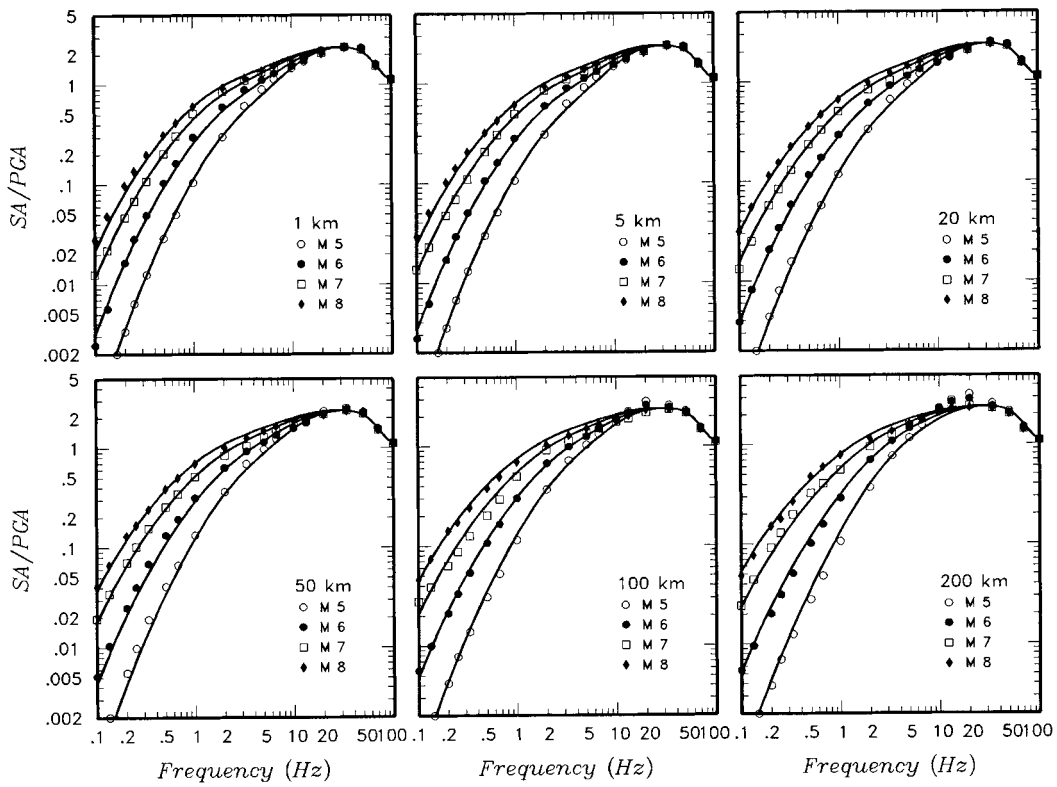


Figure 26. Example EUS single-corner response spectral shapes predicted by Equation (9) with parameters listed in Table 3 compared to the scaled and adjusted EUS spectral shape data used in the fit.

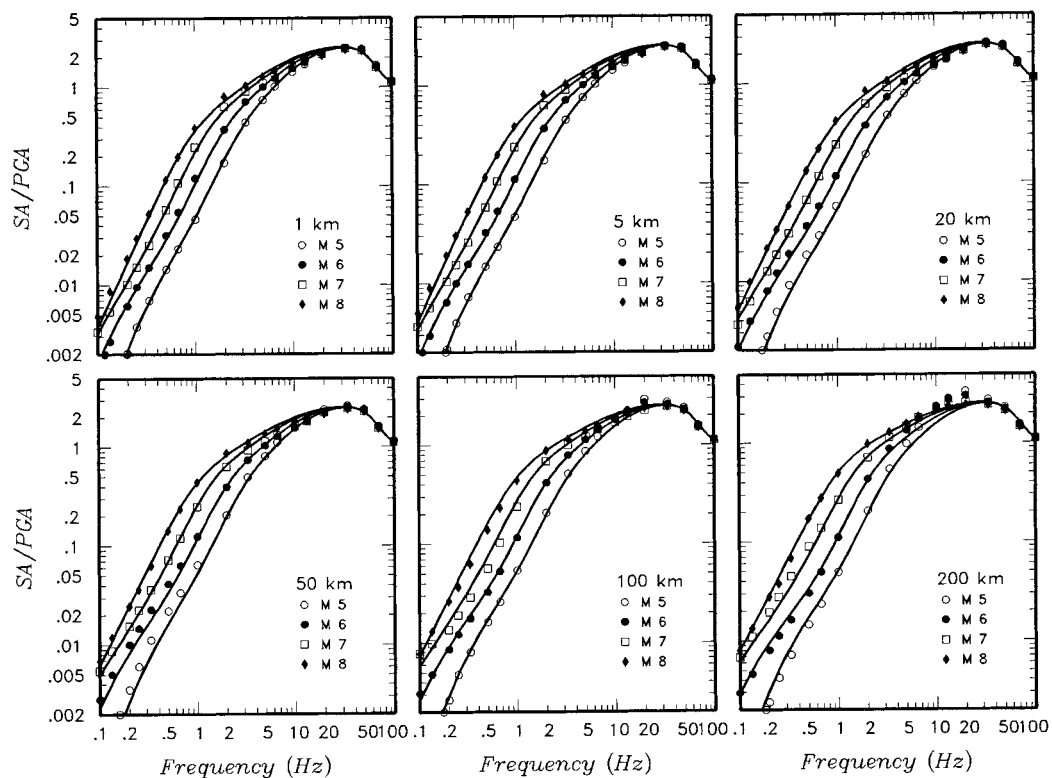
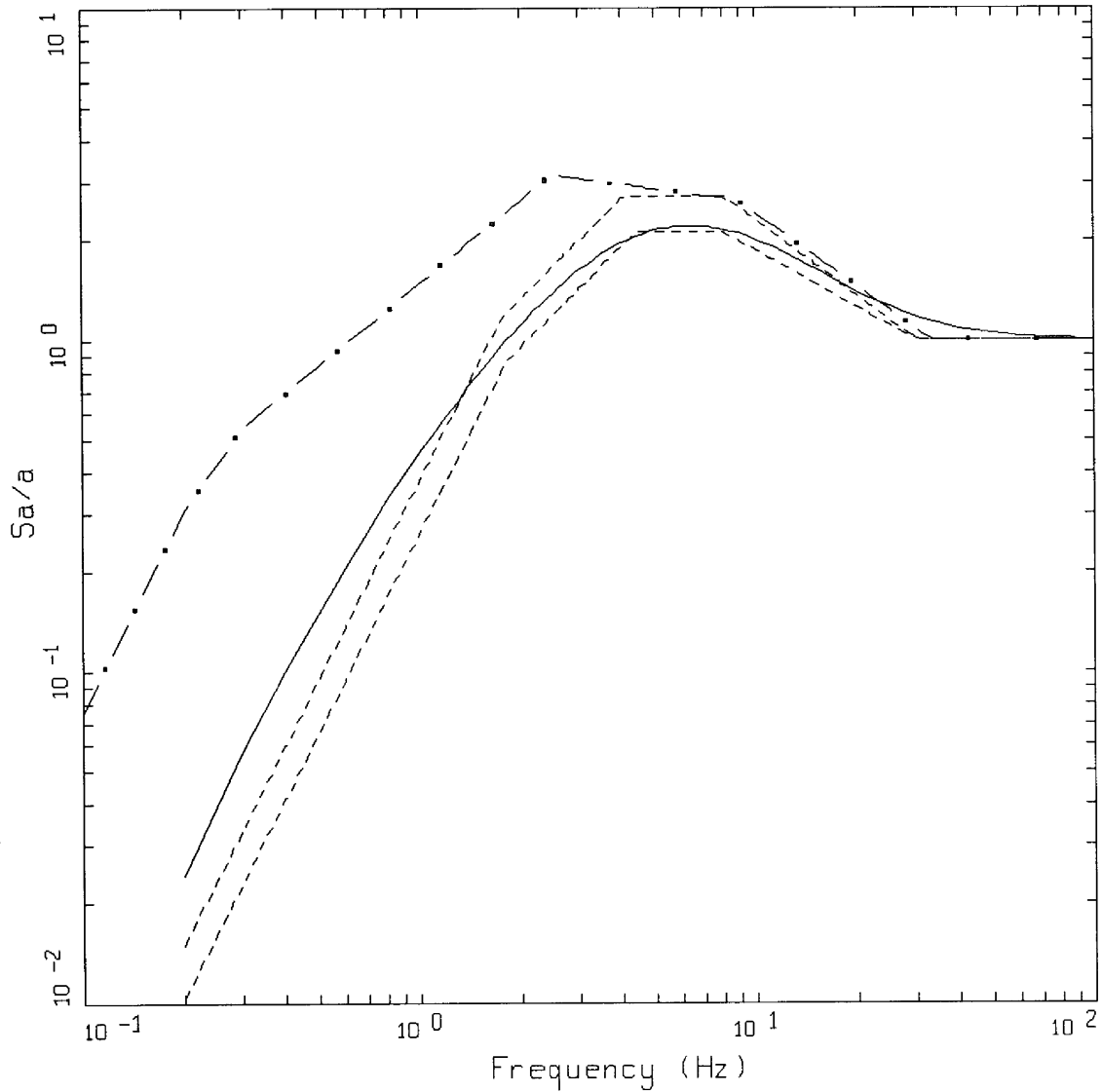


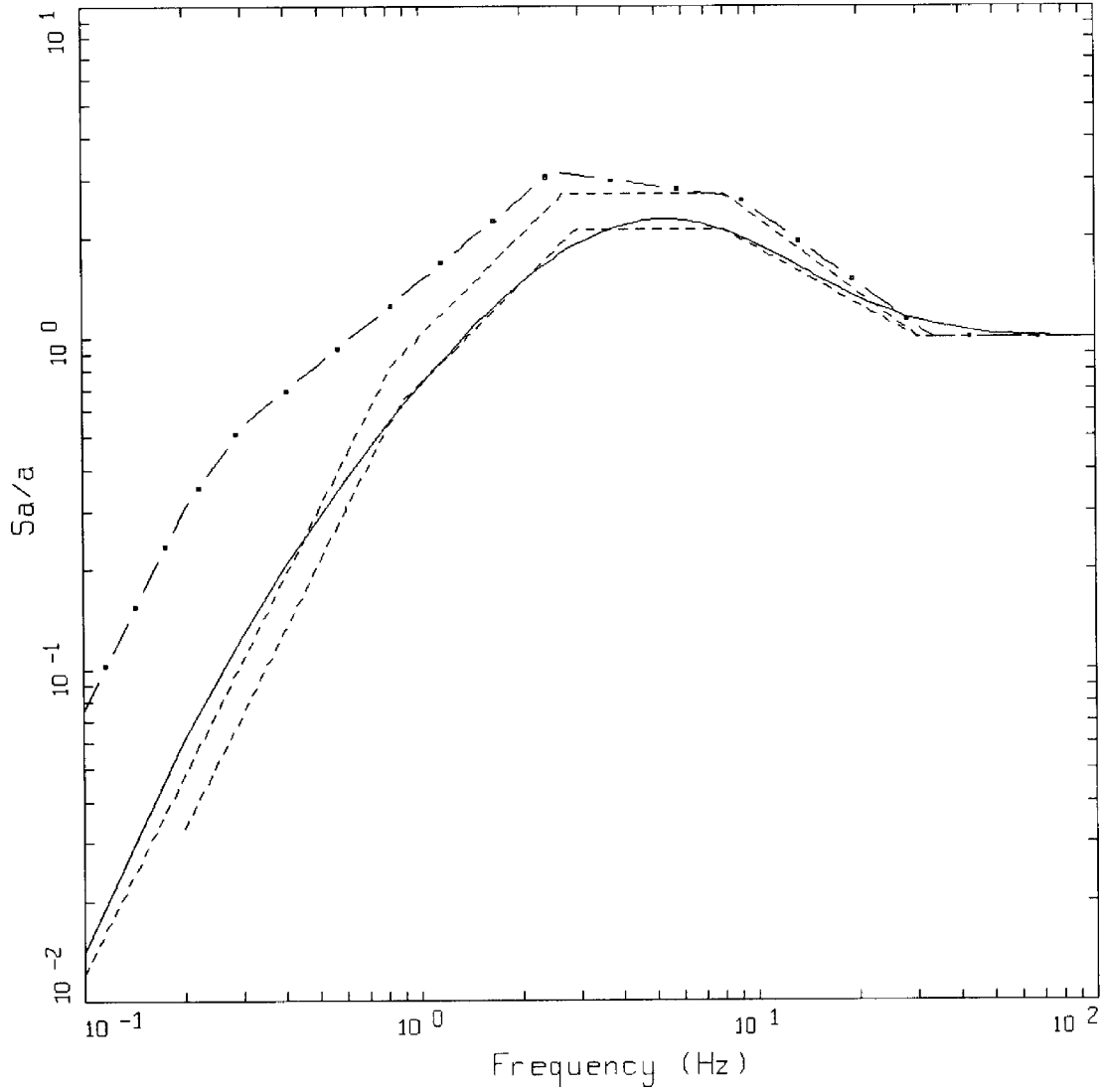
Figure 27. Example EUS double-corner response spectral shapes predicted by Equation (9) with parameters listed in Table 3 compared to the scaled and adjusted EUS spectral shape data used in the fit.



M=5.6, R=19.9 KM, ROCK  
 PGA=0.12 G, PGV=5.39 CM/S, PGD=0.57 CM

- LEGEND
- 5% DAMPED, REVISED NRC SPECTRA WUS, 50th percentile
  - - - 5% DAMPED, NEWMARK&HALL SPECTRA, 50th percentile
  - · - 5% DAMPED, NEWMARK&HALL SPECTRA, 84th percentile
  - · · 5% DAMPED, REG GUIDE 1.60

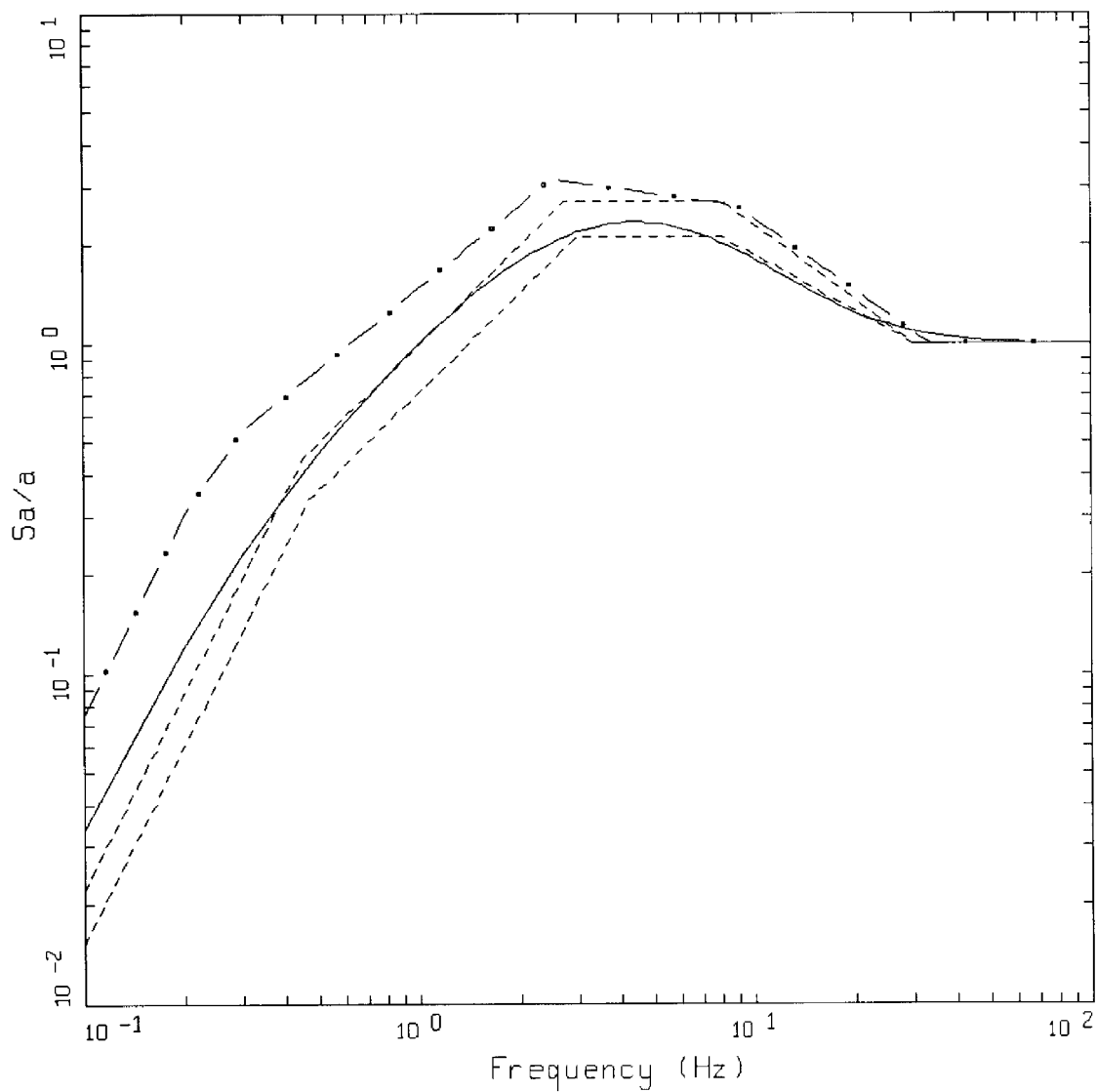
Figure Set 28a. Comparison of revised WUS shapes (solid line) to current regulatory guidance R.G. 1.60 and Newmark-Hall shapes for the distance bin 0 to 50 km and for mean magnitudes 5.6, 6.4, and 7.3. Peak parameters are taken from Table 1 for the Newmark-Hall shapes.



M=6.4, R=27.4 KM, ROCK  
 PGA=0.15 G, PGV=10.27 CM/S, PGD=2.24 CM

- LEGEND
- 5% DAMPED, REVISED NRC SPECTRA, 50th percentile
  - - - 5% DAMPED, NEWMARK&HALL SPECTRA WUS, 50th percentile
  - · - 5% DAMPED, NEWMARK&HALL SPECTRA, 84th percentile
  - · - 5% DAMPED, REG GUIDE 1.60

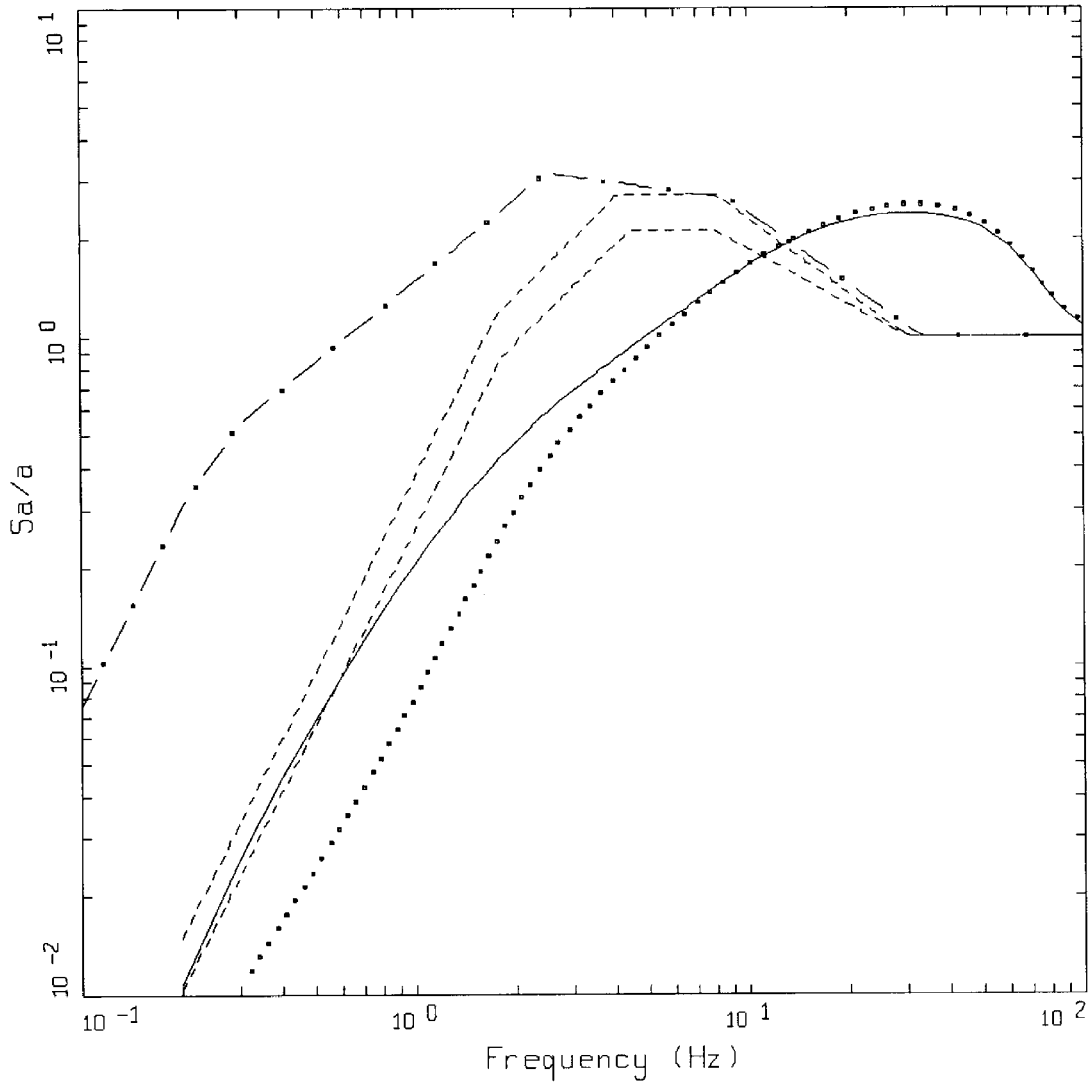
Figure 28b. (Continued)



M=7.3, R=17.6 KM, ROCK  
 PGA=0.40 G, PGV=26.82 CM/S, PGD=10.89 CM

- LEGEND
- 5% DAMPED, REVISED NRC SPECTRA, 50th percentile
  - - - 5% DAMPED, NEWMARK&HALL SPECTRA WUS, 50th percentile
  - · - 5% DAMPED, NEWMARK&HALL SPECTRA, 84th percentile
  - · - 5% DAMPED, REG GUIDE 1.6D

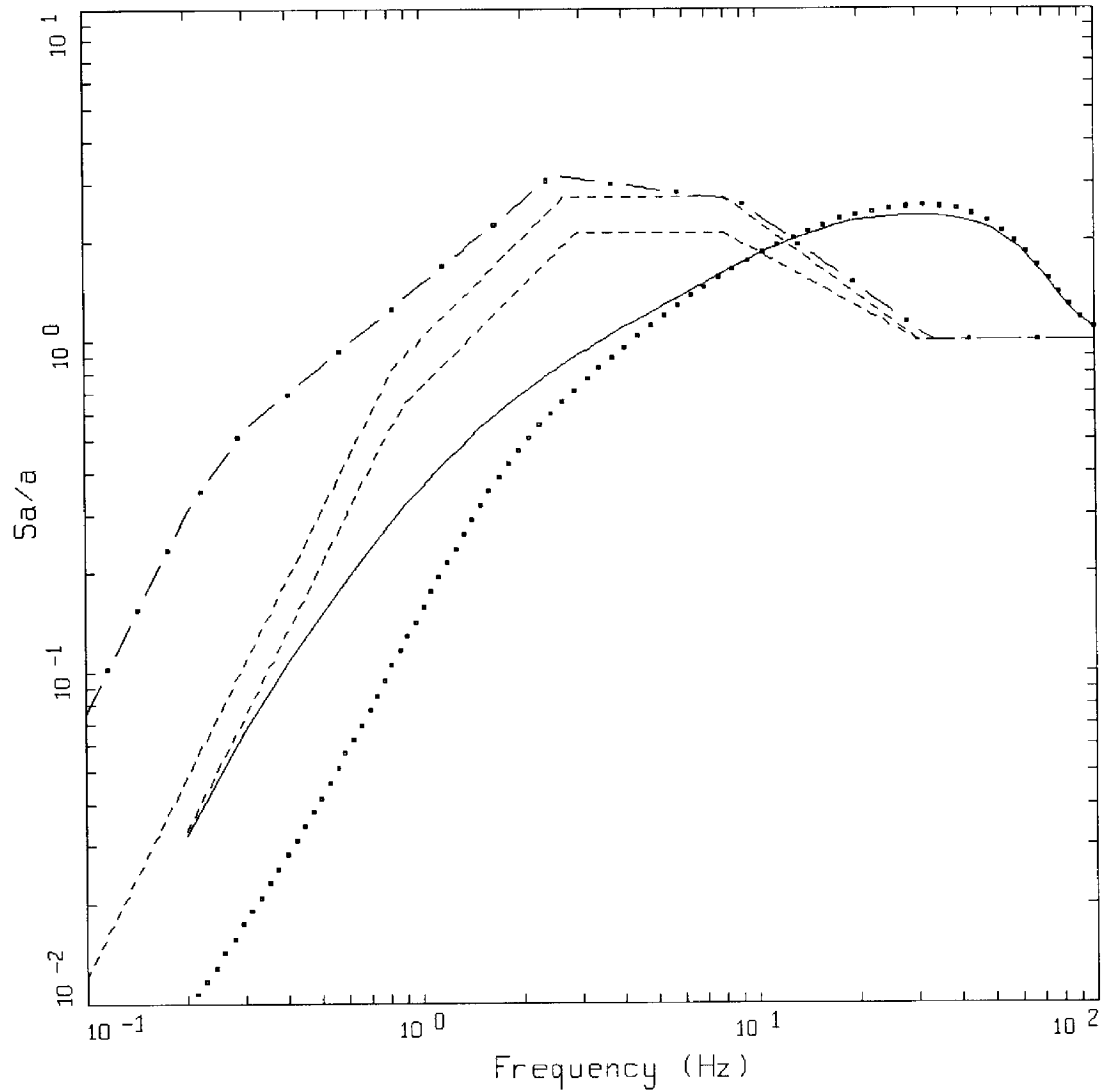
Figure 28c. (Continued)



M=5.6, R=19.9 KM, ROCK  
 PGA=0.12 G, PGV=5.39 CM/S, PGD=0.57 CM

- LEGEND
- 5% DAMPED, REVISED NRC SPECTRA CEUS 1 CORNER, 50th percentile
  - 5% DAMPED, REVISED NRC SPECTRA CEUS 2 CORNER, 50th percentile
  - 5% DAMPED, NEWMARK&HALL SPECTRA, 50th percentile
  - 5% DAMPED, NEWMARK&HALL SPECTRA, 84th percentile
  - - - - 5% DAMPED, REG GUIDE 1.60

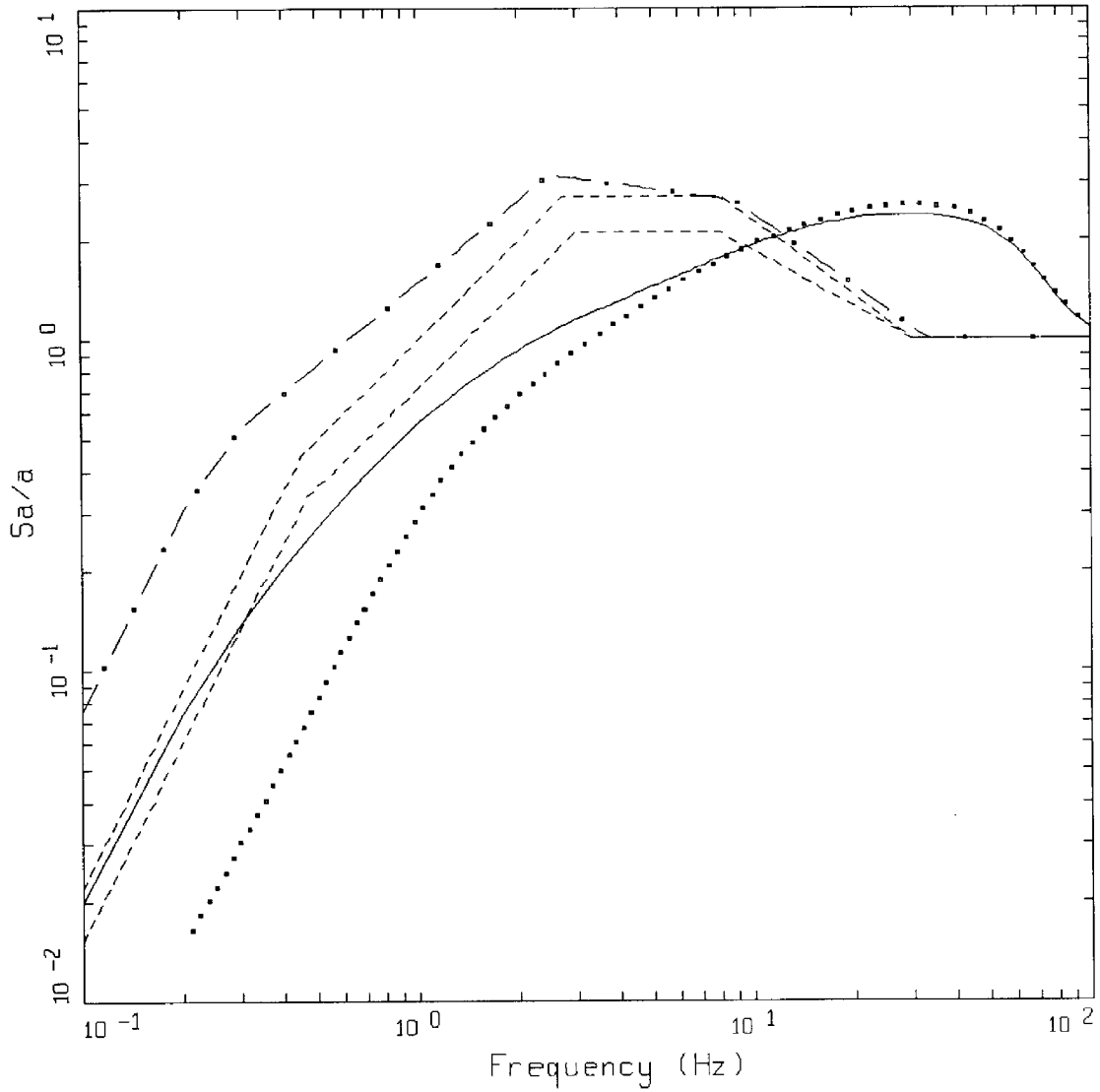
Figure Set 29a. Comparison of revised CEUS shapes (solid line) to current regulatory guidance R.G. 1.60 and Newmark-Hall shapes for the distance bin 0 to 50 km and for mean magnitudes 5.6, 4.4, and 7.3. Peak parameters are taken from Table 1 for the Newmark-Hall shapes.



M=6.4, R=27.4 KM, ROCK  
 PGA=0.15 G, PGV=10.27 CM/S, PGD=2.24 CM

- LEGEND
- 5% DAMPED, REVISED NRC SPECTRA CEUS 1 CORNER, 50th percentile
  - ..... 5% DAMPED, REVISED NRC SPECTRA CEUS 2 CORNER, 50th percentile
  - 5% DAMPED, NEWMARK&HALL SPECTRA, 50th percentile
  - - - - - 5% DAMPED, NEWMARK&HALL SPECTRA, 84th percentile
  - . - . - 5% DAMPED, REG GUIDE 1.60

Figure 29b. (Continued)



M=7.3, R=17.6 KM, ROCK  
 PGA=0.40 G, PGV=26.82 CM/S, PGD=10.89 CM

- LEGEND
- 5% DAMPED, REVISED NRC SPECTRA CEUS 1 CORNER, 50th percentile
  - ..... 5% DAMPED, REVISED NRC SPECTRA CEUS 2 CORNER, 50th percentile
  - 5% DAMPED, NEWMARK&HALL SPECTRA, 50th percentile
  - - - - 5% DAMPED, NEWMARK&HALL SPECTRA, 84th percentile
  - . - . 5% DAMPED, REG GUIDE 1.6D

Figure 29c. (Continued)

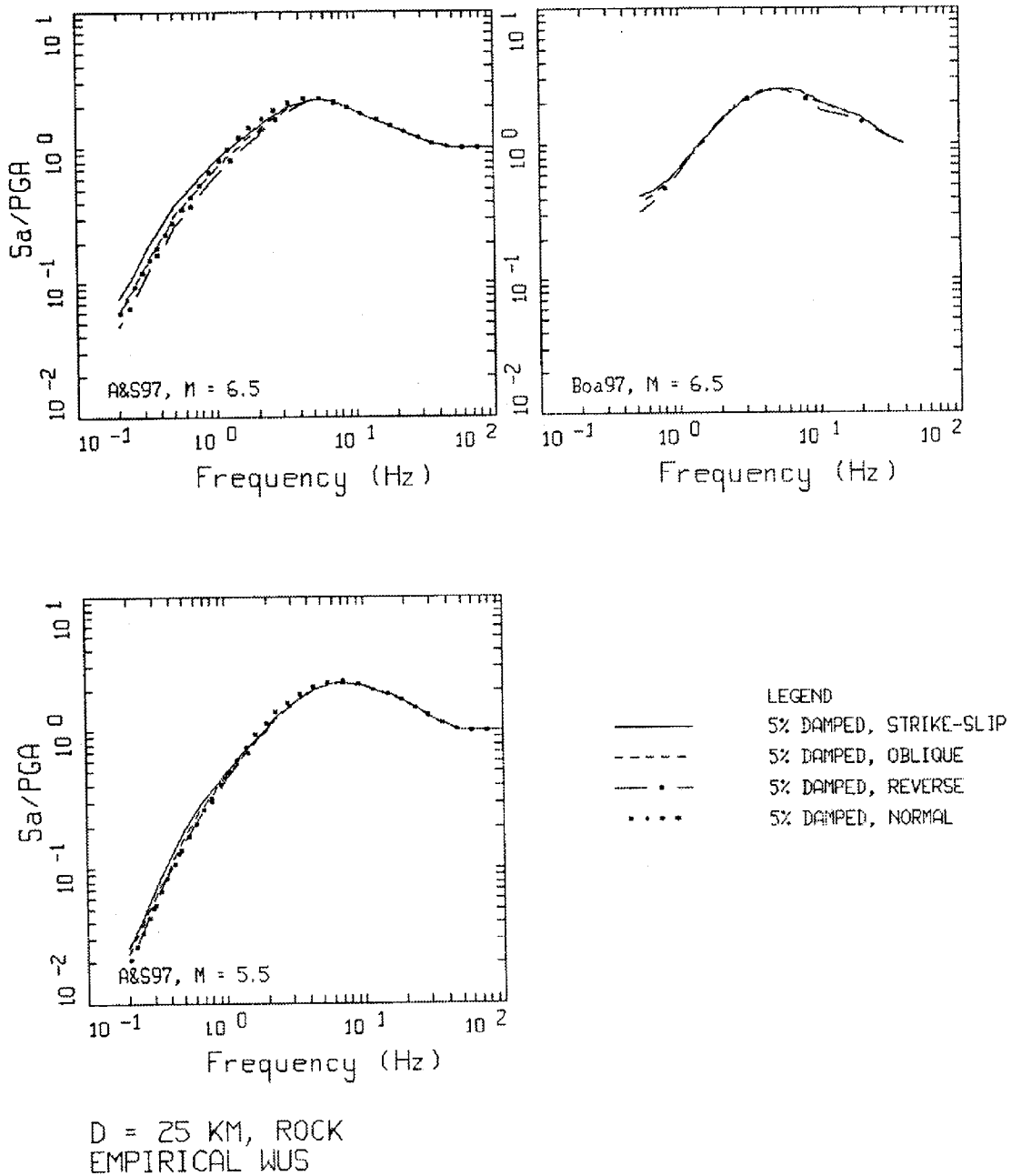
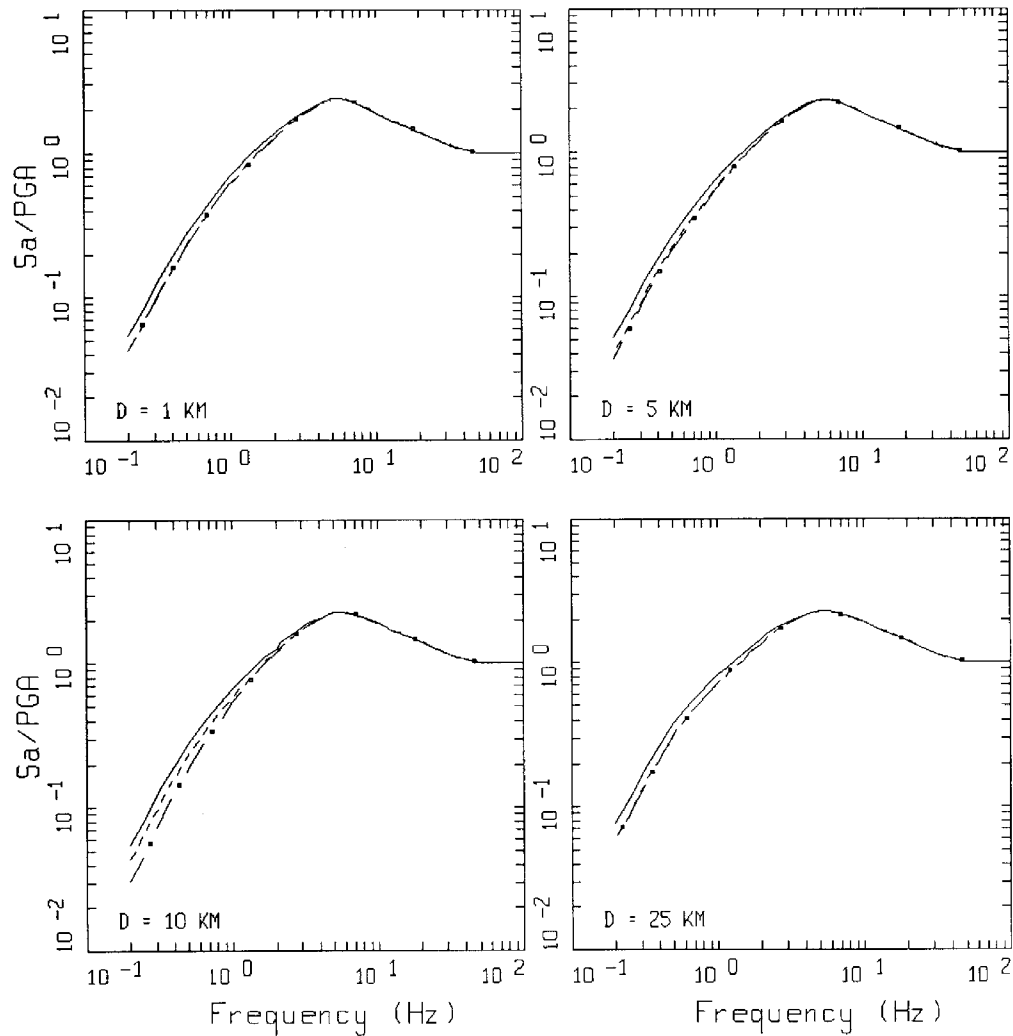


Figure 30. Predicted effects of source mechanism on spectral shapes for empirical WUS attenuation relations. For the A&S 97 empirical relation, the frequency dependence differs for small and large magnitudes.

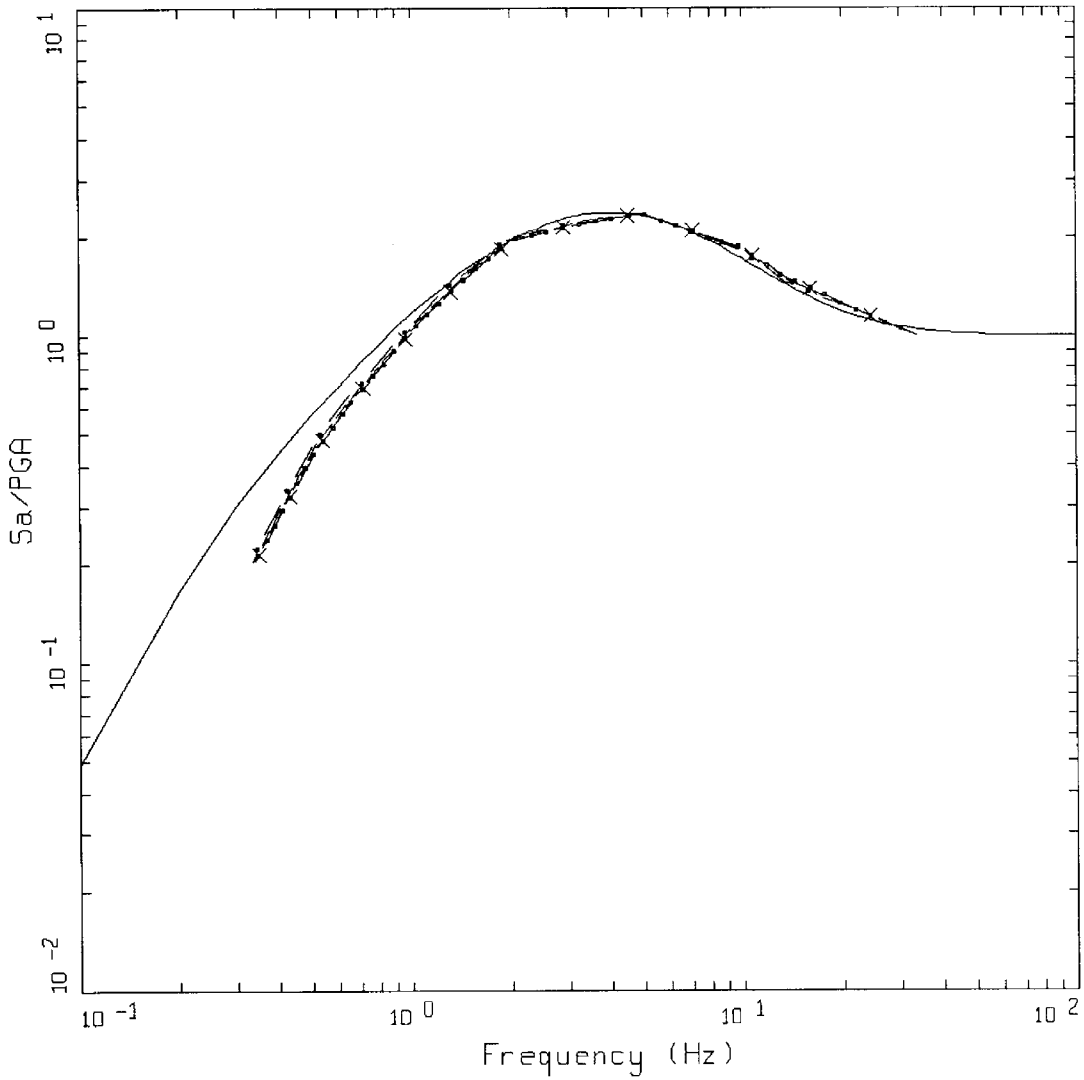


M=6.5, D=25 KM, ROCK

EMPIRICAL WUS

- LEGEND
- 5% DAMPED, STRIKE SLIP
  - 5% DAMPED, OBLIQUE, FOOT WALL
  - · - · 5% DAMPED, OBLIQUE, HANGING WALL

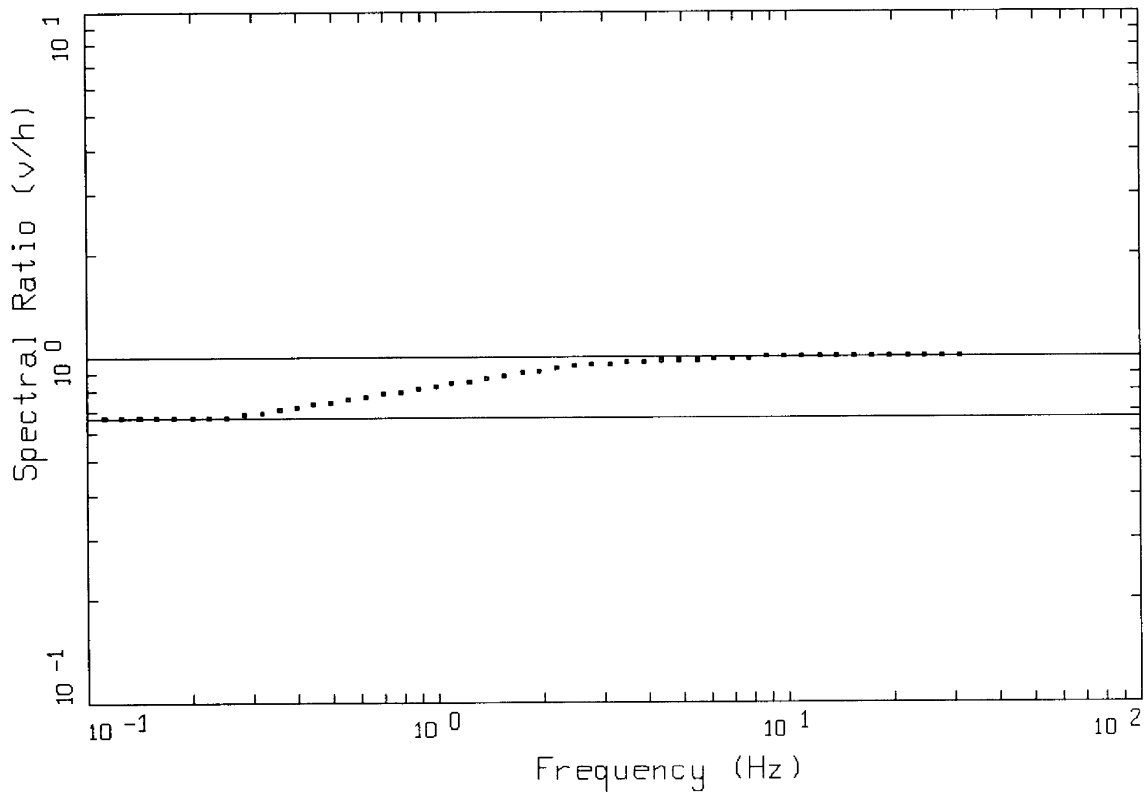
Figure 31. Predicted effects of site location (hanging wall versus foot wall) for oblique-slip source mechanisms on spectral shapes compared to strike-slip spectral shapes for an empirical WUS attenuation relation (A&S, 97).



M=9.0, ROCK, H=25 KM, INTERFACE

- LEGEND
- 5% DAMPED, REVISED NRC SPECTRA WUS, M = 8.0, DISTANCE = 25.0 KM
  - X — 5% DAMPED, M = 9.0, DISTANCE=1 KM, PGA=0.337 g
  - 5% DAMPED, M = 9.0, DISTANCE=5 KM, PGA=0.324 g
  - 5% DAMPED, M = 9.0, DISTANCE=10 KM, PGA=0.309 g
  - 5% DAMPED, M = 9.0, DISTANCE=25 KM, PGA=0.269 g
  - • — 5% DAMPED, M = 9.0, DISTANCE=50 KM, PGA=0.217 g

Figure 32. Comparison of revised shape for **M** 8.0 at  $D=25$  km to empirical subduction zone shapes for **M** 9.0 at a suite of distances (Youngs et al., 1997).



REGULATORY GUIDE 1.60  
 V/H RATIO

	LEGEND
.....	R.G. 1.60
————	1
————	2/3

Figure 33. V/H ratio for 5% damped response spectra implied by the R.G. 1.60 design motions.

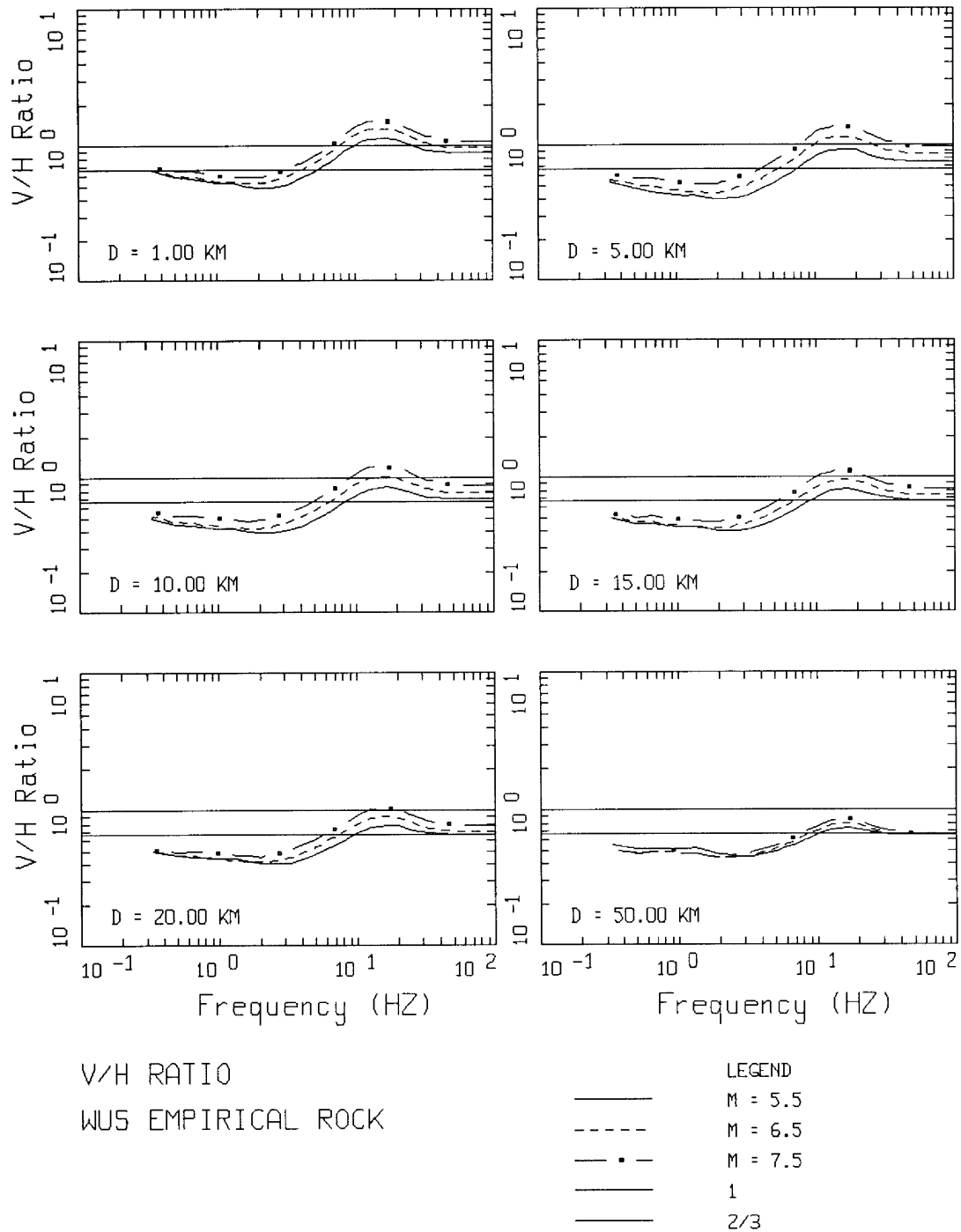
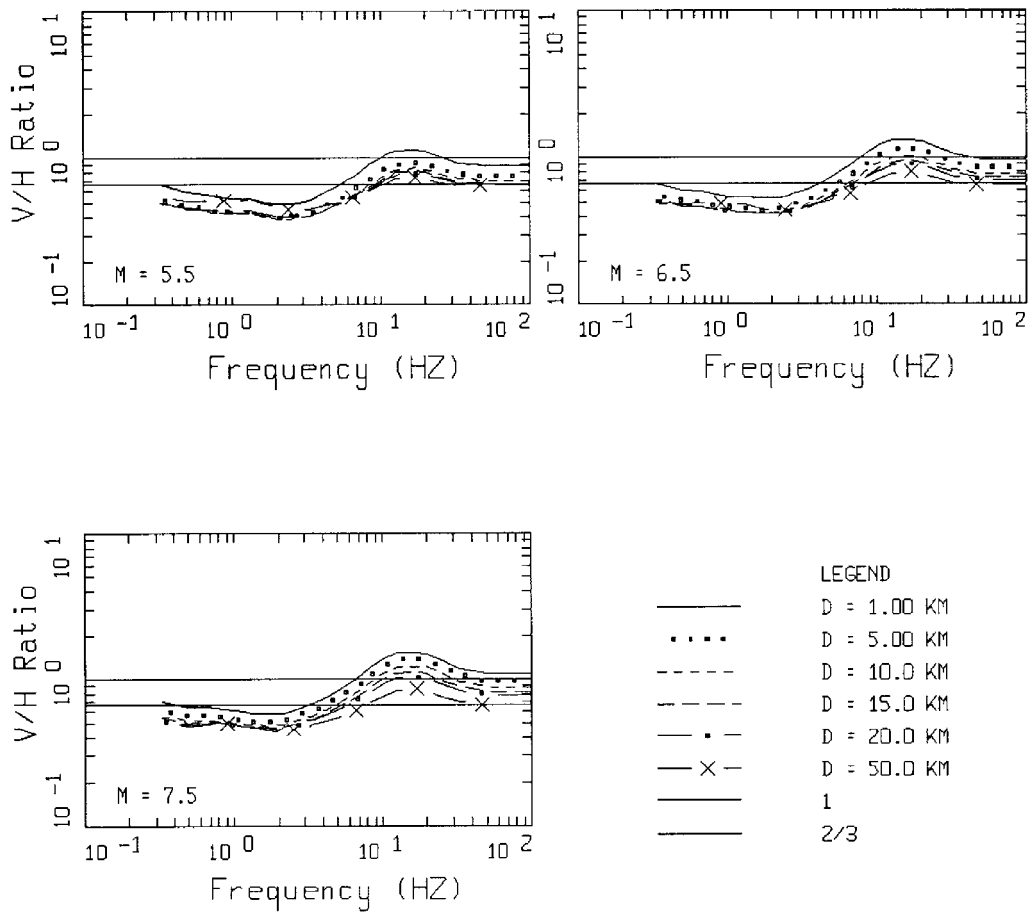
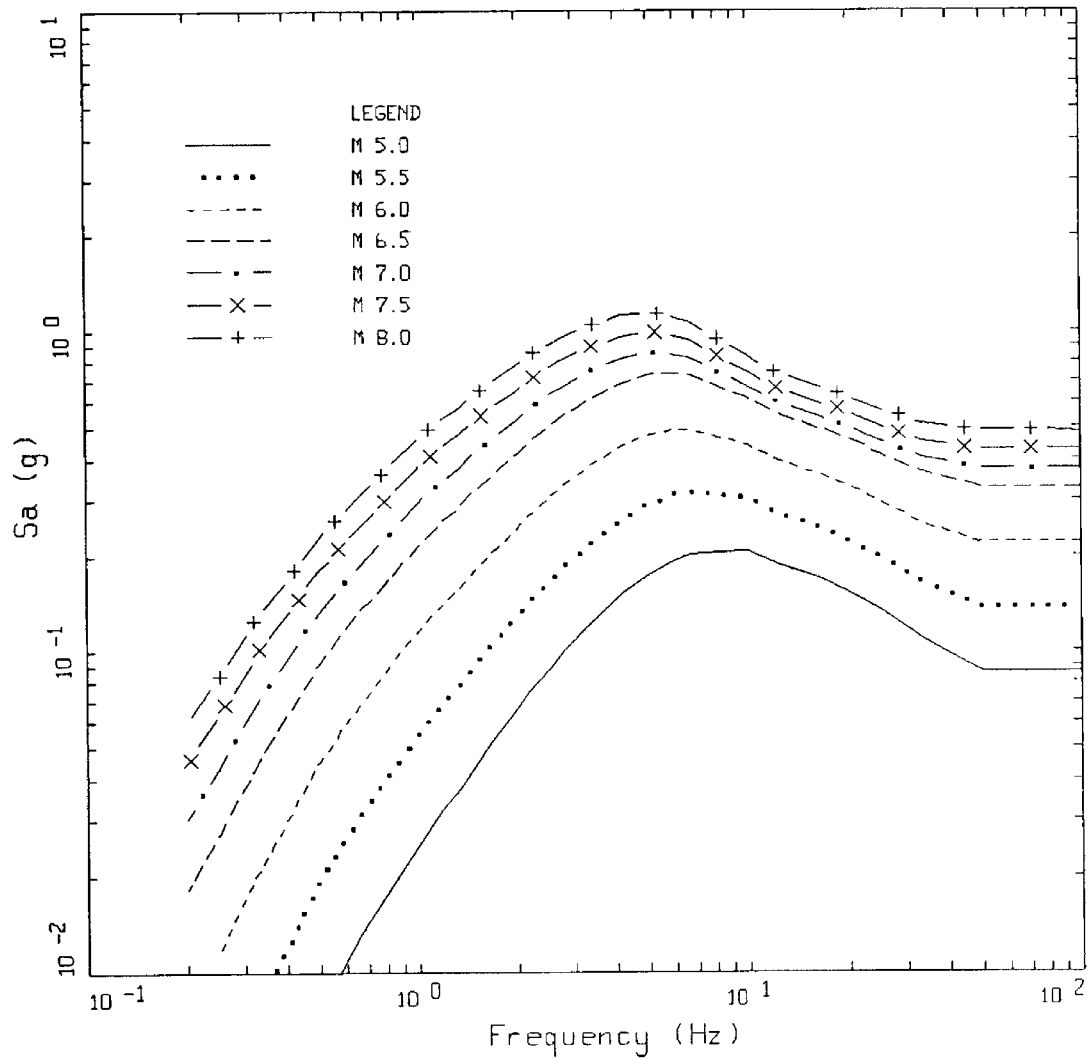


Figure 34. Average V/H ratio (5% damped) magnitude dependencies based on the A&S 97, C 97, and Sao 97 empirical WUS rock attenuation relations for a suite of distances.



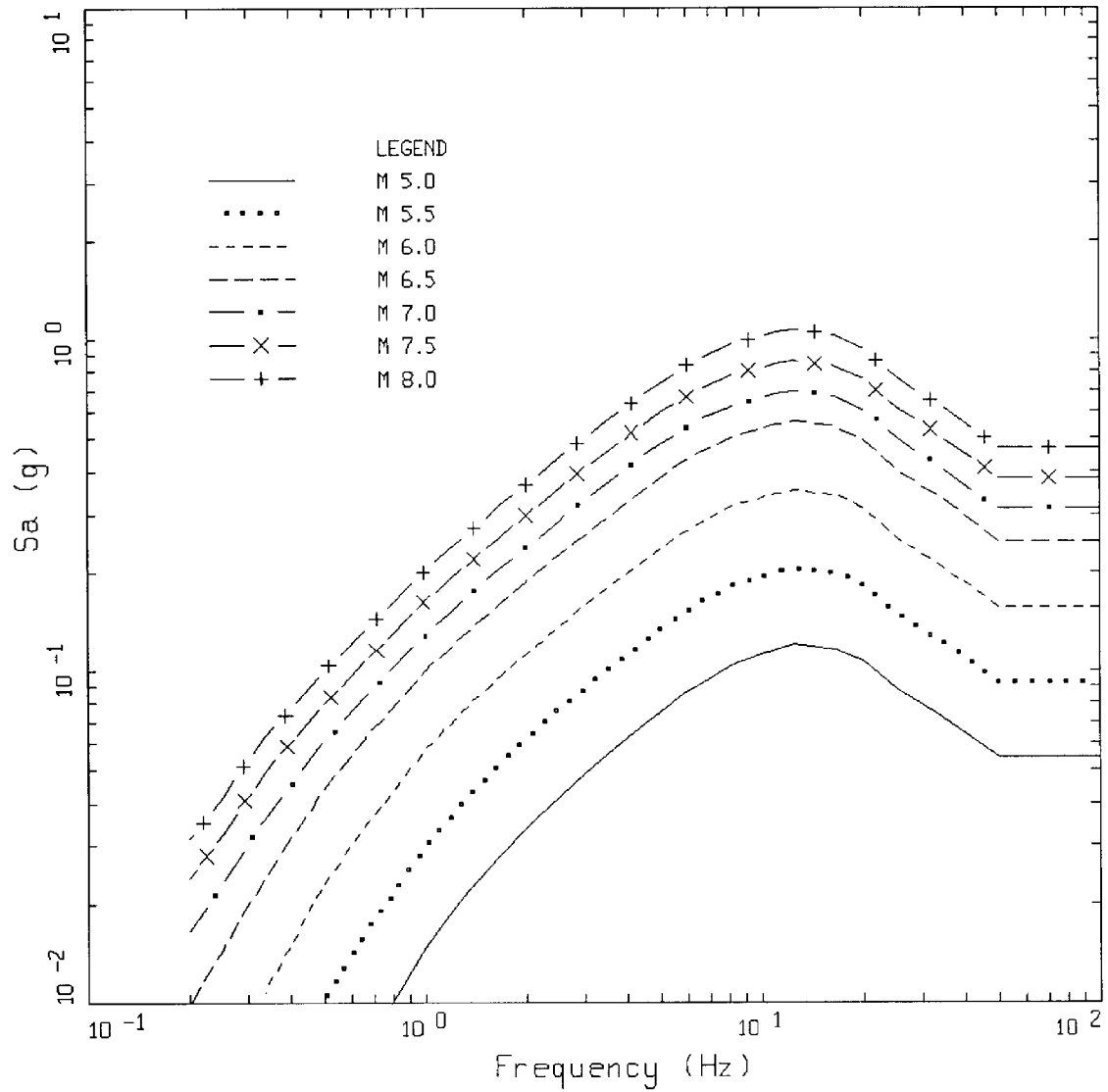
V/H RATIO  
WUS EMPIRICAL ROCK

Figure 35. Average V/H ratio (5% damped) distance dependencies based on the A&S 97, C 97, and Sao 97 empirical WUS rock attenuation relations for a suite of magnitudes.



EMPIRICAL, ROCK, HORIZONTAL  
 D = 10.0

Figure 36. Magnitude dependence of 5% damped horizontal component response spectral acceleration at a rupture distance of 10 km for a WUS rock empirical attenuation relation (A&S 97).



EMPIRICAL, ROCK, VERTICAL  
 D = 10.0

Figure 37. Magnitude dependence of 5% damped vertical component response spectral acceleration at a rupture distance of 10 km for a WUS rock empirical attenuation relation (A&S 97).

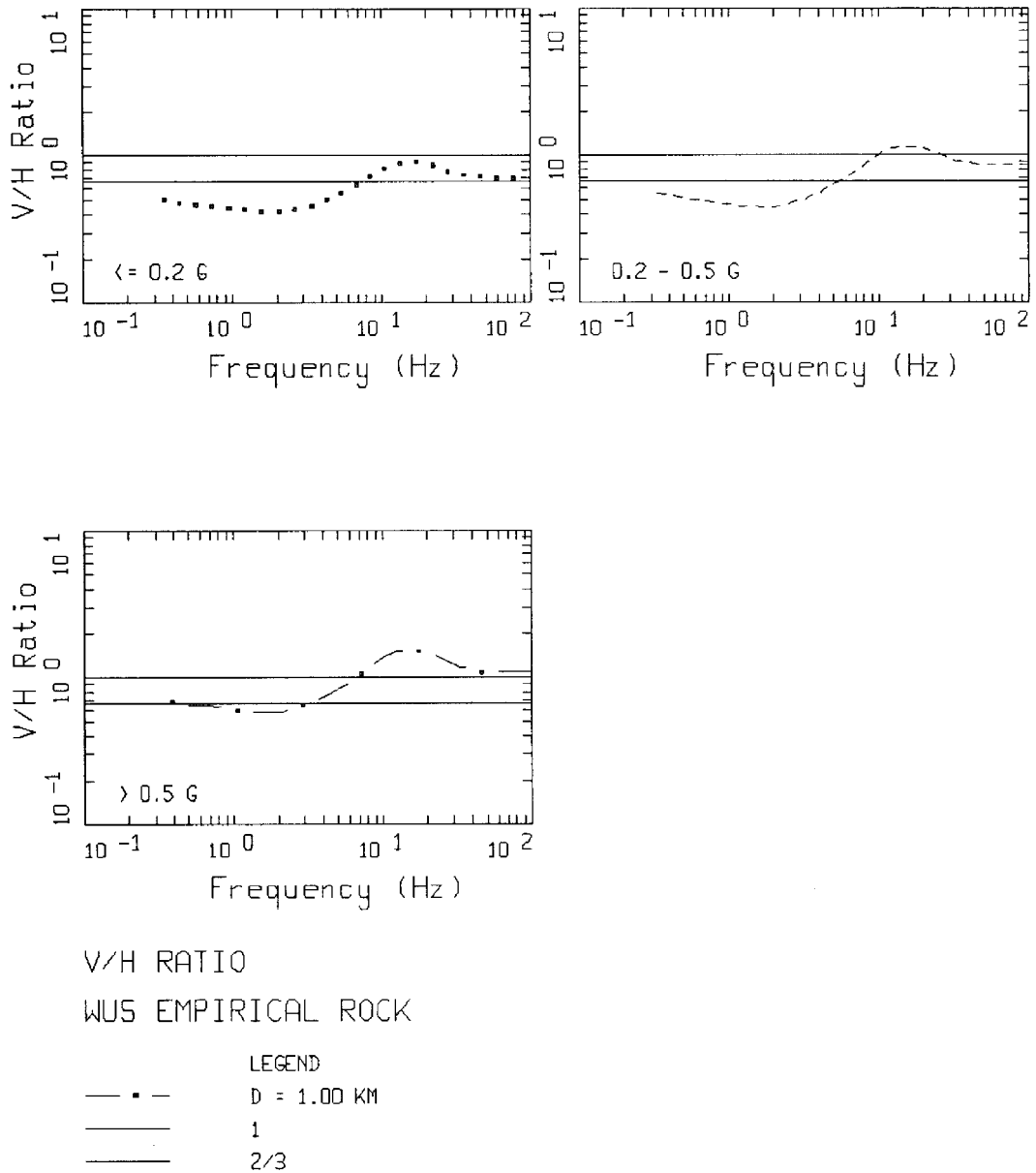
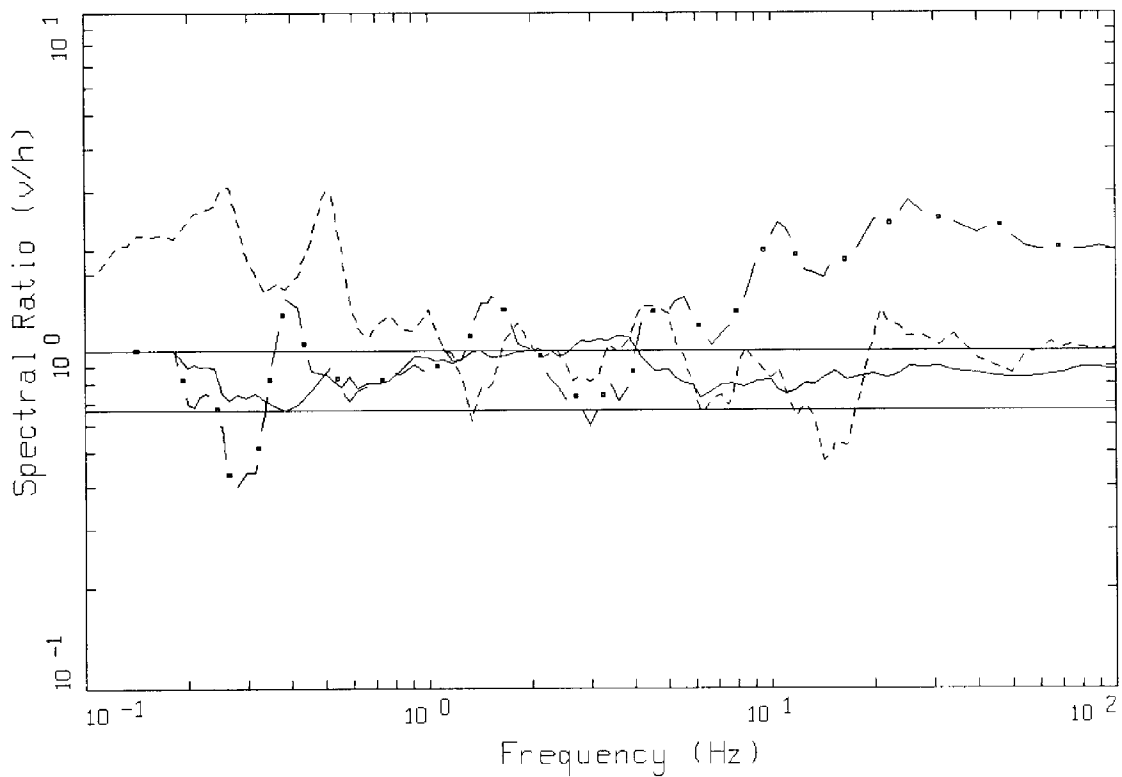


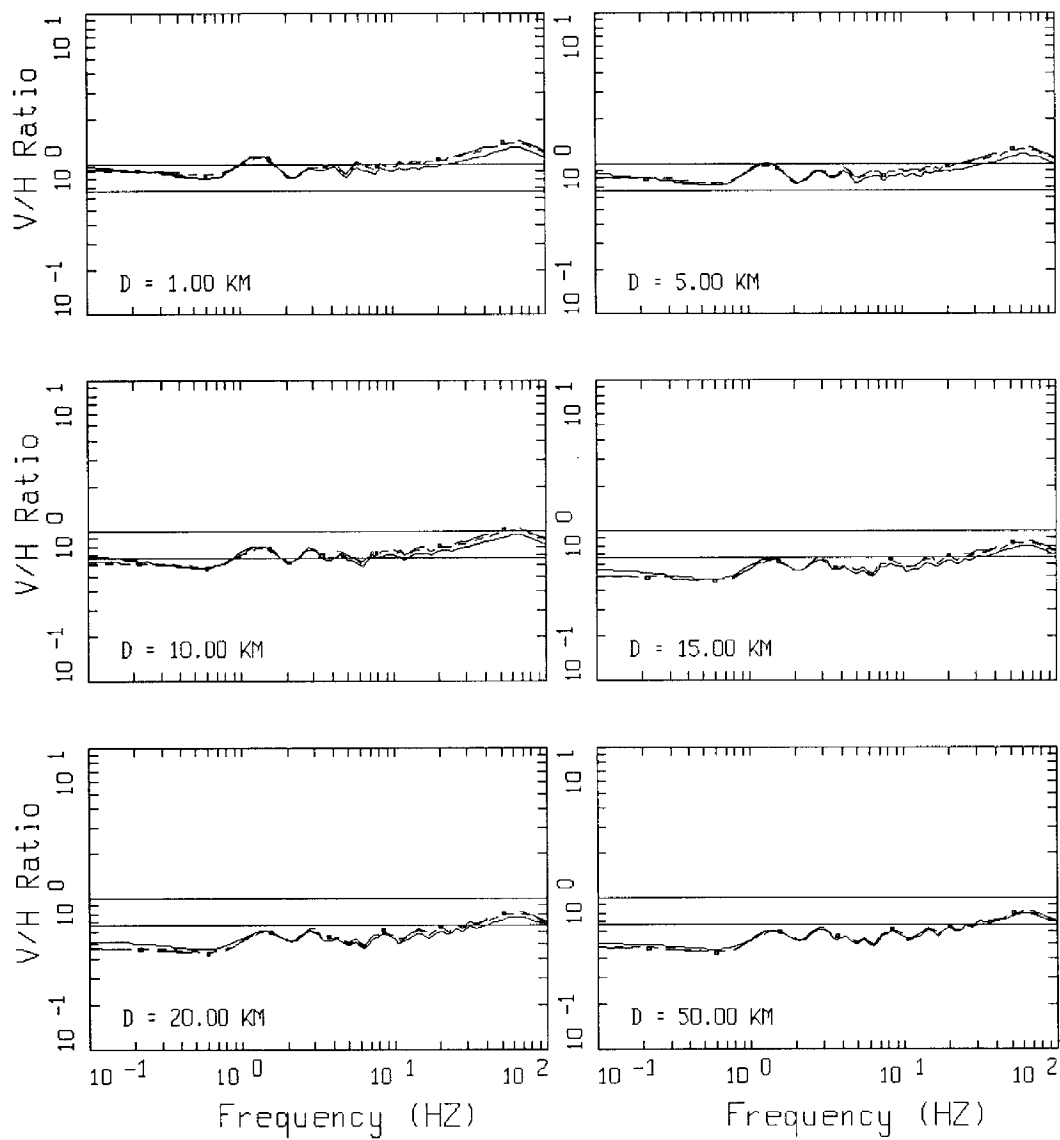
Figure 38. Recommended V/H ratios (5% damped) for WUS soft rock site conditions for ranges in horizontal component peak accelerations.



## EMPIRICAL CEUS ROCK

LEGEND	
—	SAGUENAY, M=5.9, D=111.22 KM, 18 SITES, 52-200 KM
— • —	GAZLI, NAHANNI, M=6.8, D=4.5 KM, KARAKYR, S1
- - - -	NAHANNI, M=6.8, D=16 KM, S3
—	1
—	2/3

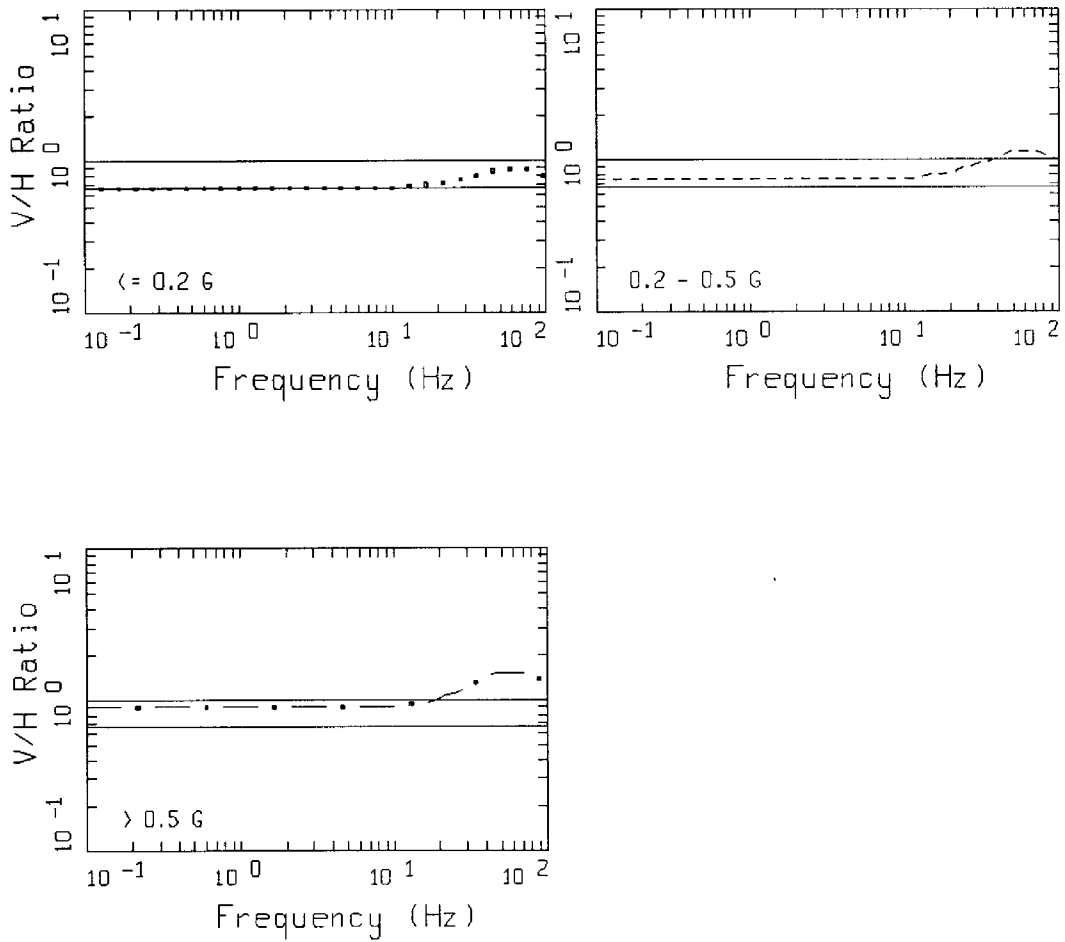
Figure 39. V/H ratios (5% damped) computed from recordings of the **M** 5.9 1988 Saguenay and **M** 6.8 1976 Gazli and 1985 Nahanni earthquakes. The Gazli and Nahanni earthquakes are considered to represent CEUS source, path, and site conditions.



V/H RATIO  
 CEUS MODEL ROCK

LEGEND	
————	M = 5.5
-----	M = 6.5
- . - .	M = 7.5
————	1
————	2/3

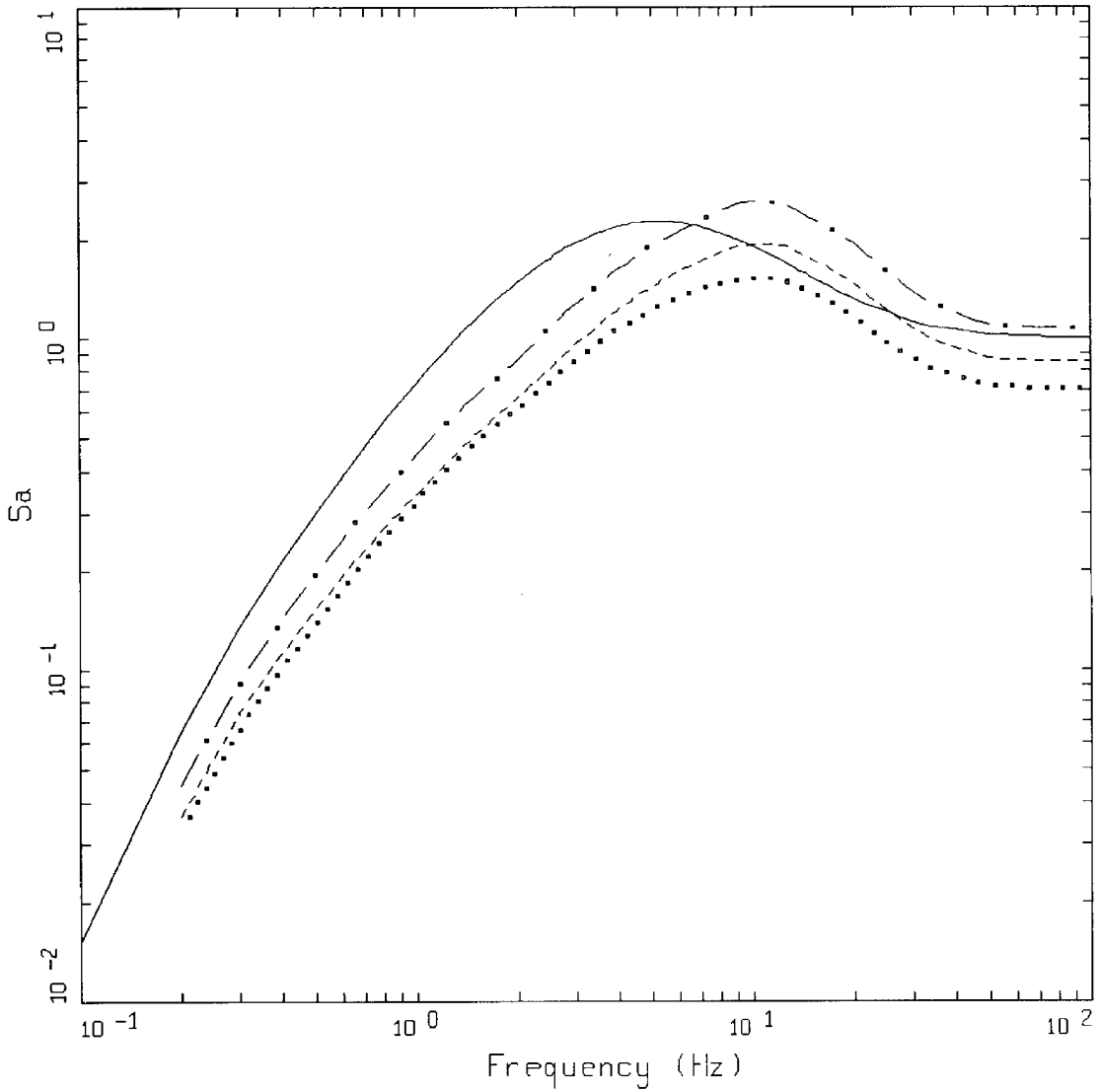
Figure 40. V/H ratios (5% damped) for CEUS rock site conditions computed with the simple point-source model.



V/H RATIO  
 CEUS RECOMMENDATIONS

LEGEND	
— • —	D = 1.00 KM
———	1
————	2/3

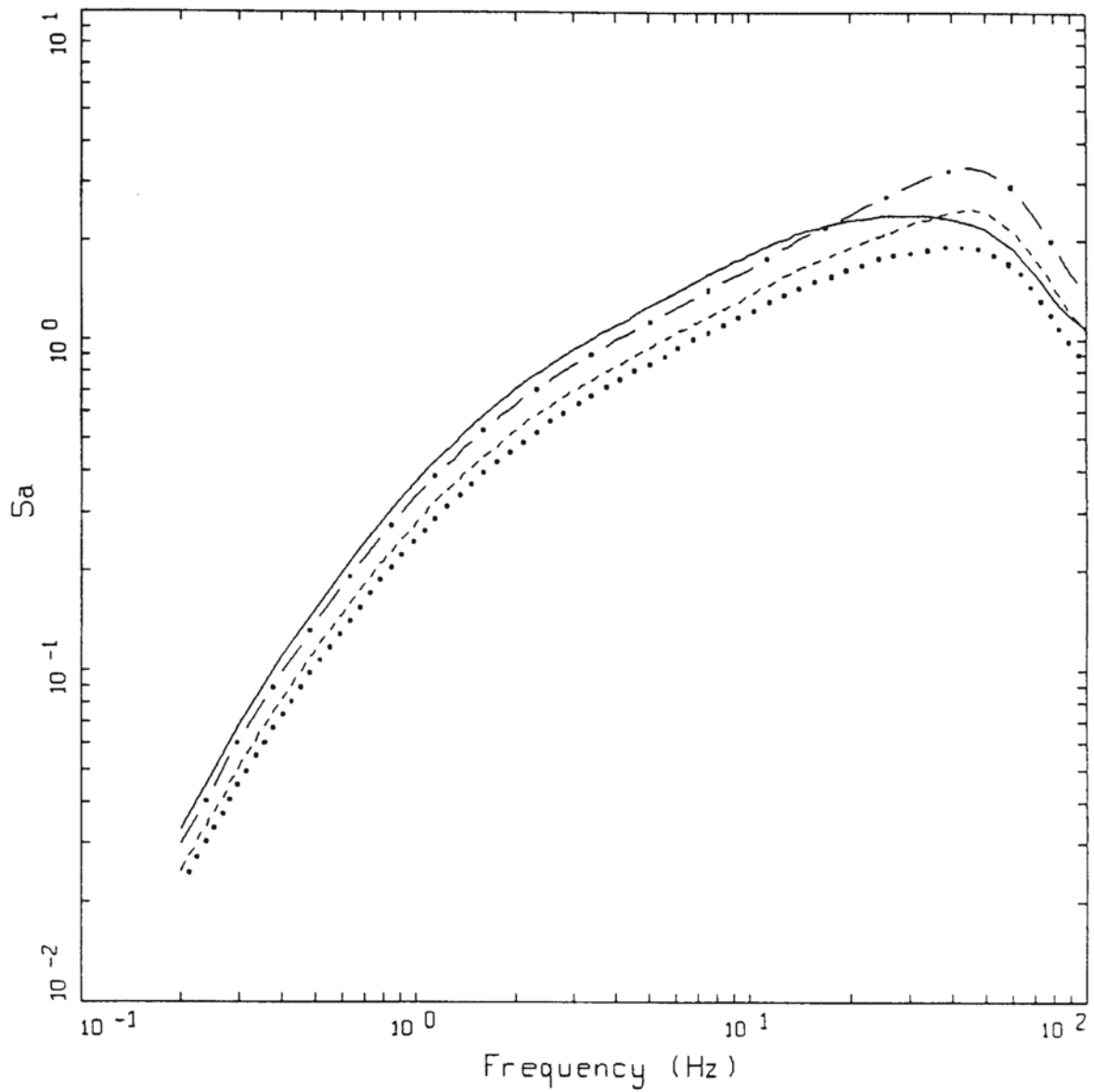
Figure 41. Recommended V/H ratios (5% damped) for CEUS hard rock site conditions for ranges in horizontal component peak accelerations.



NRC WUS V/H RATIO \* REVISED NRC SPECTRA

- LEGEND
- 5% DAMPED, REVISED NRC SHAPE, M6.4, R=27.4 km
  - - - 5% DAMPED VERTICAL > 0.5 G
  - - - 5% DAMPED VERTICAL 0.2 - 0.5 G
  - ..... 5% DAMPED VERTICAL <= 0.2 G

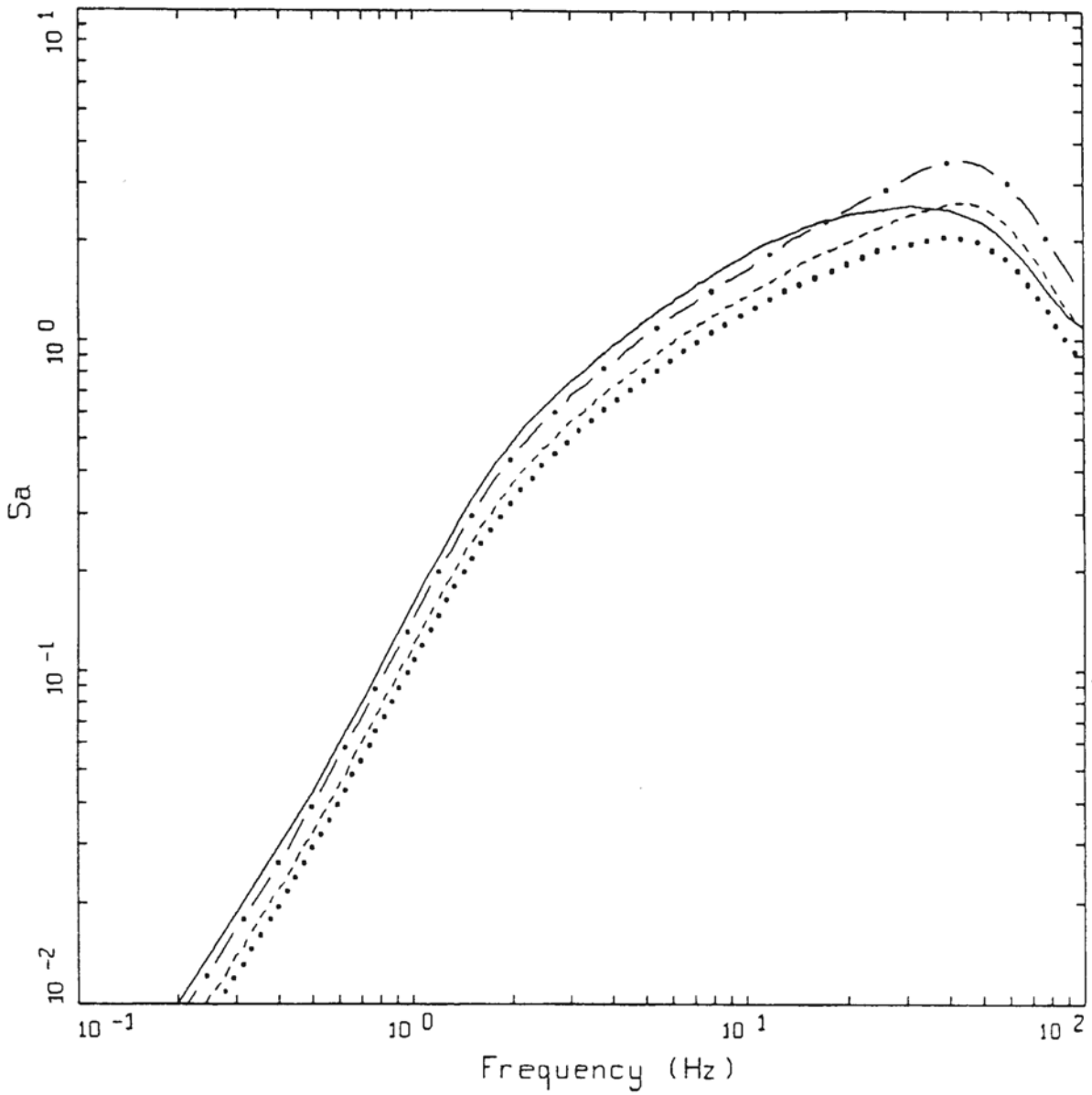
Figure 42. WUS vertical component response spectra (5% damped) based on the M 6.4, R = 27.4 km horizontal shape (Figure Set 28) and recommended V/H ratios (Table 4).



NRC CEUS V/H RATIO \* REVISED NRC SPECTRA  
1-CORNER

- LEGEND
- 5% DAMPED, REVISED NRC SHAPE, M6.4, R=27.4 km
  - · - > 0.5 G
  - - - 0.2 - 0.5 G
  - · · · <= 0.2 G

Figure 43. CEUS vertical component response spectra (5% damped) based on the M 6.4, R = 27.4 km single corner horizontal shape (Figure Set 29) and recommended V/H ratios (Table 5).



NRC CEUS V/H RATIO \* REVISED NRC SPECTRA  
2-CORNER

- LEGEND
- 5% DAMPED, REVISED NRC SHAPE, M6.4, R=27.4 km
  - · - < 0.5 G
  - - - 0.2 - 0.5 G
  - · · · <= 0.2 G

Figure 44. CEUS vertical component response spectra based on the M 6.4, R = 27.4 km double corner horizontal shape (Figure Set 28) and recommended V/H ratios (Table 5).